Arch. Comput. Meth. Engng.
Vol. **13, 2,** 249-324 (2006)

Archives of Computational Methods in Engineering
State of the art reviews

The Variational Multiscale Method for Laminar and Turbulent Flow

V. Gravemeier

Chair for Computational Mechanics
Technical University of Munich
Boltzmannstrasse 15, D-85747 Garching, Germany
vgravem@lnm.mw.tum.de

Summary

The present article reviews the variational multiscale method as a framework for the development of computational methods for the simulation of laminar and turbulent flows, with the emphasis placed on incompressible flows. Starting with a variational formulation of the Navier-Stokes equations, a separation of the scales of the flow problem into two and three different scale groups, respectively, is shown. The approaches resulting from these two different separations are interpreted against the background of two traditional concepts for the numerical simulation of turbulent flows, namely direct numerical simulation (DNS) and large eddy simulation (LES). It is then focused on a three-scale separation, which explicitly distinguishes large resolved scales, small resolved scales, and unresolved scales. In view of turbulent flow simulations as a LES, the variational multiscale method with three separated scale groups is refered to as a "variational multiscale LES". The two distinguishing features of the variational multiscale LES in comparison to the traditional LES are the replacement of the traditional filter by a variational projection and the restriction of the effect of the unresolved scales to the smaller of the resolved scales. Existing solution strategies for the variational multiscale LES are presented and categorized for various numerical methods. The main focus is on the finite element method (FEM) and the finite volume method (FVM). The inclusion of the effect of the unresolved scales within the multiscale environment via constant-coefficient and dynamic subgrid-scale modeling based on the subgrid viscosity concept is also addressed. Selected numerical examples, a laminar and two turbulent flow situations, illustrate the suitability of the variational multiscale method for the numerical simulation of both states of flow. This article concludes with a view on potential future research directions for the variational multiscale method with respect to problems of fluid mechanics.

1 INTRODUCTION

Fluids can be subdivided into liquids and gases, with water and air being the most familiar representatives of these two physical states, respectively. Liquid flows, such as water flows, may be considered incompressible flows for the most part. Under specific circumstances, such as a low Mach number, air and other gas flows may also be dealt with based on the assumption of incompressibility. The concept of incompressibility describes a presumed state of the flow where the temperature field has no influence on the velocity and pressure fields. Characteristic physical parameters, such as the density and the viscosity, are assumed to be constant in an incompressible flow. As a result of the importance of incompressible flows, this review article will focus on the incompressible version of the set of Navier-Stokes equations, which governs incompressible flow mathematically. Nevertheless, methods (solely or likewise) applied to compressible flows will also be included in this article.

The Navier-Stokes equations, either incompressible or compressible, represent the mathematical basis for two states of flow, laminar flow and turbulent flow, although these two states of flow are physically very different. The occurence of one or the other state strongly depends on the Reynolds number associated with the flow. Turbulent flows are highly unsteady flows, where the main velocity field is superimposed by random velocity fluctuations. In typical engineering applications, turbulent flows are prevalent, among other things, due to their positive features, such as a more effective transport and mixing ability with respect to a comparable laminar flow. As a result, the general interest in the turbulent state of

 ISSN: 1134–3060 Received: March 2005

flow is very high. This article accomodates this interest by paying particular attention to the numerical simulation of turbulent flows.

The analytical point of view on the Navier-Stokes equations is deficient, in particular with regard to the turbulent flow regime. There exist no analytical solutions even to the simplest turbulent flow situations. Thus, it must be hoped for a numerical way of solving this "chief outstanding" (Bradshaw [6]) problem. Currently, there are three basic conceptual alternatives for the numerical simulation of turbulence: direct numerical simulation (DNS), large eddy simulation (LES), and simulations based on the Reynolds averaged Navier-Stokes (RANS) equations (The last alternative will not be dealt with in this work, and it is refered to, e.g., Wilcox [161] for an exhaustive description of the RANS equations and related modeling approaches). The three concepts for the numerical simulation of turbulent flows in its basic form struggle with different problems in terms of computational *accuracy* and *efficiency*. Furthermore, most of the numerical approaches to laminar flows are also far from being ideal.

In view of this situation, the variational multiscale method, which was introduced as a general concept for problems of computational mechanics, appears to be a valuable framework for developing improved numerical methods in fluid mechanics. This article will try to illuminate the current situation of the variational multiscale method as a concept for the numerical simulation of laminar and turbulent flows. In the remainder of this introduction, DNS and LES will be introduced as the most promising alternatives for *accurate* numerical simulations of turbulent flows. Afterwards, the basic features of the variational multiscale method will be outlined. This will be followed by a description of its close connection to stabilized methods in the context of the finite element method. This introduction will be closed by an overview of the organization of this paper.

1.1 DNS and LES of Turbulent Flows

A DNS is the theoretically most straightforward concept for the numerical simulation of turbulent flows. It "merely" attempts to solve the Navier-Stokes equations numerically (i.e., without any additional modeling efforts), since it has been widely accepted in the meantime that the Navier-Stokes equations govern the turbulent state of flow as well as the laminar state of flow. A DNS aims at a complete resolution of all scales contained in the respective flow. Hence, no unresolved scales would be left theoretically. The problem lies in the broad range of length and time scales appearing in a turbulent flow, which makes this approach unfeasible in most of the cases. A widely used assessment of the necessary computational effort is based on the approximation

$$\frac{L}{\eta} \sim \mathrm{Re}_{\mathrm{L}}^{\frac{3}{4}} \tag{1}$$

which quantifies the ratio of the largest flow scale L and the smallest flow scale, the "Kolmogorov scale", η. This ratio is assumed to be proportional to the Reynolds number based on L and a corresponding velocity measure U, besides the kinematic viscosity ν. Assuming the computational domain to be at least as large as the largest flow scale along with the necessity to resolve the Kolmogorov scale η at the other end of the scale spectrum, a three-dimensional spatial and temporal resolution requires to solve a problem on the scale of

$$N_{\mathrm{S+T}} \approx \left(\frac{L}{\eta}\right)^4 \sim \left(\mathrm{Re}_{\mathrm{L}}^{\frac{3}{4}}\right)^4 = \mathrm{Re}_{\mathrm{L}}^3 \tag{2}$$

where $N_{\mathrm{S+T}}$ denotes the approximate sum of spatial and temporal degrees of freedom which have to be expected. Thus, the number of degrees of freedom in the simulation scales with the Reynolds number to a power of three. As a result, a DNS still is not a viable approach

to simulate high or, for the most part, even moderately high Reynolds number flows of engineering interest with the currently available computer hardware. Even for the lower Reynolds number flows which have been simulated as a DNS, the Kolmogorov scale is seldomly resolved. The smallest resolved scale usually appears to be merely of $O(\eta)$, see Moin and Mahesh [117]. Thus, there are still unresolved scales in a DNS, although the theoretical claim of a DNS assumes no unresolved scales to be left over. The basics of a DNS and its impact on the numerical simulation of turbulence, including a historical review, are provided by Moin and Mahesh [117].

As aforementioned, one usually faces the problem that adequate computational power to execute a DNS of a turbulent flow is not available. A promising alternative then is LES. The strategy of LES consists of resolving the larger flow structures and modeling the effect of the smaller flow structures on the larger structures. It has been learned from Kolmogorov's [104] hypotheses that the smaller scales exhibit a more universal character than the larger scales, which favors a more general validity of a once developed model for the smaller scales than for the larger scales. As a result, LES appears to be a promising approach in two respects. On the one hand, a coarser discretization, which is substantially coarser than a comparable DNS discretization in the majority of the cases, is sufficient for resolving the larger scales, and on the other hand, the universal character of the smaller scales simplifies the modeling process. The traditional way of performing LES is described, for instance, in the comprehensive articles by Fröhlich and Rodi [50], Lesieur and Metais [108], Piomelli [130], Rogallo and Moin [136], and in the book by Sagaut [138]. Some recent advances in LES for complex flows are reported in Moin [116]. A more mathematically oriented view on LES is provided by Guermond *et al.* [65], John [94], and Layton [106]. The traditional LES relies on a filter to separate resolved and unresolved scales. An outline of the traditional LES focusing on the aspects related to the contents of the present article can be found in the appendix of this article.

The principal difference between DNS and LES in terms of the resolved scales is displayed in Figure 1 in front of the Kolmogorov energy spectrum. It shows the energy spectrum function $E(\kappa)$ against the scalar wavenumber κ, which represents an integration over spherical shells around the origin of the three-dimensional wave number space. In the so-called "inertial subrange", the energy spectrum function follows Kolmogorov's famous "5/3-law". The spectrum in Figure 1 has been established and confirmed as a typical energy spectrum of turbulence at sufficiently high Reynolds number in the meantime. Furthergoing descriptions of the Kolmogorov energy spectrum, including the limitations of its applicability, can be found in virtually all textbooks on turbulence, such as Pope [131] and Tennekes and Lumley [149].

1.2 The Variational Multiscale Method and its Relation to Turbulence Theory

The variational multiscale method was established as a theoretical framework in Hughes [76] and further developed for general problems of computational mechanics in Hughes *et al.* [79]. It aims at problems with broad scale ranges, which often pose an unsolvable challenge for standard numerical methods. In the variational multiscale method, the scales of the underlying problem are separated into a predefined number of scale groups, and thus, a different numerical treatment of any of these scale groups is enabled. This theoretical framework was also extended to the problem of the incompressible Navier-Stokes equations in Hughes *et al.* [83], in order to generate a new approach to LES of turbulent flows. The contents of the three aforementioned publications may also be found in the recent review article by Hughes *et al.* [86].

The initial concept of the variational multiscale method, as Hughes and co-workers proposed it assumed a separation of two scale groups. Usually, it may be refered to them as "resolved scales" and "unresolved scales". Nevertheless, the framework allows various other

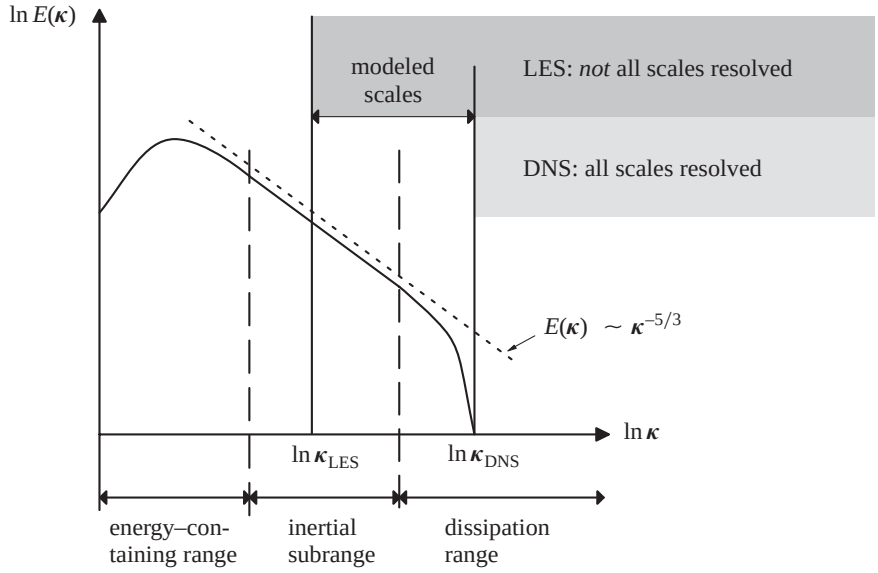

Figure 1. (Theoretical) DNS and LES in front of the Kolmogorov energy spectrum

arrangements going beyond this two-scale decomposition. In Collis [25] and Gravemeier [56], the variational multiscale method for LES, which may be abbreviated as "variational multiscale LES", was broadened by raising the number of separated scale groups beyond the original two-scale separation to three scale groups. As in the two-scale separation, a completely different numerical treatment for any of these groups is enabled. The three-scale separation accounts specifically for "large resolved scales", "small resolved scales", and "unresolved scales".

In contrast to the traditional LES, two important aspects characterize the variational multiscale LES:

- a variational projection separates scale groups within the variational multiscale method, and
- the direct influence of the subgrid-scale model is confined to the small resolved scales.

The first feature may be contrasted to the scale separation with spatial filters in the traditional LES (see appendix). As a result of the second aspect, the large resolved scales are solved as a DNS in the variational multiscale LES (i.e., without any direct influence of the modeling term). Of course, the large resolved scales are still influenced indirectly by the subgrid-scale model due to the inherent coupling of all scales. It should be remarked that the idea of restricting the modeling efforts to the small resolved scales may also be transfered back to the traditional filter-based procedure. First ideas in this direction were presented by Jeanmart and Winckelmans [93] and Vreman [153].

The restriction of the direct influence of the subgrid-scale model to the smaller resolved scales approaches an established principle in turbulence theory, namely Richardson's [135] energy cascade or, more precisely, a quantification of this rather qualitative picture. At the beginning of Richardson's energy cascade, the kinetic energy is brought into the turbulent flow by productive mechanisms at the largest scales. Following the picture of a cascade, the energy is then transmitted to smaller and smaller scales by processes not depending on the molecular viscosity ν. The viscosity merely acts at the end of the cascade, which is constituted by the smallest scales, by enforcing dissipation of the energy. The basic

constituents of a turbulent flow are eddies of various scale sizes, ranging from very large to very small ones. The energy cascade proceeds due to a breaking-up of larger eddies which transfers the energy formerly attributed to these larger eddies to smaller eddies. This goes on until a finally stable eddy motion is reached, and the dissipation of kinetic energy can then take place. Within this cascade, most of the energy that is exchanged across a certain scale-size level comes from the next larger scale-size level and goes to the next smaller scale-size level. Thus, the largest and the smallest scales have no direct effect on the energy transfer at intermediate scale-size levels (see, e.g., Tennekes and Lumley [149]).

For the three-scale separation of the variational multiscale LES, this means that it is reasonable to assume the mutual influence of the large resolved scales (i.e., the largest scales of the problem) and the unresolved scales (i.e., the smallest scales of the problem) to be of minor relevance. This is in contrast to the traditional LES, where the effect of the unresolved scales is typically taken into account equally for all resolved scales. The effect of the unresolved scales on the small resolved scales in the variational multiscale LES will be accounted for by applying a subgrid-scale model based on the subgrid viscosity concept (see appendix) to the small resolved scales in the context of the present article. This is a well-known modeling approach in the traditional LES. Aside from the main process, a drainage of energy from the resolved scales to the unresolved scales according to the picture of the energy cascade, a weak backscatter occurs in the opposite direction. This backscatter cannot be accounted for by a subgrid-viscosity model, which is a purely dissipative model, irrespective of its use in the traditional LES or in the variational multiscale LES.

At this stage, it should be pointed out that the variational multiscale method is a *theoretical* framework for the separation of scales. Thus, it is essential to develop corresponding *practical* implementations by incorporating the variational multiscale framework into a selected numerical method. For such practical methods, it is crucial that the aforementioned separation of the different scale groups is actually achieved. This study is mainly devoted to presenting various practical implementations in this context. The focus will be on the finite element method (FEM) and the finite volume method (FVM). Hence, the development of the formulations will be done with particular emphasis on these two numerical methods. In particular, the general suitability of the FEM and the FVM for unstructured grid applications is of high relevance for potential future applications in more complex geometries. Introductory textbooks on the FEM are, for example, Hughes [77], Szabo and Babuška [145], and Zienkiewicz and Taylor [165]. Particular emphasis on the FEM for flow problems is laid in the textbooks by, e.g., Donea and Huerta [30] and Gresho and Sani [63]. The FVM in fluid mechanics is addressed, for instance, in the textbooks by Ferziger and Peric [34] and Hirsch [72], [73]. For a comparison of these two numerical methods, the interested reader may consult Gresho and Sani [63] and Idelsohn and Oñate [89]. Practical strategies suitable for finite difference or spectral methods will also be briefly addressed and included in the overviews. Although spectral methods are equipped with a very simple and efficient way of separating the scales, the crucial drawback of these methods lies in their inappropriateness for even slightly complex geometries. In this respect, standard finite difference methods also reach their limitations relatively soon.

In this study, it is focused on the variational multiscale method, although many other methods exploiting the multiscale structure of the problem have been developed in recent years. To name a few explicitly declaring LES of turbulent flows as their goal, it is particularly refered to the work of Dubois, Temam, and co-workers using the non-linear Galerkin method and the incremental unknowns technique (see, e.g., Dubois *et al.* [31]) and to the multilevel algorithm of Terracol *et al.* [150]. Further interesting approaches are the modified subgrid-scale estimation model of Domaradzki and co-workers (see, e.g., Domaradzki *et al.* [29]), the Spectral Vanishing Viscosity (SVV) method of Karamanos and Karniadakis [99], and the Reproducing Kernel Particle Method (RKPM) of Wagner and Liu [155]. This

short list is by far not exhaustive. Further multiscale methods are mentioned in Gravemeier [56], Hughes *et al.* [86], and Sagaut [138].

1.3 The Variational Multiscale Method and its Relation to Stabilized Methods

The focus of this study is on the FEM and the FVM as mentioned above. However, both methods represent a risky choice for problems of fluid mechanics. This is due to potential instabilities which may appear in a straightforward application of these methods. Just to give an example in the context of the FVM, only a staggered arrangement of the variables ensures a strong coupling between the velocities and the pressure. However, the use of this arrangement for unstructured grids is difficult due to the appearance of different control volume definitions for the velocities and the pressure. On the other hand, a non-staggered (or collocated) arrangement is known to produce spurious oscillations in the pressure field in form of a "checkerboard" pressure distribution due to a decoupling of the pressure field. For elaboration of this and other stability issues in the context of the FVM, it is refered to the respective literature on the FVM (see, e.g., Ferziger and Peric [34]).

The problem of stability has particularly drawn a lot of attention in the context of the FEM in fluid mechanics in recent years. This may be learned from the huge number of publications addressing this issue. There are two stability problems related to a FEM. Independent of the effective state of flow (i.e., laminar or turbulent), it is, in general, not possible to achieve unspoilt results using the standard form of the Galerkin FEM in case of a dominating convective term (i.e., for a flow at relatively high Reynolds number) without resorting to a very fine discretization level. The second problem which must be dealt with in the context of the Navier-Stokes equations is the required fulfillment of the so-called "inf-sup" condition (or LBB condition), which is exhaustively described, e.g., in Brezzi and Fortin [10]. As a cure for these two problems, stabilized Galerkin FEMs were developed.

Overviews describing the evolution of stabilized FEMs may be found in Brezzi *et al.* [11], Donea and Huerta [30], Hughes *et al.* [82], [86], and Wall [156]. At the beginning of the 1980s, the triumphal procession of stabilized methods for convection-diffusion equations started with the "streamline upwind/Petrov-Galerkin" (SUPG) method, which was developed by Brooks and Hughes (see, e.g., Brooks and Hughes [17]), and analyzed by Johnson and co-workers under the name "streamline diffusion" method (see, e.g., Johnson and Saranen [97]). Here, the differential operator acting on the weighting function corresponds to the convective part of the underlying differential operator. The use of the complete differential operator is the feature of the "Galerkin/least-squares" (GLS) method of Hughes *et al.* [81]. Franca *et al.* [41] proposed to use the negative adjoint differential operator, which was later identified to correspond with the element Green's function and the residual-free bubble method (see, e.g., Brezzi *et al.* [12] and Hughes [76]). In the same year, the close relationship between stabilized methods and bubble methods was elaborated by Brezzi *et al.* [9]. This was continued by Brezzi and co-workers in Baiocchi et al. [1] and in Brezzi and Russo [16]. The method employing the negative adjoint differential operator was called "unusual stabilized FEM" (USFEM) by Franca, Farhat, and co-workers (see, e.g., Franca and Farhat [38] and Franca *et al.* [39]). In Franca and Valentin [49], a reactive term was included in the USFEM formulation. A comparison of various stabilized FEMs for the convection-diffusion-reaction equation was provided by Codina [22]. A special design of the stabilization parameter incorporating the flow direction was proposed in Harari *et al.* [69]. Further approaches are the finite increment calculus (FIC), which leads to very similar stabilization techniques, as could be proven by Oñate and co-workers (see, e.g., Oñate *et al.* [127] and Oñate [128]), and the nearly-optimal Petrov-Galerkin (NOPG) method (see, e.g., Barbone and Harari [2] and Nesliturk and Harari [121]).

Proceeding from the convection-diffusion-reaction equation to the Navier-Stokes equation, a second problem must be dealt with, as mentioned above: the fulfillment of the inf-sup

condition. An approach for solely addressing this problem was introduced by Hughes *et al.* [80] for the Stokes equations, where it is the only reason for introducing stabilizing terms. The method was called "pressure stabilizing Petrov-Galerkin" (PSPG), and the similarity to SUPG was obvious. Combined approaches of SUPG/PSPG are conceivable and were used (see, e.g., Hansbo and Szepessy [68] and Tezduyar and Osawa [151]). On the other hand, a stabilization of SUPG-type for elements fulfilling the inf-sup condition has recently been addressed in Gelhard *et al.* [51]. For equal-order interpolated elements violating the inf-sup condition, it is, however, more straightforward to use the GLS- or USFEM-type methods, which are already equipped with everything one needs to overcome both stability problems. Applications of stabilized methods of GLS- and USFEM-type, respectively, to the incompressible Navier-Stokes equations were reported, for instance, in Franca and Frey [40] as well as Codina [23], [24]. Oñate [129] applied a stabilized method based on the FIC to the incompressible Navier-Stokes equations. In Jansen *et al.* [91], a better consistency for the FEM with low-order functions was proposed and proven for the Navier-Stokes equations.

The variational multiscale method and the aforementioned stabilized methods are inherently linked with each other. This can be learned from the fact that the initial study on the variational multiscale method had been motivated by the desire "to better understand the origins of stabilized methods" (Hughes [76]). In fact, stabilized methods may be incorporated into the general framework of the variational multiscale method, as shown by Hughes [76] and later by Brezzi *et al.* [12]. The title of the recent review article by Hughes *et al.* [86], reading "Multiscale and stabilized methods", as well as the fact that minisymposia entitled "Stabilized and multiscale finite element methods" have now been organized by Franca, Hughes, and Masud for several years on the occasion of various conferences in the field of computational mechanics underline this inherent link. Furthermore, the idea underlying the second important characteristic of the variational multiscale LES (i.e., the direct effect of the subgrid-scale model is confined to the small resolved scales) could already be found in Guermond [64]. In that work, it was proposed to apply a subgrid-scale model only to the small resolved scales, in order to preserve *stability* for a reasonably fine discretization. Thus, the same approach may serve for two, at first sight different goals: *stabilization* (in the context of stabilized numerical methods) and *inclusion of physical effects from numerically unresolvable scales* (in the context of LES of turbulent flows).

In the case that the small scales represent the essential problem, which is the one dealt with in this study (for another problem configuration, see Hughes *et al.* [86]), two problem classes may be distinguished according to Brezzi [7]. To the first class, all the situations may be assigned, for which the chosen discretization level does not provide the necessary *stability* properties. This has to be viewed, in general, as the result of an improper treatment of the small scales of the problem. However, an actual physical effect cannot be ascribed to the small scales of these problems. This is the important difference with respect to problems associated with the second class of problems. In these problems, the *small-scale physics* is crucial. Consequently, turbulent flows have to be assigned to the second class of this simplified categorization. The final result, however, appears to be the same for the representatives of both classes in that a questionable solution may be achieved in the end due to the disregard of the small scales of the problem. As a result, it is stated, particularly for the case of turbulent flows, that there exists an inherent link between, on the one hand, *physically motivated turbulence modeling* and, on the other hand, *numerically motivated modeling to account for inevitable errors due to an inadequate discretization*, as already pointed out in Collis [25] and Gravemeier [56].

1.4 Guideline and Organization of the Paper

The present paper is organized along the aforementioned two important features of the variational multiscale method for the numerical simulation of flow problems. After a variational FE and FV formulation of the incompressible Navier-Stokes equation will have been given in Section 2, the following sections address the main aspects of the variational multiscale method from a practical point of view as follows.

- Section 3 describes various solutions strategies for a three-scale separation within the variational multiscale method. The emphasis is on the practical realization of the theoretically prescribed variational projection for separating the scale groups. Non-projective scale-separating procedures, which have also been applied in this context, will be addressed, too. The main focus is on approaches within the FEM and the FVM, but approaches used in spectral and finite difference methods will also be included. Overall, two different views on the final equation system, which consists of the equations governing the large and the small resolved scales, will be distinguished.

- The direct influence of the subgrid-scale model is confined to the small resolved scales in the variational multiscale LES. Irrespective of this restriction, the need for subgrid-scale modeling still persists as in a traditional LES. Specific modeling approaches for the variational multiscale LES have not been developed as yet, except for a recent one which will be addressed in the outlook at the end of the present article. Thus, models based on the subgrid viscosity concept, the Smagorinsky [144] model and its dynamic versions, have been used in the applications so far. In Section 4, the basic Smagorinsky model and various related dynamic modeling procedures with respect to their application within the multiscale environment will be addressed.

Numerical results for one laminar flow example as well as two turbulent flow examples will be presented in Section 5, along with an overview of further turbulent flow examples which have been investigated using the variational multiscale LES. In Section 6, conclusions from this study will be drawn and some future prospects will be assessed. A brief survey of the traditional filter-based LES is provided in the appendix of this study.

2 VARIATIONAL MULTISCALE FORMULATION OF THE NAVIER-STOKES EQUATIONS

At the outset of this section, the problem statement in form of the incompressible Navier-Stokes equations with an appropriate set of initial and boundary conditions will be given, which is then taken into a weighted residual formulation. This weighted residual formulation will lead to both a finite element (FE) and finite volume (FV) formulation, depending on the respective function space definitions and integration-by-parts procedures. Afterwards, two and three scale groups will be distinguished, respectively, leading to different formulations. These formulations will then be interpreted in view of a DNS and LES.

2.1 Problem Statement and Weighted Residual Formulation

The set of incompressible Navier-Stokes equations is given as

$$\frac{\partial \mathbf{u}}{\partial t} + \nabla \cdot (\mathbf{u} \otimes \mathbf{u}) + \nabla p - 2\nu \nabla \cdot \varepsilon(\mathbf{u}) = \mathbf{f} \qquad \text{in} \quad \Omega \times (0,T) \tag{3}$$

$$\nabla \cdot \mathbf{u} = 0 \qquad \text{in} \quad \Omega \times (0,T) \tag{4}$$

where $\mathbf{u}$ denotes the velocity vector, p the kinematic pressure (i.e., pressure divided by density), ν the kinematic viscosity, $\varepsilon(\mathbf{u})$ the rate-of-deformation tensor, defined as the symmetric part of the spatial gradient of the velocity subject to

$$\varepsilon(\mathbf{u}) = \frac{1}{2}\left[\nabla\mathbf{u} + (\nabla\mathbf{u})^{\mathrm{T}}\right] \tag{5}$$

$\mathbf{f}$ the body force vector, Ω the spatial domain and T the simulation time. The inflow boundary of the spatial domain, Ω with domain boundary Γ is defined as

$$\Gamma^{-} = \{\mathbf{x} \in \Gamma | \mathbf{u}(\mathbf{x}) \cdot \mathbf{n}_{\Gamma}(\mathbf{x}) < 0\} \tag{6}$$

where $\mathbf{n}_{\Gamma}$ indicates the normal vector to the domain boundary Γ. The outflow boundary Γ^{+} is consistently defined subject to $\Gamma^{+} = \Gamma - \Gamma^{-}$. A Dirichlet boundary condition as

$$\mathbf{u} = \mathbf{g} \qquad \text{on} \quad \Gamma_g \times (0,T) \tag{7}$$

where Γ_g denotes the Dirichlet part of the domain boundary Γ, is defined. Moreover, a Neumann boundary condition for the total momentum flux, such that

$$\boldsymbol{\sigma}_{\mathrm{tot}} \cdot \mathbf{n} = (-\mathbf{u} \otimes \mathbf{u} - p\mathbf{I} + 2\nu\varepsilon(\mathbf{u})) \cdot \mathbf{n} = \mathbf{h}^{-} \qquad \text{on} \quad \Gamma_h^{-} \times (0,T) \tag{8}$$

where Γ_h^{-} denotes the Neumann part of the inflow boundary Γ^{-}, and a Neumann boundary condition for the traction, such that

$$\boldsymbol{\sigma} \cdot \mathbf{n} = (-p\mathbf{I} + 2\nu\varepsilon\mathbf{u})) \cdot \mathbf{n} = \mathbf{h}^{+} \qquad \text{on} \quad \Gamma_h^{+} \times (0,T) \tag{9}$$

where Γ_h^{+} denotes the Neumann part of the outflow boundary Γ^{+}, are defined. Γ_h^{-} and Γ_h^{+} compose the Neumann part Γ_h of the domain boundary Γ subject to $\Gamma_h = \Gamma_h^{-} \cup \Gamma_h^{+}$ and the Neumann boundary conditions (8) and (9) are summarized as

$$\mathbf{h} = \left\{ \begin{array}{ll} \mathbf{h}^{-} & \text{on} \quad \Gamma_h^{-} \times (0,T) \\ \\ \mathbf{h}^{+} & \text{on} \quad \Gamma_h^{+} \times (0,T) \end{array} \right\} \tag{10}$$

It is assumed that $\Gamma = \Gamma_g \cup \Gamma_h$ and $\Gamma_g \cap \Gamma_h = \emptyset$. An initial condition

$$\mathbf{u} = \mathbf{u}_0 \qquad \text{in} \quad \Omega \times \{0\} \tag{11}$$

is given, where the initial velocity field $\mathbf{u}_0$ is assumed to be divergence-free.

A weighted residual formulation of the Navier-Stokes equations reads

$$B_{\mathrm{NS}}^{\mathrm{WR}}(\mathbf{v}, q; \mathbf{u}, p) = (\mathbf{v}, \mathbf{f})_{\Omega} \tag{12}$$

where $\mathbf{v}$ and q denote the weighting functions. The L_2-inner product in the domain Ω on the right hand side of (12) is defined as usual:

$$(\mathbf{v}, \mathbf{f})_{\Omega} = \int_{\Omega} \mathbf{v}\mathbf{f} d\Omega \tag{13}$$

Using the notation in (13), the form $B_{\mathrm{NS}}^{\mathrm{WR}}(\mathbf{v}, q; \mathbf{u}, p)$ on the left hand side, which is linear on the first slot (i.e., $\mathbf{v}, q$) and non-linear on the second slot (i.e., $\mathbf{u}$, p), is defined as

$$B_{\mathrm{NS}}^{\mathrm{WR}}(\mathbf{v}, q; \mathbf{u}, p) = \left(\mathbf{v}, \frac{\partial \mathbf{u}}{\partial t}\right)_{\Omega} + (\mathbf{v}, \nabla \cdot (\mathbf{u} \otimes \mathbf{u}))_{\Omega} + (\mathbf{v}, \nabla p)_{\Omega} - (\mathbf{v}, 2\nu\nabla \cdot \varepsilon(\mathbf{u}))_{\Omega} + (q, \nabla \cdot \mathbf{u}))_{\Omega} \tag{14}$$

2.2 Discretization: FEM and FVM

The weighted residual equation (12) may serve as the starting point for either a FE or a FV formulation. As a first step towards a FE or FV formulation, respectively, the weighted residual formulation (12) is transformed into a variational formulation by applying appropriate integration-by-parts procedures, as will be seen below. Additionally, appropriate vectorial solution and weighting function spaces $\mathcal{S}_u$ and $\mathcal{V}_u$ for the velocity $\mathbf{u}$ and the corresponding velocity weighting function $\mathbf{v}$ have to be defined. Usually, the d-dimensional vectorial version of the function space $H^1(\Omega)$, where d denotes the number of spatial dimensions, is chosen. Analogously, scalar solution and weighting function spaces $\mathcal{S}_p$ and $\mathcal{V}_p$ for the pressure p and the corresponding pressure weighting function q are required. Usually, the scalar space $L_2(\Omega)$ is chosen, where the integral mean value of the pressure over the domain Ω may be prescribed to be zero for the case $\Gamma_h = \emptyset$. Further specifications defining the function spaces for the FEM and the FVM, respectively, will be given below. In combined form, the solution and weighting function spaces may be written as

$$\mathcal{S}_{up} := \mathcal{S}_u \times \mathcal{S}_p, \qquad \mathcal{V}_{up} := \mathcal{V}_u \times \mathcal{V}_p \tag{15}$$

For both methods, the prerequisite for the application is a discretization of the domain Ω into n_{el} elements or n_{cv} control volumes Ω_i, respectively, where $i = 1 \dots n_{\text{el/cv}}$, with the respective element or control volume boundaries Γ_i. The continuous solution and weighting functions in the weighted residual equation (12) are replaced by discrete FE or FV functions, respectively, to be defined below. Moreover, the finite-dimensional subspaces $\mathcal{S}_{up}^h \subset \mathcal{S}_{up}$ and $\mathcal{V}_{up}^h \subset \mathcal{V}_{up}$ replace the infinite-dimensional function spaces $\mathcal{S}_{up}$ and $\mathcal{V}_{up}$, respectively.

In the FEM, the weighting function values on the Dirichlet boundary are prescribed as

$$\mathbf{v}^h = \mathbf{0} \qquad \text{on} \quad \Gamma_g \times (0,T) \tag{16}$$

and the solution function values are expected to take on the (discretely) prescribed Dirichlet boundary condition, such that

$$\mathbf{u}^h = \mathbf{g}^h \qquad \text{on} \quad \Gamma_g \times (0,T) \tag{17}$$

The usual FE solution functions are constituted by unknown velocity parameters $\mathbf{u}_B^h$ and pressure parameters p_B^h, which will have to be determined, and shape functions N_B, which are commonly represented by polynomial functions, such that

$$\mathbf{u}^h = \sum_{B=1}^{n_{\text{dofs}}} N_B \mathbf{u}_B^h, \qquad p^h = \sum_{B=1}^{n_{\text{dofs}}} N_B p_B^h \tag{18}$$

where n_{dofs} indicates the number of degrees of freedom of the problem. Choosing similar functions for the approximation of the weighting functions subject to

$$\mathbf{v}^h = \sum_{A=1}^{n_{\text{dofs}}} N_A \mathbf{v}_A^h, \qquad q^h = \sum_{A=1}^{n_{\text{dofs}}} N_A q_A^h \tag{19}$$

provides us with a standard Galerkin method, which may also be termed "Bubnov-Galerkin" method. Different choices for the solution and weighting functions are usually categorized under the label "Petrov-Galerkin" method.

Two different concepts for the shape functions N in (18) and (19) are possible: standard Lagrange-based shape functions and hierarchical shape functions. Elementary descriptions

of the hierarchical concept can be found in Szabo and Babuška [145], Zienkiewicz *et al.* [164] and Zienkiewicz and Taylor [165]. Within the standard Lagrangean concept, the parameters, for example p_B, are entirely assigned to nodal values, whereas this is, in general, not the case for the hierarchical concept. The crucial second difference lies in the respective generation of the polynomial shape functions N. In the standard concept, every polynomial order k is associated with a completely different set of shape functions entirely built by functions of this specific order k, whereas the hierarchical shape functions of a particular order k are assembled by functions of order k and of lower order. This feature of the hierarchical concept constitutes the basic reason for the suitability of this concept for the variational multiscale method: the hierarchical basis of order $k-1$ is a subset of the one of order k, which amounts to a "natural" scale separation. The hierarchical concept is exploited for a scale separation to be outlined in Section 3.2.1. Nevertheless, another scale separation outside of the hierarchical concept will also be addressed. The merits and troubles of the hierarchic concept in comparison to the Lagrangean concept were addressed, for instance, in Whiting and Jansen [159] and Zienkiewicz *et al.* [164]. One may benefit from an improved conditioning of the resulting matrix with respect to matrices stemming from standard Lagrangean concepts. Furthermore, the special structure of the matrix consisting of submatrices, which may be preserved, allows for some potential computational savings as well as assistance in the case of grid refinement. Some problems associated with the hierachical concept, however, should be remarked as well. Difficulties arise particularly with the coverage of initial and boundary conditions as well as with the post-processing of the solutions. These problems do not occur in the standard concept.

The FE equation may be formulated as follows: find $\{\mathbf{u}^h, p^h\} \in \mathcal{S}^h_{up}$ such that

$$B^{\mathrm{FE}}_{\mathrm{NS}}(\mathbf{v}^h, q^h; \mathbf{u}^h, p^h) = (\mathbf{v}^h, \mathbf{f})_\Omega + (\mathbf{v}^h, \mathbf{h})_{\Gamma_h} \qquad \forall \{\mathbf{v}^h, q^h\} \in \mathcal{V}^h_{up} \tag{20}$$

where the additional Neumann boundary term on the right hand side of (20), compared to (12), reads

$$(\mathbf{v}, \mathbf{h})_{\Gamma_h} = \int_{\Gamma_h} \mathbf{v}\mathbf{h} d\Gamma \tag{21}$$

and

$$B^{\mathrm{FE}}_{\mathrm{NS}}(\mathbf{v}^h, q^h; \mathbf{u}^h, p^h) = \left(\mathbf{v}^h, \frac{\partial \mathbf{u}^h}{\partial t}\right)_\Omega - (\nabla \cdot \mathbf{v}^h, \mathbf{u}^h \otimes \mathbf{u}^h)_\Omega - (\nabla \cdot \mathbf{v}^h, p^h)_\Omega + \\ + (\varepsilon(\mathbf{v}^h), 2\nu\varepsilon(\mathbf{u}^h))_\Omega + (q^h, \nabla \cdot \mathbf{u}^h)_\Omega \tag{22}$$

on the left hand side of (20) is obtained after integration-by-parts of the convective term, the pressure term, and the viscous term.

The FV weighting functions read

$$\mathbf{v}^h = \sum_i \mathbf{v}^h_i, \qquad q^h = \sum_i q^h_i \tag{23}$$

where

$$\mathbf{v}^h_i = \mathbf{1}, \qquad q^h_i = 1 \qquad \text{in} \quad \Omega_i \tag{24}$$

and zero elsewhere. In (24), $\mathbf{1}$ explicitly means that each component of $\mathbf{v}^h_i$ is of unit value. The FV solution functions are similar in their structure to the FE weighting functions. They may be given as

$$\mathbf{u}^h = \sum_i N_i \mathbf{u}^h_i, \qquad p^h = \sum_i N_i p^h_i \tag{25}$$

for a collocated volume-centered variable arrangement, where polynomial shape functions as well as velocity and pressure parameters are used as in the FEM. The respective velocity

parameters $\mathbf{u}_i^h$ and the respective pressure parameter p_i^h are determined at the center of the control volume Ω_i. Other arrangements are possible, see the respective literature on the FVM. In accordance with the usual application of low-order shape functions in the FV method, only linear shape functions N_i are considered here. A particular procedure for taking into account Dirichlet boundary conditions for such a variable arrangement was described in Gravemeier [58]. With (23)-(24) and (25) at hand, the FV equation may be formulated for each $\mathbf{v}_i^h$ and q_i^h: find $\{\mathbf{u}^h, p^h\} \in \mathcal{S}_{up}^h$, such that

$$B_{\mathrm{NS}}^{\mathrm{FV}}(\mathbf{v}_i^h, q_i^h; \mathbf{u}^h, p^h) = (\mathbf{v}_i^h, \mathbf{f})_\Omega + (\mathbf{v}_i^h, \mathbf{h})_{\Gamma_h} \tag{26}$$

where

$$\begin{aligned} B_{\mathrm{NS}}^{\mathrm{FV}}(\mathbf{v}_i^h, q_i^h; \mathbf{u}^h, p^h) = &\left(\mathbf{v}_i^h, \frac{\partial \mathbf{u}^h}{\partial t}\right)_\Omega + (\mathbf{v}_i^h, (\mathbf{u}^h \otimes \mathbf{u}^h)\cdot\mathbf{n})_{\Gamma_i} + (\mathbf{v}_i^h, p^h\mathbf{n})_{\Gamma_i} \\ &-(\mathbf{v}_i^h, 2\nu\varepsilon(\mathbf{u}^h)\cdot\mathbf{n})_{\Gamma_i} + (q_i^h, \mathbf{u}^h\cdot\mathbf{n})_{\Gamma_i} \end{aligned} \tag{27}$$

is obtained after applying Gauss' theorem to the convective term, the pressure term, the viscous term, and the continuity term. Γ_i denotes the boundary of the support of $\mathbf{v}_i^h$ and q_i^h, respectively, and $\mathbf{n}$ the respective outward normal vector of unit length to this boundary of support. The Neumann boundary integral, where condition (10) is prescribed, can be shifted to the right hand side of (26). Note that the FV formulation (26) is *locally conservative* with respect to each control volume Ω_i.

It is important to note that the Galerkin FEM may be mathematically interpreted as a projection. An exhaustive discussion of this specific aspect of the Galerkin FEM can be found in Gresho and Sani [63], appendix 3. The main aspects for the present purpose were summarized in Gravemeier [56]. Similar considerations may be pursued for the FVM. Overall, it is stated that a variational projection identifies the resolved scales of the problem as a result of the straightforward application of both the FEM and the FVM. This may be contrasted to the use of a spatial filtering process for the identification of the resolved scales of the problem in the traditional LES, at least according to its basic theory, see appendix.

2.3 Separation of Two Scale Groups

At first, two scale groups are separated: resolved scales and unresolved scales. In terms of the underlying weighting and solution function spaces $\mathcal{V}_{up}$ and $\mathcal{S}_{up}$, this scale separation reads

$$\mathcal{V}_{up} = \mathcal{V}_{up}^h \otimes \hat{\mathcal{V}}_{up} \tag{28}$$

$$\mathcal{S}_{up} = \mathcal{S}_{up}^h \otimes \hat{\mathcal{S}}_{up} \tag{29}$$

where the resolved scales are indicated by the characteristic discretization length h and the unreolved scales by $\hat{(\cdot)}$. The weighting functions are composed as

$$\mathbf{v} = \mathbf{v}^h + \hat{\mathbf{v}}, \qquad q = q^h + \hat{q} \tag{30}$$

and the solution functions as

$$\mathbf{u} = \mathbf{u}^h + \hat{\mathbf{u}}, \qquad p = p^h + \hat{p} \tag{31}$$

Since the weighted residual equation (12) is linear with respect to the weighting functions, it may be separated into a system of two equations as

$$B_{\mathrm{NS}}(\mathbf{v}^h, q^h; \mathbf{u}^h + \hat{\mathbf{u}}, p^h + \hat{p}) = (\mathbf{v}^h, \mathbf{f})_\Omega \qquad \forall \{\mathbf{v}^h, q^h\} \in \mathcal{V}_{up}^h \tag{32}$$

$$B_{\mathrm{NS}}(\hat{\mathbf{v}}, \hat{q}; \mathbf{u}^h + \hat{\mathbf{u}}, p^h + \hat{p}) = (\hat{\mathbf{v}}, \mathbf{f})_\Omega \qquad \forall \{\hat{\mathbf{v}}, \hat{q}\} \in \hat{\mathcal{V}}_{up} \tag{33}$$

In the general statement of the two-scale equation system (32)-(33) as well as the three-scale equation system in the subsequent section, the superscripts for B_{NS} are omitted, since the scale-separating procedure is basically valid for all previously introduced versions of B_{NS}. In particular, it is valid for the FE equation (20) and the FV equation (26). The form B_{NS} in the equation for the resolved scales of the problem (32) is linearized with respect to the convective term according to Hughes *et al.* [83] by expanding it as

$$\begin{aligned} B_{\mathrm{NS}}(\mathbf{v}^h, q^h; \mathbf{u}^h + \hat{\mathbf{u}}, p^h + \hat{p}) &= B_{\mathrm{NS}}(\mathbf{v}^h, q^h; \mathbf{u}^h, p^h) \\ &+ \frac{d}{d\varepsilon} B_{\mathrm{NS}}(\mathbf{v}^h, q^h; \mathbf{u}^h + \varepsilon\hat{\mathbf{u}}, p^h + \varepsilon\hat{p})|_{\varepsilon=0} + \frac{1}{2}\frac{d^2}{d\varepsilon^2} B_{\mathrm{NS}}(\mathbf{v}^h, q^h; \mathbf{u}^h + \varepsilon\hat{\mathbf{u}}, p^h + \varepsilon\hat{p})|_{\varepsilon=0} \\ &= B_{\mathrm{NS}}(\mathbf{v}^h, q^h; \mathbf{u}^h, p^h) + B^1_{\mathrm{NS}}(\mathbf{v}^h, q^h; \mathbf{u}^h; \hat{\mathbf{u}}, \hat{p}) + B^2_{\mathrm{NS}}(\mathbf{v}^h; \hat{\mathbf{u}}) \end{aligned} \tag{34}$$

where $B_{\mathrm{NS}}(\mathbf{v}^h, q^h; \mathbf{u}^h, p^h)$ is given according to (14). The linearized form

$$\begin{aligned} B^1_{\mathrm{NS}}(\mathbf{v}^h, q^h; \mathbf{u}^h; \hat{\mathbf{u}}, \hat{p}) &= \frac{d}{d\varepsilon} B_{\mathrm{NS}}(\mathbf{v}^h, q^h; \mathbf{u}^h + \varepsilon\hat{\mathbf{u}}, p^h + \varepsilon\hat{p})|_{\varepsilon=0} \\ &= \left(\mathbf{v}^h, \frac{\partial\hat{\mathbf{u}}}{\partial t}\right)_\Omega + (\mathbf{v}^h, \nabla\cdot(\mathbf{u}^h \otimes \hat{\mathbf{u}}) + \nabla\cdot(\hat{\mathbf{u}} \otimes \mathbf{u}^h))_\Omega + (\mathbf{v}^h, \nabla\hat{p})_\Omega \\ &\quad -(\mathbf{v}^h, 2\nu\nabla\cdot\varepsilon(\hat{\mathbf{u}}))_\Omega + (q^h, \nabla\cdot\hat{\mathbf{u}})_\Omega \end{aligned} \tag{35}$$

is linear on the first slot (i.e., $\mathbf{v}^h$, q^h) as well as on the third slot (i.e., $\hat{\mathbf{u}}$, $\hat{p}$), and affine on the second slot (i.e., $\mathbf{u}^h$). The form

$$B^2_{\mathrm{NS}}(\mathbf{v}^h; \hat{\mathbf{u}}) = \frac{1}{2}\frac{d^2}{d\varepsilon^2} B_{\mathrm{NS}}(\mathbf{v}^h, q^h; \mathbf{u}^h + \varepsilon\hat{\mathbf{u}}, p^h + \varepsilon\hat{p})|_{\varepsilon=0} = (\mathbf{v}^h, \nabla\cdot(\hat{\mathbf{u}} \otimes \hat{\mathbf{u}}))_\Omega \tag{36}$$

is linear on the first slot (i.e., $\mathbf{v}^h$) and non-linear on the second slot (i.e., $\hat{\mathbf{u}}$)). Rearranging (32) with the help of (34) yields

$$B_{\mathrm{NS}}(\mathbf{v}^h, q^h; \mathbf{u}^h, p^h) = (\mathbf{v}^h, \mathbf{f})_\Omega - B^1_{\mathrm{NS}}(\mathbf{v}^h, q^h; \mathbf{u}^h; \hat{\mathbf{u}}, \hat{p}) - B^2_{\mathrm{NS}}(\mathbf{v}^h; \hat{\mathbf{u}}) \tag{37}$$

The last two terms on the right hand side of (37) may be identified as the influence of the unresolved scales onto the resolved scales. In terms of the aforementioned interpretation of the FE and FV method as a variational projection, these two terms can be viewed as the *projection of the unresolved scales onto the subspace of the resolved scales*. Hence, it is only this projection that has to be represented by a subgrid- scale model in the equation for the resolved scales, see also Collis [25].

In view of the equation for the unresolved scales of the problem (33), it is stated that it is not intended to explicitly resolve any quantities which are termed "unresolved" *a priori*: "the name is the game". Taking into account the effect of the unresolved scales on the small resolved scales in form of the unknown projective terms on the right hand side of (37) is the only desire. Several approaches lend themselves to this purpose (see Gravemeier [56]), but the focus here will be on the subgrid viscosity concept (see appendix) as a usual and well-established way of taking into account the effect of unresolved scales in the numerical simulation of turbulent flows. It is emphasized that it is merely accounted for an energetic or, more precisely, a purely dissipative effect of the unresolved scales on the resolved scales by using this concept.

As a result, the equation for the unresolved scales (33) is neglected, and the modeled form of the equation for the resolved scales (32) reads

$$B_{\mathrm{NS}}(\mathbf{v}^h, q^h; \mathbf{u}^h, p^h) - (\mathbf{v}^h, \nabla\cdot(2\nu_T\varepsilon(\mathbf{u}^h)))_\Omega = (\mathbf{v}^h, \mathbf{f})_\Omega \tag{38}$$

with a subgrid viscosity term in form of a weighted integral term added to the left hand side of (32). The appropriate integration-by-parts procedure, analogous to the one applied to the molecular viscosity term for the FEM in (22) or the FVM in (27), respectively, has to be applied to this term as well. Appropriate modeling approaches for the subgrid viscosity ν_T will be discussed in Section 4. Note that the reason for introducing a model term in this context is mathematically different from the usual necessity to introduce a model term due to the appearance of a subfilter-scale (or subgrid-scale) stress tensor in the strong formulation of the Navier-Stokes equations in a traditional LES, see appendix. Nevertheless, the physical necessity to account for the missing effect of unresolved scales onto the resolved scales is the same in both cases.

In Gravemeier *et al.* [62], it was shown that the same equation for the resolved scales (37) may be achieved by following an intuitive procedure. This procedure consists of a straightforward adoption of the separation of velocity and pressure according to (31) and its introduction into the respective basic variational formulation. In terms of a traditional LES, the variational projection may then be interpreted as an implicit filter, see appendix. However, the equation for the unresolved scales (33) never appears in this straightforward derivation, since there is no separation of the weighting functions subject to (30).

2.4 Separation of Three Scale Groups

The scales of the problem are now separated into three scale groups, as proposed in Collis [25] and Gravemeier [56]: large resolved scales, small resolved scales, and unresolved scales. In terms of the underlying weighting and solution function spaces $\mathcal{V}_{up}$ and $\mathcal{S}_{up}$, this scale separation yields

$$\mathcal{V}_{up} = \bar{\mathcal{V}}_{up}^h \otimes \mathcal{V}_{up}'^h \otimes \hat{\mathcal{V}}_{up} \tag{39}$$

$$\mathcal{S}_{up} = \bar{\mathcal{S}}_{up}^h \otimes \mathcal{S}_{up}'^h \otimes \hat{\mathcal{S}}_{up} \tag{40}$$

where the large and small resolved scales are distinguished by $\bar{(\cdot)}$ and $(\cdot)'$, respectively. According to this, the weighting functions read

$$\mathbf{v} = \bar{\mathbf{v}}^h + \mathbf{v}'^h + \hat{\mathbf{v}}, \qquad q = \bar{q}^h + q'^h + \hat{q} \tag{41}$$

and, analogously, the solution functions are composed as

$$\mathbf{u} = \bar{\mathbf{u}}^h + \mathbf{u}'^h + \hat{\mathbf{u}}, \qquad p = \bar{p}^h + p'^h + \hat{p} \tag{42}$$

With the same rationale as before (i.e., the fact that the formulations are linear in the weighting functions), the respective equation may now be separated into a system of three variational equations:

$$B_{\mathrm{NS}}(\bar{\mathbf{v}}^h, \bar{q}^h; \bar{\mathbf{u}}^h + \mathbf{u}'^h + \hat{\mathbf{u}}, \bar{p}^h + p'^h + \hat{p}) = (\bar{\mathbf{v}}^h, \mathbf{f})_\Omega \qquad \forall \{\bar{\mathbf{v}}^h, \bar{q}^h\} \in \bar{\mathcal{V}}_{up}^h \tag{43}$$

$$B_{\mathrm{NS}}(\mathbf{v}'^h, q'^h; \bar{\mathbf{u}}^h + \mathbf{u}'^h + \hat{\mathbf{u}}, \bar{p}^h + p'^h + \hat{p}) = (\mathbf{v}'^h, \mathbf{f})_\Omega \qquad \forall \{\mathbf{v}'^h, q'^h\} \in \mathcal{V}_{up}'^h \tag{44}$$

$$B_{\mathrm{NS}}(\hat{\mathbf{v}}, \hat{q}; \bar{\mathbf{u}}^h + \mathbf{u}'^h + \hat{\mathbf{u}}, \bar{p}^h + p'^h + \hat{p}) = (\hat{\mathbf{v}}, \mathbf{f})_\Omega \qquad \forall \{\hat{\mathbf{v}}, \hat{q}\} \in \hat{\mathcal{V}}_{up} \tag{45}$$

With the linearization procedure in (34), the large-scale equation (43) and the small-scale equation (44) can be written as

$$B_{\mathrm{NS}}(\bar{\mathbf{v}}^h, \bar{q}^h; \mathbf{u}^h, p^h) = (\bar{\mathbf{v}}^h, \mathbf{f})_\Omega - B_{\mathrm{NS}}^1(\bar{\mathbf{v}}^h, \bar{q}^h; \mathbf{u}^h; \hat{\mathbf{u}}, \hat{p}) - B_{\mathrm{NS}}^2(\bar{\mathbf{v}}^h; \hat{\mathbf{u}}) \tag{46}$$

$$B_{\mathrm{NS}}(\mathbf{v}'^h, q'^h; \mathbf{u}^h, p^h) = (\mathbf{v}'^h, \mathbf{f})_\Omega - B_{\mathrm{NS}}^1(\mathbf{v}'^h, q'^h; \mathbf{u}^h; \hat{\mathbf{u}}, \hat{p}) - B_{\mathrm{NS}}^2(\mathbf{v}'^h; \hat{\mathbf{u}}) \tag{47}$$

where the large- and small-scale part of the solution functions have been merged again. Thus, the only difference to (37) is highlighted, which is the fact that only the large- and the small-scale part of the weighting functions appear in (46) and (47), respectively.

It is assumed that

$$B^1_{\mathrm{NS}}(\bar{\mathbf{v}}^h, \bar{q}^h; \mathbf{u}^h; \hat{\mathbf{u}}, \hat{p}) + B^2_{\mathrm{NS}}(\bar{\mathbf{v}}^h; \hat{\mathbf{u}}) \approx 0 \tag{48}$$

which relies on a clear separation of the large-scale space and the space of unresolved scales, as discussed in Section 1.2. Using (48), the large-scale equation (43) is simplified to

$$B_{\mathrm{NS}}(\bar{\mathbf{v}}^h, \bar{q}^h; \bar{\mathbf{u}}^h + \mathbf{u}'^h, p^h + p'^h) = (\bar{\mathbf{v}}^h, \mathbf{f})_\Omega \qquad \forall \{\bar{\mathbf{v}}^h, \bar{q}^h\} \in \bar{\mathcal{V}}^h_{up} \tag{49}$$

As in the previous case, where two scale groups have been separated, it is not intended to explicitly resolve any quantities which are termed "unresolved" *a priori*. Thus, the equation for the unresolved scales (45) is not solved. After introducing a subgrid viscosity term in weighted integral form to represent the effect of the unresolved scales only within the small-scale equation (47), this equation reads

$$B_{\mathrm{NS}}(\mathbf{v}'^h, q'^h; \bar{\mathbf{u}}'^h + \mathbf{u}'^h, \bar{p}^h + p'^h) - (\mathbf{v}'^h, \nabla \cdot (2\nu'_T \varepsilon(\mathbf{u}'^h)))_\Omega = (\bar{\mathbf{v}}^h, \mathbf{f})_\Omega \tag{50}$$

As mentioned for (38), the appropriate integration-by-parts procedure for the FEM or the FVM, respectively, has to be applied to the subgrid viscosity term in weighted integral form. Due to assumption (48), the subgrid viscosity term directly acts only on the small resolved scales, and the final large-scale equation (49) contains no term depending on the unresolved scales of the problem. An indirect influence of the unresolved scales on the large resolved scales, however, is ensured due to the coupling of the large- and the small-scale equation. Appropriate modeling approaches for the subgrid viscosity ν'_T, where the prime indicates the specific dependence on the small resolved scales, will be discussed in Section 4.

2.5 Interpretation of the Two- and Three-Scale Separation in the Sense of a DNS and LES

In a DNS, it is assumed that, theoretically, the complete range or, practically, the predominant part of the scale spectrum is resolved. As a result

$$B^1_{\mathrm{NS}}(\mathbf{v}^h, q^h; \mathbf{u}^h; \hat{\mathbf{u}}, \hat{p}) + B^2_{\mathrm{NS}}(\mathbf{v}^h, \hat{\mathbf{u}}) = 0 \tag{51}$$

in the equation for the resolved scales (37) within the two-scale separation, at least theoretically. As mentioned above, merely the projection of the unresolved scales onto the subspace of the resolved scales is assumed to be zero by stating (51). In a three-scale separation, the *projection* of the unresolved scales onto the subspace of the *large* resolved scales is assumed to be zero, as a result of assumption (48). Hence, the larger of the resolved scales are essentially solved as a DNS. Additionally, the projection of the unresolved scales onto the subspace of the small resolved scales would have to be presumed as

$$B^1_{\mathrm{NS}}(\mathbf{v}'^h, q'^h; \mathbf{u}^h; \hat{\mathbf{u}}, \hat{p}) + B^2_{\mathrm{NS}}(\mathbf{v}'^h, \hat{\mathbf{u}}) = 0 \tag{52}$$

in the small-scale equation (47), at least theoretically, in order to establish a DNS over *all* resolved scales in the three-scale separation.

In Figure 2, the Kolmogorov energy spectrum is displayed for various situations within a two- and a three-scale separation. The respective situation is depicted symbolically by indicating the range of scales "captured" by the (solution) function space. It is observable

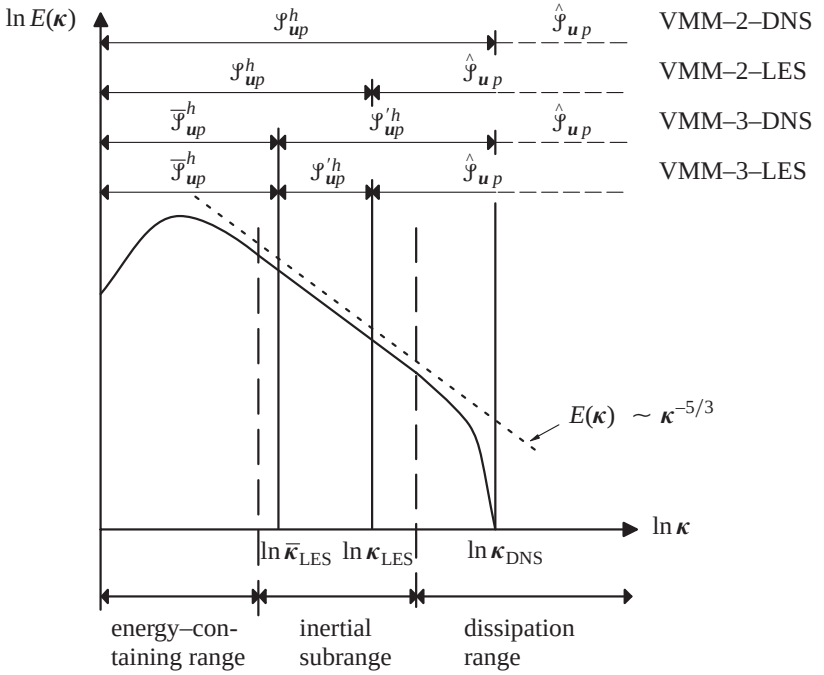

Figure 2. DNS and LES within a two- and three-scale separation of the variational multiscale method

that there are two ways of performing a DNS or LES, respectively. A DNS may result from completely resolving all scales necessary therefore by the space of resolved scales. Alternatively, the same may be done by subdividing these scales into a large- and a small-scale space of resolved scales. Whereas this distinction may be more or less of academic nature for a DNS, it is a crucial decision for a LES. In Figure 2, it is assumed that the overall resolution level for a "VMM-2-LES" and for a "VMM-3-LES" is identical (i.e., it is only a matter of "distributing" this particular amount of scales into one or two scale groups, respectively). In contrast to a VMM-2-LES, a VMM-3-LES provides one with the opportunity of letting the subgrid-scale model directly act only on the space of small resolved scales. Hence, the large scales are solved as a DNS, guaranteeing consistency if an adequate resolution is already achieved by the large-scale space. This last case represents a natural switch to a "VMM-2-DNS", see Figure 2. In order to clarify the notation, it is emphasized that only the VMM-3-LES represents what is refered to as the variational multiscale LES below.

In general, it is remarked that using a variational projection theoretically allows for a clear separation of scales and, accordingly, scale spaces, in contrast to, for example, discrete smooth filters, which are widely used in the traditional LES. Ultimately, the preservation of this clear separation in a practical application of the variational multiscale method depends on the specific choice of the applied numerical method. Of course, this applies both to the basic separation of unresolved and resolved scales as well as a potential further separation of the resolved scales into large and small resolved scales. This issue will be extensively discussed in Section 3 by presenting and analyzing various existing approaches.

An important question is the one of how large the size of the space containing the large as well as the small resolved scales should be chosen, both absolutely and in comparison to each other. The combined extension of both spaces is definitely restricted by the computational effort which can be afforded overall. This essential restriction for the overall size of both

spaces, however, still leaves room for deciding on the relative extension of the spaces. A first basic requirement for choosing the "cutoff-level" of the large-scale space may demand this space to cover at least the range of energy-containing modes. In other words, the location of the cutoff-level is supposed to be within the inertial subrange. This basic requirement has already been taken into account in the depiction of the Kolmogorov energy spectrum in Figure 1, and it will also be depicted this way in the following figures showing the spectrum. Aside from this, several numerical tests of the dynamic modeling procedure according to Germano *et al.* [53] in the traditional LES revealed an optimal value for the cutoff-level associated with a test filter which is about twice as large as the one associated with the basic filter (see, e.g., Sagaut [138]). This may be accepted as a first hint for an adequate choice of the respective relation of large- and small-scale space within the variational multiscale method. It is refered to the related discussion in Hughes *et al.* [83].

It is without doubt that the aforementioned choices strongly affect the actual impact of a potential subgrid-scale model. On the one hand, the combined size of large- and small-scale space influences the overall impact. For a very fine resolution (i.e., a very large size of large- and small-scale space together), there are only few unresolved scales left to be modeled. However, the overall impact of the subgrid-scale model will become crucial if this combined resolution of large- and small-scale space is rather poor. This rather general perception is definitely valid for both ways of performing LES, the traditional and the multiscale approach. On the other hand, the relative size of large- and small-scale space influences the specific impact within the variational multiscale method. A dominant large-scale space in comparison to the small-scale space leaves the majority of the scales without the addition of a modeling term. This eventually results in a pure DNS for the extreme case that all scales, with no unresolved scales left, are contained in the large-scale space. In contrast to this, a diminutive large-scale space tends towards the traditional approach of LES again, since the subgrid-scale model is added to a substantial margin of the resolved scales. Here, the extreme case with all scales, but still leaving unresolved scales, contained in the small-scale space must be considered as the traditional LES approach again. It is refered to Collis [25] for further discussion. After all, the absolute as well as the relative choice of the respective spaces considerably influence the overall procedure. In fact, its actual selection is an important parameter of the method as a whole.

At the end of this section, Figure 3 graphically reemphasizes the essential difference between the new approach, the variational multiscale LES, and the traditional LES approach. Whereas the subgrid-scale model is directly acting on the complete range of resolved scales in the traditional approach, its direct influence is restricted to the range of small resolved scales in the variational multiscale LES. Assuming that one is not able to perform a DNS in most of the cases, these two approaches represent the feasible ways for numerically simulating turbulent flows out of the four depicted in Figure 2. In the upcoming section, solution strategies for a three-scale separation within the variational multiscale method which have already been successfully applied to laminar and/or turbulent flows and published afterwards will be presented.

3 SOLUTION STRATEGIES FOR A THREE-SCALE SEPARATION

Two different solution strategies are distinguished.

- The first strategy appears to be the "natural" way to address the problem. It aims at explicitly solving both constituents of the two-equation system of the variational multiscale LES (i.e., the large-scale equation (49) and the small-scale equation (50)). One practical realization of this strategy in a FEM will be outlined, and prospects for improving this approach in view of its still existing shortcomings will be addressed.

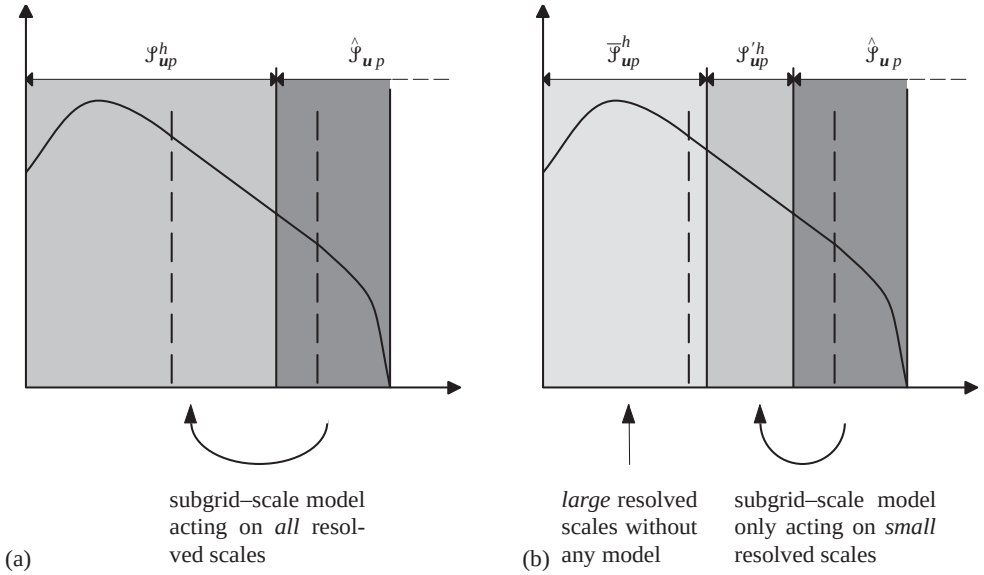

Figure 3. Modeling approach: (a) variational multiscale LES; (b) traditional LES

- The second strategy assumes a formal "reunification" of the large-scale equation (49) and the small-scale equation (50). The separation of scales remains to be observable due to the subgrid viscosity term, which is still acting directly only on the small resolved scales. Several potential strategies within various numerical methods will be described, but the focus remains on the FEM and the FVM.

The inherent link between multiscale and stabilized methods has already been addressed in the introduction. It has to be emphasized that a practical multiscale implementation does not need to be stable *per se*. On the contrary, most of the approaches to be presented in the following rather demand for additional stabilization to represent a viable numerical method.

3.1 Explicitly Solving the Large- and the Small-Scale Equation

The large-scale equation (49) and the small-scale equation (50) are repeated here for the convenience of the reader:

$$B_{\mathrm{NS}}(\bar{\mathbf{v}}^h, \bar{q}^h; \bar{\mathbf{u}}^h + \mathbf{u}'^h, \bar{p}^h + p'^h) = (\bar{\mathbf{v}}^h, \mathbf{f})_\Omega \tag{53}$$

$$B_{\mathrm{NS}}(\mathbf{v}'^h, q'^h; \bar{\mathbf{u}}^h + \mathbf{u}'^h, \bar{p}^h + p'^h) - (\mathbf{v}'^h, \nabla \cdot (2\nu_T' \varepsilon(\mathbf{u}'^h)))_\Omega = (\mathbf{v}'^h, \mathbf{f})_\Omega \tag{54}$$

As Hughes *et al.* [83] already pointed out, this amounts to a pair of coupled non-linear variational equations. Consequently, the large- and the small-scale part of the solution is expected to be obtained by solving these coupled non-linear equations. For instance, if one is able to solve (54) for the small scales of the problem, inserting this solution into (53) enables the solution of the large scales of the problem. As a result, the solution for the complete range of resolvable scales is available. Due to the mutual dependence of the large and the small scales, the just described solution approach may only be done in an iterative manner in practice. However, this iteration may be effectively combined with the iteration which is anyway necessary for solving the basically non-linear problem.

In the following section, one particular approach, a two-level FEM, which will later be extended to a three- level FEM, will be presented. The two-level FEM uses a localized

approximation on the small-scale level. To the best of the author's knowledge, this approach represents the only practical realization of the first strategy which has been reported to date. The reasonability of a localization strategy for the small resolved scales is also supported by perceptions from turbulence theory. In this respect, it is refered to the tendency of decorrelation in a turbulent flow with increasing spatial separation of two points in the flow domain. This tendency has been discovered by analyzing two-point correlations in turbulent flows (see, e.g., Pope [131]). The smaller the scales are, the shorter is the distance over which the scales have to be expected to correlate strongly. Thus, a locally confined resolution of the smaller scales should be a reasonable strategy. The following approach represents a first step in this direction by implementing a rather restrictive localization on the small-scale level.

3.1.1 Two-Level FEM based on residual-free bubbles and a stabilizing term

Residual-free bubbles are used to localize the solution of the small-scale equation. In brief, using residual- free bubbles means obeying two basic rules.

- The governing differential equation has to be satisfied by the complete solution function in strong form on every individual element domain Ω_i of the basic discretization.
- Zero Dirichlet boundary conditions are assumed for the small-scale part of the solution function on the boundaries of every individual element domain Ω_i.

For the underlying case of a separation of the resolved solution function into a large- and a small-scale part, following these rules amounts to selecting the small-scale bubble part of the solution function such that the governing equation is solved in every individual element up to the large-scale part of the solution function. Correspondingly, the residual of the large-scale part of the solution function appears on the right hand side of the residual-free bubble equation, representing the "driving force" of this equation. This equation is subject to homogeneous Dirichlet boundary conditions. Publications by Brezzi, Farhat, Franca, Hughes, Russo and co-workers generally addressing residual-free bubbles and, in particular, residual-free bubbles for convection-diffusion problems are, e.g., [12], [13], [16], [38], and [39].

The strong form of the small-scale equation reads

$$\begin{aligned}&\frac{\partial \mathbf{u}'}{\partial t} + \nabla \cdot (\mathbf{u}' \otimes \mathbf{u}) + \nabla p' - 2\nu \nabla \cdot \varepsilon(\mathbf{u}') \\ &\quad = -\frac{\partial \bar{\mathbf{u}}^h}{\partial t} - \nabla \cdot (\bar{\mathbf{u}}^h \otimes \mathbf{u}) - \nabla \bar{p}^h + 2\nu \nabla \cdot \varepsilon(\bar{\mathbf{u}}^h) + \mathbf{f} \qquad \text{in} \quad \Omega_i \times (0,T) \end{aligned} \tag{55}$$

$$\nabla \cdot \mathbf{u}' = -\nabla \cdot \bar{\mathbf{u}}^h \qquad \text{in} \quad \Omega_i \times (0,T) \tag{56}$$

$$\mathbf{u}' = \mathbf{0} \qquad \text{on} \quad \Gamma_i \times (0,T) \tag{57}$$

Note the zero Dirichlet boundary conditions on all element boundaries. Note also that there are no superscripts "h" attached to the small-scale variables, indicating non-discrete values for the time being. The non-discrete complete velocity $\mathbf{u}$ in the convective term is taken care of iteratively in the actual solution procedure. Furthermore, the convective term and the viscous term are simplified by using the respective conventional form, see Gravemeier [56] for discussion.

The problem statement (55)-(57) represents an analytical problem formulation in every individual element domain Ω_i expecting the small-scale solution to capture all remaining scales not captured by the discrete large-scale solution. Thus, the right hand side of the

small-scale momentum equation (55) is constituted by the residual of the large-scale momentum equation for the discrete large-scale part of the problem variables $\Re_{\mathrm{NS}}^{\mathrm{M}}(\bar{\mathbf{u}}^h, \bar{p}^h)$, and the right hand side of the small-scale continuity equation (56) is constituted by the residual of the large-scale continuity equation for the discrete large-scale part of the velocity $\Re_{\mathrm{NS}}^{\mathrm{C}}(\bar{\mathbf{u}}^h)$.

The small-scale continuity equation (56) may be replaced by a small-scale pressure Poisson equation as

$$\Delta p' + \nabla \cdot (\mathbf{u} \cdot \nabla \mathbf{u}' - \nu \Delta \mathbf{u}') = -\nabla \cdot [\Re_{\mathrm{NS}}^{\mathrm{M}}(\bar{\mathbf{u}}^h, \bar{p}^h)] \qquad \text{in} \quad \Omega_i \times (0,T) \tag{58}$$

where the structure of a consistent pressure Poisson equation according to Gresho and Sani [63] has been adapted for the small scales. The right hand side of (58) is constituted by the negative divergence of $\Re_{\mathrm{NS}}^{\mathrm{M}}(\bar{\mathbf{u}}^h, \bar{p}^h)$.

Firstly, it is focused on the small-scale momentum equation (55). To the author's knowledge, the first attempt of using residual-free bubbles for the stabilization of a linearized stationary Navier-Stokes problem has to be credited to Russo [137]. The separation of function spaces, which is merely carried out for the weighting function space here, reads

$$\mathcal{V}_{up} \approx \bar{\mathcal{V}}_{up}^h \otimes \mathcal{V}'_{u,\mathrm{RFB}} = \bar{\mathcal{V}}_{up}^h \otimes_{\Omega_i} (B(\Omega_i))^d, \qquad i = 1, \ldots, n_{\mathrm{el}} \tag{59}$$

with the usual assumption being $B(\Omega_i) = H_0^1(\Omega_i)$ in each spatial dimension d. As may be observed by inspecting the subscripts of the weighting function spaces, the bubble space exclusively enhances the velocity approximation (i.e., $p' = 0$). Insights into approaches to satisfy the inf-sup condition emphasize the reasonability of this concept, see Gravemeier [56]: by choosing $p' = 0$, a larger function space for the approximation of the velocity in comparison to the one for the approximation of the pressure is guaranteed. As a result, the small-scale momentum equation (55) can now be simplified to

$$\begin{aligned} &\frac{\partial \mathbf{u}'}{\partial t} + \nabla \cdot (\mathbf{u}' \otimes \mathbf{u}) - 2\nu \nabla \cdot \varepsilon(\mathbf{u}') \\ &\quad = -\frac{\partial \bar{\mathbf{u}}^h}{\partial t} - \nabla \cdot (\bar{\mathbf{u}}^h \otimes \mathbf{u}) - \nabla \bar{p}^h + 2\nu \nabla \cdot \varepsilon(\bar{\mathbf{u}}^h) + \mathbf{f} \qquad \text{in} \quad \Omega_i \times (0,T) \end{aligned} \tag{60}$$

If one were able to solve (60) in every element of the basic discretization, the small-scale velocity would be obtained as a sum of these elementwise solutions. The result for $\mathbf{u}'$, along with the assumption $p' = 0$, may then be integrated into the variational large-scale equation (49) leaving *one* final equation to be solved.

Secondly, it is returned to the small-scale continuity equation (56), which has been left out so far. Note that this equation is actually not needed any more, since there is no small-scale pressure in the small-scale momentum equation to be governed by the small-scale continuity equation. As will be seen below, however, it may be helpful to revitalize some kind of small-scale pressure which is completely independent of the small-scale momentum equation. More precisely, it is focused on the small-scale pressure Poisson equation (58) and tried to find a solution. This should be helpful in fulfilling the continuity condition on the small-scale level. The fulfillment of the continuity condition is generally known to become more important with increasing Reynolds number (see, e.g., Gresho and Sani [63], Tezduyar and Osawa [151], and Wall [156]). Therefore, it is supposed to be a crucial ingredient of the solution strategy, particularly for the simulation of flows at high Reynolds numbers.

The residual $\Re_{\mathrm{NS}}^{\mathrm{M}}(\bar{\mathbf{u}}^h, \bar{p}^h)$ on the right hand side of (58) is assumed to be divergence-free. Otherwise, a potential component is subsumed in a modified small-scale pressure, such that

$$\Delta p'_{\mathrm{mod}} = \Delta p' + \nabla \cdot [\Re_{\mathrm{NS}}^{\mathrm{M}}(\bar{\mathbf{u}}^h, \bar{p}^h)] \tag{61}$$

The following Poisson equation for the modified small-scale pressure is then obtained from (58):

$$\Delta p'_{\mathrm{mod}} = -[\mathbf{u} \cdot \nabla(\nabla \cdot \bar{\mathbf{u}}^h) - \nu\Delta(\nabla \cdot \bar{\mathbf{u}}^h)] = -\left[\mathbf{u} \cdot \nabla - \nu\Delta\right](\nabla \cdot \bar{\mathbf{u}}^h) \tag{62}$$

It is not advisable to solve this differential equation for the small-scale pressure on the element level besides the burden of solving the momentum equation, let alone the difficult question of useful pressure boundary conditions for (62) on the element boundaries. Here, it is rather intended to incorporate the effect of the small-scale pressure Poisson equation and, thus, the small-scale continuity equation into the final (large-scale) equation via an additional term in the form of a stabilizing term. Thus, p' is approximated as

$$p' \approx -\tau_i^C(\nabla \cdot \bar{\mathbf{u}}^h) = -\tau_i^C \Re_{\mathrm{NS}}^{\mathrm{C}}(\bar{\mathbf{u}}^h) \tag{63}$$

where τ_i^C denotes an elementwise algebraic stabilization parameter. In the large-scale equation, a bulk viscosity term as

$$\cdots + \sum_{i=1}^{n_{\mathrm{el}}} (\nabla \cdot \bar{\boldsymbol{\nu}}^h, \tau_i^C(\nabla \cdot \bar{\mathbf{u}}^h))_{\Omega_i} \ldots \tag{64}$$

is added to the left hand side. Recently, it has been shown in Franca and Oliveira [46] that the derivation of this stabilizing term can be traced back to the introduction of so-called "pressure bubbles". For τ_i^C, the definition in Codina [24] is adopted, which is given as

$$\tau_i^C = \left[\nu^2 + \left(\frac{c_2}{c_1}|\bar{\mathbf{u}}^h|h\right)^2\right]^{\frac{1}{2}} \tag{65}$$

where the two constants are subject to

$$c_1 \geq c_2^2 \tag{66}$$

The strategy may be summarized now. Residual-free bubbles are used to solve the small-scale momentum equation. Additionally, the effect of the small-scale continuity equation is taken into account via a stabilizing term in the final (large-scale) equation. Thus, it amounts to a combined residual-free bubble/stabilizing strategy. After all, the main assumption $p' = 0$ in the small-scale momentum equation means that the small-scale velocity is exclusively driven by the residual of the large-scale momentum equation and not by the residual of the continuity equation, see Codina [24]. Furthergoing discussions related to this assumption may be found in Gravemeier [56] and Gravemeier *et al.* [61], respectively. It is emphasized that the strategy described in this section results in a *completely stable* method. Hence, there is no need to include any additional stabilizing term.

In terms of the small-scale momentum equation (55) or (60), respectively, it has been dealt with an analytical problem formulation in every individual element domain Ω_i so far, expecting the small-scale solution to capture *all* remaining scales not captured by the discrete large-scale solution. Since an analytical solution of this equation is not feasible, in general, an approximative approach is used: the two-level FEM. The idea of using a two-level FEM for the practical computation of residual-free bubble functions can be traced back to Franca and Macedo [42], where this methodology was proposed for the Helmholtz equation. In the same year, the application of this approach to convection-diffusion equations was published in Franca *et al.* [45]. Afterwards, a stationary incompressible Navier-Stokes equations was addressed in Franca and Nesliturk [44] as well as Nesliturk [120]. In Gravemeier *et al.* [61], the basic idea of this method was extended, in order to use it for the

instationary incompressible Navier-Stokes equations with a semi-discretization in time. At the same time, the validity of this approach for any kind of convection-diffusion-reaction equation was shown.

On every individual element domain Ω_i of the initial discretization, with its characteristic element length denoted by $\bar{h}$, a submesh is introduced. This discretization on a second level or, more precisely, the number of n_{el} discretizations on a second level is the support for the small-scale part of the solution (i.e., the small-scale momentum equation (60) subject to the residual-free bubble assumption). Its characteristic element length is denoted by h', where $h' < \bar{h}$. Details of a particular approach which aims at solving directly for shape function components of the small-scale velocity as well as furthergoing assumptions which enable such a separation into shape function components are described in Gravemeier [56]. The resulting shape function components of the small-scale velocity are eventually substituted into the large-scale equation in the course of a static condensation procedure. The decomposition process is described in detail in Gravemeier [56]. Finally, one obtains a certain number of scalar convection-diffusion-reaction equations with identical left-hand-side structure and varying right hand sides. Due to this, a representative equation in the form of a normalized equation (i.e., an equation with the right hand side set equal to one) is used below to explain the solution process on the second level and, later, on an additional third level in Section 4.2.3. This normalized residual-free bubble equation is given as

$$\frac{1}{\delta t}\mathcal{B}_1 + \mathbf{u}\cdot\nabla\mathcal{B}_1 - \nu\Delta\mathcal{B}_1 = 1 \qquad \text{in} \quad \Omega_i \tag{67}$$

subject to the usual zero Dirichlet boundary conditions, where δt denotes the discrete time step. In (67), $\mathcal{B}_1$ is a place-holder for the respective shape function components. In order to obtain (67), starting from (60), both the convective and the viscous term have been simplified using the continuity equation (4).

Since one is normally unable to find an analytical solution to even this simplified equation (67), it is attempted to find an approximate residual-free bubble function $\mathcal{B}_1^{h'}$ in every element of the original discretization. This is done with the aid of the elementwise submeshes. The approximate residual-free bubble $\mathcal{B}_1^{h'}$ then replaces the actually sought-after exact residual-free bubble function $\mathcal{B}_1$. A variational form of (67) with the submesh weighting function $w^{h'}$ is given as

$$\left(w^{h'}, \frac{1}{\delta t}\mathcal{B}_1^{h'} + \mathbf{u}\cdot\nabla\mathcal{B}_1^{h'}\right)_{\Omega_i} + (\nabla w^{h'}, \nu\nabla\mathcal{B}_1^{h'})_{\Omega_i} = (w^{h'}, 1)_{\Omega_i} \tag{68}$$

The constituents of the two-level FEM (i.e., the discretizations on the two levels) and the solution strategy are comprisingly depicted in Figure 4. Level 1 is represented by standard FE spaces $\mathcal{S}_{up}^h$ and $\mathcal{V}_{up}^h$, which are linked with a basic discretization. This basic discretization is the support of the large-scale part of the solution and also the "source" of the discretization on level 2, since this discretization is restricted to individual elements of the basic discretization. The stabilizing term in the form of a bulk viscosity term (BVT), which is eventually added to the final (large-scale) equation besides the approximate residual-free bubble (RFB) functions, is also indicated in Figure 4.

3.1.2 Advanced boundary conditions for the residual-free bubble equations

In the preceding section, efforts have been focused on getting an approximate solution for the residual-free bubble equation (67) as close to the analytical solution as possible. This will be enhanced with the help of a dynamic subgrid viscosity approach in Section 4.2.3. However, in order to pursue this computationally attractive strategy of localization for the

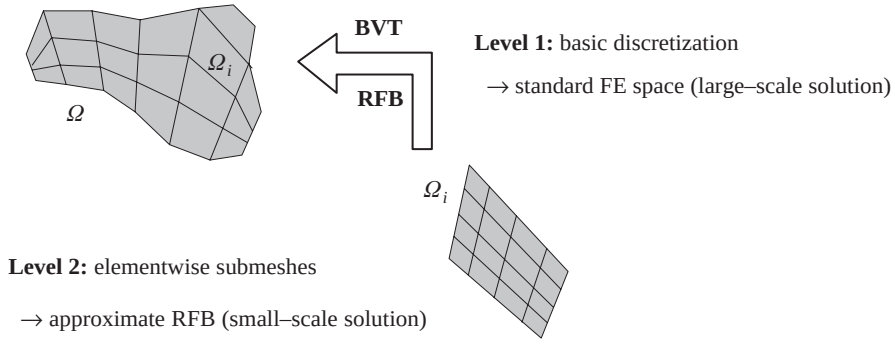

Figure 4. Two-level FEM: discretizations and strategy

small-scale solution including a subsequent static condensation, a high prize has to be paid: artificial zero Dirichlet boundary conditions for the small-scale part of the solution on Γ_i have to be accepted, which are undoubtedly incorrect in general. It is intended to think beyond this simple "zero-strategy" now. At first, one may think of the "ideal" residual-free bubble equation in each element (i.e., the one with the correct Dirichlet and/or Neumann boundary conditions on Γ_i). This would definitely be a situation of paramount attraction. The correct boundary conditions will not be accessible, however, and even a slight deviation may leave us behind with an ill-posed problem, let alone that the correct problem is not solved any more.

One idea in this context providing, at least, some improvement with respect to the zero-strategy is the use of non-conforming bubbles. Farhat *et al.* [35] (see also Farhat *et al.* [36]) introduced inter-element Lagrange multipliers and developed a discontinuous enrichment method herewith. Their enrichment contains free-space solutions of the underlying homogeneous differential equation that are not represented by the basic polynomial approximation. For the main goal of this work, the Navier-Stokes equations, the search for such free-space solutions is certainly ambitious and mostly impossible. The Lagrange multipliers represent the means for approximating the flow over the element boundaries Γ_i and, thus, what has to be considered as the correct Neumann boundary conditions for the enrichment. Consequently, approximate boundary conditions are obtained, but it has to be paid for that with additional degrees of freedom, which are related to the Lagrange multipliers and appear in the final equation system. The elementwise solution process of the residual-free bubble equation is replaced by an elementwise static condensation process. Comparing this approach to the residual-free bubble approach, it is stated that better boundary conditions, which, in fact, never appear as boundary conditions in the method, can be expected. Furthermore, the user gets rid of the elementwise solution procedures. In exchange for this, however, it has to be paid with an elementwise static condensation (with potentially expensive matrix inversions), a larger final equation system, and the necessity to provide a framework for dealing computationally with the Lagrange multipliers.

Another idea is the "occupation" of the element edges in the two-dimensional case (likewise, the element faces and edges in the three-dimensional case) with additional functions. Brezzi [8] already suggested the addition of, at least some (in fact, not too many), edge functions with special shape. This should be done in an iterative manner using information from previous solution steps. The main drawback is that, similar to the discontinuous enrichment method, all these additional functions will appear in the final equation system, since they do not go away during the static condensation process. In this context, it is further refered to Brezzi and Marini [15] providing the reader with a very general framework related to augmented spaces and two-level methods.

Due to the aforementioned drawback of a larger equation system, the attention is now turned to a different approach ensuring the final equation system to maintain the same size. Such an idea was already pursued by Hughes *et al.* [79]. As a first step in this direction, they added residual-free edge functions in the two-dimensional case as a furthergoing means to resolve the remaining residual on the element edges. It is straightforward to think of a three-dimensional counterpart including also residual-free face functions. The problem that all these edge functions are globally coupled is overcome by focusing on one respective edge, which is linked to two elements. This is certainly a severe approximation, but Hughes *et al.* [79] hoped to get some improvement with respect to the exclusive use of residual-free bubbles. However, this approach appears to be inappropriate for the ultimate goal of this work, the numerical simulation of turbulent flows, which are usually linked with very small physical viscosities, since the jump terms on the element boundaries, which have been omitted in the wake of the residual-free bubble approximation, are diffusive or viscous terms, respectively (For the Navier-Stokes equations, this is only the case for continuous pressure interpolations, see Gravemeier [56]). This means that by approaching a very small diffusion or viscosity, respectively, the influence of these terms vanishes more and more. Therefore, it makes little sense to put extra effort in taking into account these edge functions unless a diffusion-dominated problem has to be solved. For exactly this kind of problem, namely the Stokes problem, the benefit of these edge-functions (on a macro-element) was demonstrated by Franca and Russo [48]. The idea of using such macro-elements for improving the solution quality was picked up by Sangalli [140] for elliptic problems with rapidly varying coefficients.

A theoretically promising approach is the one recently proposed by Franca *et al.* [43]. They call the resulting functions "multiscale functions". These functions are based on additional residual-free functions on the element edges (or element faces and edges in three dimensions) which are determined in a different procedure compared to the above-mentioned. The main drawback lies in the necessity to solve for these additional functions separately, as shown in Gravemeier [56]. The stimulation for the formulation of the edge functions in the two-dimensional case goes back to an approach for elliptic problems in Hou and Wu [75]. The basic idea of Franca *et al.* [43] was extended to convection-diffusion-reaction equations in Franca *et al.* [47] and Gravemeier [56] as well as to the three-dimensional case in Gravemeier [56]. The respective computational algorithms can be found in Gravemeier [56]. Early results in Franca *et al.* [43] showed a superior performance of this procedure with respect to stabilized methods and approaches based on residual-free bubbles with zero Dirichlet boundary conditions for reaction-dominated diffusion-reaction problems. However, a straighforward transfer to convection-dominated convection-diffusion-reaction problems in Gravemeier [56] exhibited problems at internal element boundaries. Similar problems were also observed by Franca *et al.* [47]. In order to find a remedy, Franca *et al.* [47] proposed a combined approach, where residual-free bubbles are used in most of the domain and multiscale functions at the outflow boundary. This helped improving results for a convection-dominated convection-diffusion-reaction problem, particularly towards the boundary. However, further investigations appear to be necessary for providing suitability also in the context of the Navier-Stokes equations.

3.2 Solving a Monolithic Equation System with the Scales Separated a Priori

The large-scale equation (53) and the small-scale equation (54) are reunified as

$$\begin{aligned} & B_{\mathrm{NS}}(\mathbf{v}^h, q^h; \mathbf{u}^h, p^h) - \left(\mathbf{v}'^h, \nabla \cdot \left(2\nu_T' \varepsilon(\mathbf{u}'^h)\right)\right)_\Omega \\ & = B_{\mathrm{NS}}(\bar{\mathbf{v}}^h + \mathbf{v}'^h, \bar{q}^h + q'^h; \bar{\mathbf{u}}^h + \mathbf{u}'^h, \bar{p}^h + p'^h) - \left(\mathbf{v}'^h, \nabla \cdot \left(2\nu_T' \varepsilon(\mathbf{u}'^h)\right)\right)_\Omega \\ & = (\bar{\mathbf{v}}^h + \mathbf{v}'^h, \mathbf{f})_\Omega = (\mathbf{v}^h, \mathbf{f})_\Omega \end{aligned} \tag{69}$$

where, however, the separation of scales is still obvious due to the subgrid viscosity term, which depends only on the small resolved scales. In the following, potential strategies within various numerical methods will be described. The focus remains on the FEM and the FVM. In the context of these two numerical methods, two different scale-separating approaches are distinguished: a "p-type" scale separation and an "h-type" scale separation. The nomenclature follows the usual notation in the FEM. Since low-order shape functions are usually applied in the FV method, and this "restriction" is also obeyed in the present work, p-type scale separations are only identified within the FEM, for the time being. However, there is no reason for completely excluding p-type scale separation in the FVM, although it might appear less simple and appropriate than in the FEM. In fact, a discontinuous Galerkin FEM, which will also be addressed in the context of the p-type scale separation, already exhibits characteristics very similar to the FVM. According to Ramakrishnan and Collis [134], the discontinuous Galerkin FEM can be thought of as a hybrid of FVM and FEM with a number of potential advantages for the application in the context of the variational multiscale method. The h-type scale separation will be developed in parallel for the FEM and the FVM. Subsequent to the presentation of the scale-separating approaches in the FEM and FVM, scale separation within the finite difference method and spectral methods will be outlined. In particular, spectral methods have been used several times for the variational multiscale LES in simple geometries in the meantime. It will be pointed out that the scale separation in spectral methods is a p-type scale separation, and that the scale separation in the finite difference method represents an h-type scale separation.

3.2.1 p-type scale separation within the FEM

The upcoming section is divided into three parts. In the first two parts, multiscale concepts for continuous (in space) Galerkin FEMs will be outlined, one for a FEM with hierarchical shape functions and one for a FEM with non-hierarchical shape functions. In the third part, multiscale concepts for the discontinuous Galerkin FEM will be briefly discussed.

Continuous Galerkin FEM with a hierarchical basis

The hierarchical concept of the FEM has already been briefly addressed in Section 2.2. The essential feature is a "natural" scale separation within the set of shape functions of order k. All polynomials up to a certain $\bar{k}$ are chosen for the polynomial representation of the space of large resolved scales. These "large-scale polynomials" and further polynomials up to a necessarily higher order k are then chosen for the representation of the complete range of resolved scales. The polynomial(s) of order k' subject to

$$\bar{k} < k' \leq k, \qquad [\bar{k}, k', k] \in \mathbb{N} \tag{70}$$

are then assigned to the small resolved scales. Adjusting the three-scale separation (39)-(40) to this approach yields

$$\mathcal{V}_{up} = \bar{\mathcal{V}}_{up}^{h,\bar{k}} \otimes \mathcal{V}_{up}'^{h,k'} \otimes \hat{\mathcal{V}}_{up} \tag{71}$$

$$\mathcal{S}_{up} = \bar{\mathcal{S}}_{up}^{h,\bar{k}} \otimes \mathcal{S}_{up}'^{h,k'} \otimes \hat{\mathcal{S}}_{up} \tag{72}$$

Accordingly, large- and small-scale shape functions may be distinguished, so as to get the large-scale approximations of the velocity weighting and solution functions as

$$\bar{\mathbf{v}}^h = \sum_{\bar{A}=1}^{\bar{n}_{\text{dofs}}} \bar{N}_{\bar{A}} \bar{\mathbf{v}}_{\bar{A}}^h, \qquad \bar{\mathbf{u}}^h = \sum_{\bar{B}=1}^{\bar{n}_{\text{dofs}}} \bar{N}_{\bar{B}} \bar{\mathbf{u}}_{\bar{B}}^h \tag{73}$$

and the small-scale approximations of the velocity weighting and solution functions as

$$\mathbf{v}'^h = \sum_{A'=1}^{n'_{\text{dofs}}} N'_{A'} \mathbf{v}'^h_{A'}, \qquad \mathbf{u}'^h = \sum_{B'=1}^{n'_{\text{dofs}}} N'_{B'} \mathbf{u}'^h_{B'} \tag{74}$$

with the respective number of degrees of freedom $\bar{n}_{\text{dofs}}$ and n'_{dofs} for the two approximation spaces. A separation of the pressure weighting and solution function is unnecessary, since the scale separation in (69) only applies to the velocity degrees of freedom. Note that both the large- and the small-scale approximations are subject to the same discretization with the characteristic element length h. The only distinction lies in the different assignement of shape functions of certain polynomial orders to either the large- or the small-scale approximation. An alternative hierarchical basis particularly suited for the variational multiscale method was addressed in Gravemeier [56].

For continuous Galerkin FE methods, the hierarchical concept without recourse to the variational multiscale method was successfully applied in the framework of a stabilized method to incompressible and compressible laminar flows and for a DNS of a turbulent channel flow by Whiting and co-workers in Whiting [158], Whiting and Jansen [159], and Whiting *et al.* [160]. Jansen and Tejada-Martinez then showed the suitability of the hierarchical approach for the variational multiscale LES in Jansen and Tejada-Martinez [92]. The hierarchical basis for all these applications was provided by the mesh-entity based construction of shape functions proposed by Shephard *et al.* [143]. An important remark concerns the fact that the stability of the hierarchical-based Galerkin FEM is not guaranteed without additional provisions. The separation of the scales is the only goal of this strategy. Thus, there is no "help" in stabilizing the two problems encountered in a Galerkin FEM (i.e., the problem of a dominating convective term and the required fulfillment of the inf-sup condition), as it has been the case for the two-level FEM in Section 3.2.1. Therefore, stabilizing terms must be added, in general, to the variational equation (69).

Continuous Galerkin FEM with an explicit L_2-projection

A p-type scale separation outside of the hierarchical concept was proposed by John and Kaya [95] (see also John *et al.* [96] and Kaya and Layton [100] for related work on convection-diffusion equations). Those authors developed an explicit L_2-projection procedure. They basically start with the reunified equation (69) as a FE equation. However, the subgrid viscosity term is applied to all scales, and another subgrid viscosity term related to the large scales is subtracted. As a result, the problem formulation reads: find $\{\mathbf{u}^h, p^h\} \in \mathcal{S}^h_{up}$ and $\bar{\gamma}^h \in \bar{\mathcal{L}}^h$, such that

$$\begin{aligned} &B^{FE}_{\text{NS}}(\mathbf{v}^h, q^h; \mathbf{u}^h, p^h) + (\varepsilon(\mathbf{v}^h), 2\nu'_T \varepsilon(\mathbf{u}^h))_\Omega - (\varepsilon(\mathbf{v}^h), 2\nu'_T \bar{\gamma}^h)_\Omega \\ &= (\mathbf{v}^h, \mathbf{f})_\Omega + (\mathbf{v}^h, \mathbf{h})_{\Gamma_h} \qquad \forall \{\mathbf{v}^h, q^h\} \in \mathcal{V}^h_{up} \end{aligned} \tag{75}$$

$$\left(\bar{\lambda}^h, \bar{\gamma}^h - \varepsilon(\mathbf{u}^h)\right)_\Omega = 0 \qquad \forall \bar{\lambda}^h \in \bar{\mathcal{L}}^h \tag{76}$$

where

$$\bar{\mathcal{L}}^h \subset \mathcal{L} = \{\lambda \in (L_2(\Omega))^{d \times d} | \lambda = \lambda^{\text{T}}\} \tag{77}$$

and it is prescribed that $\nu'_T \geq 0$. Now, the following assumption is made: if the L_2-projection onto the large-scale space $\mathcal{P}_{\bar{\mathcal{L}}^h} : \mathcal{L} \rightarrow \bar{\mathcal{L}}^h$ is defined for $\varepsilon(\mathbf{v}) \rightarrow \mathcal{P}_{\bar{\mathcal{L}}^h}\lceil\varepsilon(\mathbf{v})\rceil$ with

$$(\bar{\lambda}^h, \mathcal{P}_{\bar{\mathcal{L}}^h}\lceil\varepsilon(\mathbf{v})\rceil - \varepsilon(\mathbf{v}))_\Omega = 0 \qquad \forall \bar{\lambda}^h \in \bar{\mathcal{L}}^h \tag{78}$$

then $\bar{\gamma}^h = \mathcal{P}_{\bar{\mathcal{L}}^h}[\varepsilon[\mathbf{u}^h)]$ in (75)-(76) (i.e., $\bar{\gamma}^h$ is the large-scale part of the rate-of-deformation tensor $\varepsilon(\mathbf{u}^h)$ based on the L_2-projection).

In order to show that this approach is indeed identical to the variational multiscale approach, the equation system (75)-(76) may be rewritten in one equation as

$$B_{\mathrm{NS}}^{FE}(\mathbf{v}^h, q^h; \mathbf{u}^h, p^h) + \Big(\varepsilon(\mathbf{v}^h), 2\nu_T' \varepsilon(\mathbf{u}^h)\Big)_\Omega - \Big(\varepsilon(\mathbf{v}^h), 2\nu_T' \mathcal{P}_{\bar{\mathcal{L}}^h}\big[\varepsilon(\mathbf{u}^h)\big]\Big)_\Omega = (\mathbf{v}^h, \mathbf{f})_\Omega + (\mathbf{v}^h, \mathbf{h})_{\Gamma_h} \tag{79}$$

Using

$$\Big(\varepsilon(\mathbf{v}^h), 2\nu_T' \varepsilon(\mathbf{u}^h)\Big)_\Omega - \Big(\varepsilon(\mathbf{v}^h), 2\nu_T' \mathcal{P}_{\bar{\mathcal{L}}^h}\big[\varepsilon(\mathbf{u}^h)\big]\Big)_\Omega = \Big(\big(I - \mathcal{P}_{\bar{\mathcal{L}}^h}\big)\big[\varepsilon(\mathbf{v}^h)\big], 2\nu_T' \big(I - \mathcal{P}_{\bar{\mathcal{L}}^h}\big)\big[\varepsilon(\mathbf{u}^h)\big]\Big)_\Omega \tag{80}$$

equation (79) may be changed to

$$B_{\mathrm{NS}}^{FE}(\mathbf{v}^h, q^h; \mathbf{u}^h, p^h) + \Big(\varepsilon(\mathbf{v}^h) - \mathcal{P}_{\bar{\mathcal{L}}^h}[\varepsilon(\mathbf{v}^h)], 2\nu_T' \big(\varepsilon(\mathbf{u}^h) - \mathcal{P}_{\bar{\mathcal{L}}^h}[\varepsilon(\mathbf{u}^h)]\big)\Big)_\Omega = (\mathbf{v}^h, \mathbf{f})_\Omega + (\mathbf{v}^h, \mathbf{h})_{\Gamma_h} \tag{81}$$

John and Kaya [95] proved that the definition of the large scales by an L_2-projection commutes with differentiation subject to

$$\mathcal{P}_{\bar{\mathcal{L}}^h}\lceil\varepsilon(\mathbf{v})\rceil = \varepsilon(\mathcal{P}_{\bar{\mathcal{L}}^h}\lceil\mathbf{v}\rceil) \qquad \forall \mathbf{v} \in \mathcal{V}_u \tag{82}$$

if $\bar{\mathcal{L}}^h = \varepsilon(\bar{\mathcal{V}}_u^h)$. This is a property which cannot be proven, in general, for the filtering approach in the traditional LES, see appendix. Using (82) and setting $\bar{\mathbf{u}}^h := \mathcal{P}_{\bar{\mathcal{L}}^h}[\mathbf{u}^h]$ as well as $\bar{\mathbf{v}}^h := \mathcal{P}_{\bar{\mathcal{L}}^h}[\mathbf{v}^h]$, equation (81) may be simplified to

$$B_{\mathrm{NS}}^{FE}(\mathbf{v}^h, q^h; \mathbf{u}^h, p^h) + (\varepsilon(\mathbf{v}^h - \bar{\mathbf{v}}^h), 2\nu_T' \varepsilon(\mathbf{u}^h - \bar{\mathbf{u}}^h))_\Omega = B_{\mathrm{NS}}^{FE}(\mathbf{v}^h, q^h; \mathbf{u}^h, p^h) + (\varepsilon(\mathbf{v}'^h), 2\nu_T' \varepsilon(\mathbf{u}'^h))_\Omega = (\mathbf{v}^h, \mathbf{f})_\Omega + (\mathbf{v}^h, \mathbf{h})_{\Gamma_h} \tag{83}$$

The space $\bar{\mathcal{L}}^h$ represents the large scales in this approach. There are two options to define $\bar{\mathcal{L}}^h$: either it may be defined on a coarser grid, which would amount to an h-type scale separation, or it may be defined by the respective polynomial orders (i.e., a p-type scale separation). In their numerical simulations, John and Kaya [95] chose the second option (i.e., the reason why this approach is mentioned in the context of the p-type scale separation), using hexahedral elements with continuous triquadratic functions for the velocity approximation and discontinuous linear functions for the pressure approximation. This is an element definition known to fulfill the inf-sup condition, see Gresho and Sani [63]. Discontinuous constant and linear functions are then chosen to represent the large-scale space $\bar{\mathcal{L}}^h$, using L_2-orthogonal bases of piecewise Legendre polynomials. The addition of the subgrid viscosity to the small resolved scales acts here as a stabilization according to Guermond's [64] approach, in order to deal with the problem of a dominating convective term. Thus, the approach of John and Kaya [95] can be proven to be *completely stable*.

Discontinuous Galerkin FEM

It is definitely impossible to present the complete concept of the discontinuous Galerkin FEM in a short section. Thus, it is focused on the basic idea, some references providing

the details as well as two advantages and a crucial drawback of the method for the underlying problems. The basic idea of the discontinuous Galerkin FEM consists of a more "autonomous" treatment of each element of the discretization. More precisely, a polynomial approximation within each element is enforced, but these approximations are allowed to be discontinuous between adjoining elements. The resulting gap between the values on either side of an element boundary is "closed" by weakly enforcing continuity in the discontinuous Galerkin formulation.

Concerning the details of discontinuous Galerkin methods, it is refered to the respective literature. In particular, the compilation by Cockburn *et al.* [21], which contains, among other things, a description of the history and the state of the art of these methods, is a valuable source. Aside from this, it is refered to Baumann and Oden [4] for work related to the Euler and Navier-Stokes equations and Engel *et al.* [32] for an exhaustive comparison of continuous and discontinuous Galerkin methods, combined with stabilized methods. Among other things, Engel *et al.* [32] refer to convection-diffusion problems. First steps towards an application of discontinuous Galerkin methods for the numerical simulation of compressible turbulent flows using the variational multiscale method have recently been presented in Collis [26], [27], Ramakrishnan [132], and Ramakrishnan and Collis [134].

Two advantages may be ascribed to the discontinuous Galerkin method in the context of fluid mechanics. On the one hand, potential velocity oscillations may be precluded by avoiding to strongly prescribe Dirichlet boundary conditions at outflow boundaries. Nevertheless, instabilities can occur for certain problems. In these cases, the introduction of stabilizing techniques to overcome these problems is required, see Engel *et al.* [32]. On the other hand, the discontinuous Galerkin method provides a formulation which is locally conservative within each element, similar to the local conservation property of the FVM with respect to each control volume. Local conservation is mentioned in Hughes *et al.* [83] to be an attribute for several methods used for LES. However, the continuous Galerkin method may also be altered to be an elementwise conserving scheme. This can be done by adding a postprocessing procedure proposed in Hughes [77], p. 107, and Hughes *et al.* [78]. The conservation properties of stabilized continuous Galerkin formulations have also recently been investigated in Hughes and Wells [87].

A crucial drawback of the discontinuous Galerkin method is the substantial increase of the number of degrees of freedom, at least for lower-order interpolated elements. Each element "meeting" at a certain node of the discretization "brings in" its particular degree of freedom in the discontinuous Galerkin method. An analysis of the number of degrees of freedom was performed in Engel *et al.* [32] for one-, two- , and three-dimensional elements. The ratio relating the number of degrees of freedom for the discontinuous Galerkin method (DGM) to the one for the continuous Galerkin method (CGM) is, e.g., for two-dimensional quadrangles given as

$$\frac{n_{\text{dofs}}(\text{DGM})}{n_{\text{dofs}}(\text{CGM})} = \left(\frac{k+1}{k}\right)^2 \tag{84}$$

The ratio in (84) moves towards 1 for increasing polynomial order k. For low and moderately high polynomial orders (i.e., for linear, quadratic, cubic, and quartic interpolations), evaluating (84) results in ratios of 4, 2.25, 1.78, and 1.56, respectively. Thus, discontinuous Galerkin method become competitive in terms of computational *efficiency* not until polynomials of considerably high order are applied.

3.2.2 h-type scale separation within the FEM and FVM

The h-type scale separation relies on a level of complete resolution indicated by the characteristic discretization length h. In terms of the velocity, this reads

$$\mathbf{u}^h = (\bar{\mathbf{u}} + \mathbf{u}')^h \tag{85}$$

With respect to this complete resolution level, a large-scale resolution level is identified *a priori*. This level is characterized by the length $\bar{h}$, where $\bar{h} > h$, and, accordingly, yields a large-scale velocity $\bar{\mathbf{u}}^h$. The small-scale velocity is obtained on the complete resolution level, characterized by the length h, as

$$\mathbf{u}'^h = \mathbf{u}^h - \bar{\mathbf{u}}^h \tag{86}$$

where $\bar{\mathbf{u}}^h$ is the large-scale value transfered to this level. Adjusting the three-scale separation (39)-(40) to this approach yields

$$\mathcal{V}_{up} = \bar{\mathcal{V}}_{up}^{\bar{h}} \otimes \mathcal{V}_{up}'^h \otimes \hat{\mathcal{V}}_{up} \tag{87}$$

$$\mathcal{S}_{up} = \bar{\mathcal{S}}_{up}^{\bar{h}} \otimes \mathcal{S}_{up}'^h \otimes \hat{\mathcal{S}}_{up} \tag{88}$$

In Koobus and Farhat [103] (see also Farhat *et al.* [37]), a mixed FEM/FVM was developed for the compressible Navier-Stokes equations, where all the terms also appearing in the incompressible Navier-Stokes equations are weighted by FV weighting functions, except for the viscous term, which is weighted by FE weighting functions. In Gravemeier [57]-[59], a complete FVM was applied to the incompressible Navier-Stokes equations (i.e., all terms are weighted by FV weighting functions). Nevertheless, all techniques to be presented below may also be applied to a complete FEM. For both the FEM and the FVM, only linear interpolations will be used in the following. As in the case of the hierarchical p-type scale separation, it is remarked that the separation of the scales is the only goal of this strategy. Thus, there is basically no "help" in stabilizing the formulation, and it has to be accounted for this separately.

Grid generation

Two alternative techniques for the generation of the necessary grids may be distinguished in principle: one generating the grid for the large-scale resolution level from the grid for the complete resolution level and one proceeding in the opposite direction (i.e., from the grid for the large-scale resolution level to the grid for the complete resolution level).

Koobus and Farhat [103] initially discretize the flow domain by a grid with tetrahedral elements, from which a dual grid defined by control volumes is derived. This represents the grid for the complete resolution level. By a volume-agglomeration procedure according to Lallemand *et al.* [105], macro-volumes are created. The characteristic large-scale length $\bar{h}$ and, hence, the ratio of $\bar{h}$ and h may be varied by varying the extension of the macro-volumes, which depends on the number of subsets of neighbors included in the macro-volumes, see Farhat *et al.* [37].

Gravemeier [57]-[59] also creates two grids, a coarser grid, which is called the "parent" grid, and a finer grid, which is called the "child" grid, but by proceeding in the opposite direction. Starting from the parent grid, the child grid is obtained by an isotropic hierarchical subdivision of the parent grid according to the procedure described by Mavriplis [114]. The notation "parent" and "child" mirrors a usual notation in multigrid methods. However, in contrast to a usual parent-child relationship in multigrid solvers, where the parent needs to know only the number of its children, a complete parent-child knowledge base is set up. As a result, every parent knows about every child and vice versa. More details concerning the implementation can be found in Gravemeier [58].

The implementation in Gravemeier [58] aims at hybrid unstructured grids. Hybrid unstructured grids can contain tetrahedra, hexahedra, prisms, and pyramids. However, only two different types of faces, namely triangles and quadrangles, occur for these four different types of control volumes. Based on the fact that a factor of two is most often used

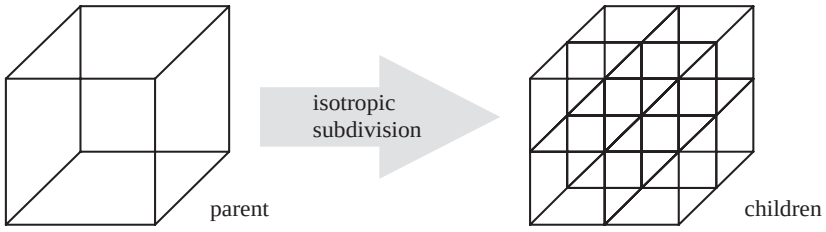

Figure 5. Parent hexahedron with eight child hexahedra

in a dynamic modeling procedure for the relation of the cutoff length scale for the large resolved scales to the one for all resolved scales, an initial subdivision procedure using this factor is chosen. Both a parent triangular face and a parent quadrangular face subdivided isotropically result in four child faces of the same type. For three-dimensional control volumes, isotropic subdivision of either a parent tetrahedron or hexahedron, for example, results in eight children. A parent hexahedron along with its eight child hexahedra is depicted in Figure 5. Illustrations of subdivided tetrahedra, prisms, and pyramids can be found in Mavriplis [114]. Obviously, this kind of refinement is not restricted to a subdivision by a factor of two. Other integer factors (e.g., three or four) may be applied and result in considerably lower ratios of the spaces containing the large resolved scales to the spaces containg the small resolved scales. As a result, the characteristic complete-scale length h is varied for the purpose of varying the ratio of $\bar{h}$ and h, contrary to the other grid generation technique. In the following, the notation parent grid and child grid will be used, irrespective of how the two grids have been generated.

Multigrid scale separation

Several references concerning multigrid methods in general may be found in literature. An introductory work with particular emphasis on applications in computational fluid dynamics is, for instance, Wesseling [157]. In particular, Chapter 5 of Wesseling [157] deals with the topics of restriction and prolongation. Some sections in Ferziger and Peric [34] are also devoted to multigrid methods in the context of computational fluid dynamics.

The general class of scale-separating operators based on multigrid operators was defined in Gravemeier [58] as

$$\bar{\mathbf{u}}^h = S^{\mathrm{m}}[\mathbf{u}^h] = P \circ R[\mathbf{u}^h] = P[\bar{\mathbf{u}}^{\bar{h}}] \tag{89}$$

where the multigrid scale-separating operator S^{m} consists of the sequential application of a restriction operator R and a prolongation operator P. Applying the restriction operator on $\mathbf{u}^h$ yields a large-scale velocity $\bar{\mathbf{u}}^{\bar{h}}$ defined at the degrees of freedom of the parent grid, which is then prolongated to obtain a large-scale velocity $\bar{\mathbf{u}}^h$ defined at the degrees of freedom of the child grid. Various restriction as well as prolongation operators may be used in (89).

Two special combinations of restriction and prolongation operators were investigated in Gravemeier [58]. Both of them rely on the same restriction operator, but apply different prolongation operators afterwards. The restriction operator is defined to be a volume-weighted average over all the child control volumes within one parent control volume subject to

$$\bar{\mathbf{u}}_j^{\bar{h}} = \frac{\sum\limits_{i=1}^{n_{\mathrm{cop}}} |\Omega_i| \mathbf{u}_i^h}{\sum\limits_{i=1}^{n_{\mathrm{cop}}} |\Omega_i|} \tag{90}$$

where $\bar{\mathbf{u}}_j^{\bar{h}}$ denotes the large-scale velocity at the center of the parent control volume $\bar{\Omega}_j$ and n_{cop} the number of child control volumes in $\bar{\Omega}_j$. The first prolongation operator P^{p} yields a constant prolongation, which is given as

$$\bar{\mathbf{u}}_i^h = P^{\text{p}}[\bar{\mathbf{u}}_j^{\bar{h}}]_i = \bar{\mathbf{u}}_j^{\bar{h}} \qquad \forall \Omega_i \subset \bar{\Omega}_j \tag{91}$$

and zero elsewhere. It was shown in Gravemeier [58] that the scale-separating operator defined as

$$S^{\text{pm}} := P^{\text{p}} \circ R \tag{92}$$

has the property of a projector, which is indicated by the additional superscript "p". The projector (92) is exactly the operator also used in Farhat *et al.* [37] and Koobus and Farhat [103], although it was not derived from the general formulation (89) and, thus, not split up into a restriction and prolongation operator there. The present operator was also addressed in Vreman [154].

The second prolongation operator considered in Gravemeier [58] yields a linear prolongation subject to

$$\bar{\mathbf{u}}_i^h = P^{\text{s}}[\bar{\mathbf{u}}_j^{\bar{h}}]_i = \bar{\mathbf{u}}_j^{\bar{h}} + (\nabla^{\bar{h}} \bar{\mathbf{u}}_j^{\bar{h}})(\mathbf{r}_i - \bar{\mathbf{r}}_j) \qquad \forall \Omega_i \subset \bar{\Omega}_j \tag{93}$$

and zero elsewhere. The vectors $\mathbf{r}_i$ and $\bar{\mathbf{r}}_j$ denote geometrical vectors pointing to the centers of the child control volume Ω_i and the parent control volume $\bar{\Omega}_j$, respectively. $\nabla^{\bar{h}}$ describes the discrete gradient operator on the parent grid. Due to this, values from neighbouring parent control volumes and, consequently, child control volumes contained in these neighbouring parent control volumes influence the final large-scale value in the child control volume Ω_i. The prolongation P^{s} does not provide us with a projective scale-separating operation, as shown in Gravemeier [58]. It rather produces a smoothing prolongation, which is, at least, smoother than the prolongation produced by P^{p}. Thus, it is indicated by the additional superscript "s", and the complete scale-separating operator is defined as

$$S^{\text{sm}} := P^{\text{s}} \circ R \tag{94}$$

Nevertheless, S^{sm} still exhibits a fundamentally different character than discrete smooth filters, which have been widely used in the traditional LES.

The definitions for the restriction and prolongation operators go well on a pure FV grid as in Gravemeier [57]–[59] or on a dual grid as in Farhat *et al.* [37] and Koobus and Farhat [103]. Alternative operators must be defined for a nodal-based FEM. For example, a projector similar to S^{pm} can be created without the generation of a dual grid. For this purpose, the restriction operator is constituted by an injector, which simply injects the values from those nodes of the child elements which are geometrically identical to a respective node of the parent element. For example, this results in 8 injected values at the parent nodes in Figure 5. An appropriate prolongation operator then defines the values at all child nodes. These are the nodes of the child elements which are not geometrically identical to a parent node. This may, for instance, be a simple linear interpolation similar to (93). In Figure 6, the situation is depicted for a simple two-dimensional parent quadrangle with its child quadrangles. The property of a projector is ensured by the injective *restriction* operator in a nodal-based FEM. This may be contrasted to S^{pm} in (92), where the *prolongation* operator P^{p} provides an injective operation and ensures the projective property as a result.

Alternative definitions for the restriction as well as the prolongation operator are certainly conceivable in both cases. For example, differential operators with additional volume weighting on non-uniform grids were proposed in Terracol *et al.* [150] to define the restriction and prolongation operators for their FV multilevel algorithm. However, their specific

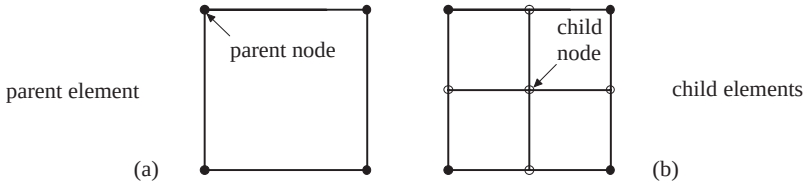

Figure 6. Nodes in two-grid nodal-based FEM (2-D case): (a) parent element; (b) child elements

choice for the parameters of the differential operators extended the scope of the operators beyond the nearest neighbour of a coarse grid control volume. This is due to the fact that their restriction operator takes into account fine grid control volumes located in neighbouring coarse grid control volumes, in addition to the fact that their prolongation operator, similar to P^{s}, is influenced by neighbouring coarse grid control volumes. At boundaries, in particular, such an extended range of influence, which includes child control volumes within the next to nearest neighbour parent control volume, might lead to substantial problems, as shown in Gravemeier [58]. However, the overall strategy in Terracol *et al.* [150] proceeded further in that actual solution steps on the parent grid and further, even coarser grids were performed in the basic sense of a multigrid solver. This may substantially raise the computational *efficiency* of the method with respect to the solver. However, in Farhat *et al.* [37], Gravemeier [57]-[59], and Koobus and Farhat [103], the focus was on the influence of the multigrid scale separation on the quality of the results (i.e., *accuracy* was the main goal of those studies).

Large- and small-scale boundaries in the FVM

Nevertheless, it was shown in Gravemeier [58] that substantial gain in computational *efficiency* may be achieved for the projective scale-separating operator S^{pm} in the context of a FV method due to another reason. In the FVM, the large-scale weighting function may be defined as

$$\bar{\mathbf{v}}^{\bar{h}} = \sum_j \bar{\mathbf{v}}_j^{\bar{h}} \tag{95}$$

where

$$\bar{\mathbf{v}}_j^{\bar{h}} = \mathbf{1} \qquad \text{in} \quad \bar{\Omega}_j \tag{96}$$

and zero elsewhere. As above, $\bar{\Omega}_j$ denotes the j-th control volume of the parent grid with the characteristic control volume length $\bar{h}$. The reunified equation (69) is now expressed on the basis of a FV formulation with the aid of (95). This yields the following problem statement for each $\mathbf{v}_i^h$, q_i^h, and $\bar{\mathbf{v}}_i^{\bar{h}}$, where the child grid control volume Ω_i is contained in the parent grid control volume $\bar{\Omega}_i$: find $\{\mathbf{u}^h, p^h\} \in \mathcal{S}_{up}^h$ such that

$$\begin{aligned}
&B_{\mathrm{NS}}^{\mathrm{FV}}(\mathbf{v}_i^h, q_i^h; \mathbf{u}^h, p^h) - (\mathbf{v}_i'^h, \nu_T'(\nabla \mathbf{u}'^h)\cdot\mathbf{n})_{\Gamma' i} \\
&\quad = B_{\mathrm{NS}}^{\mathrm{FV}}(\mathbf{v}_i^h, q_i^h; \mathbf{u}^h, p^h) - \left(\mathbf{v}_i^h, \nu_T'(\nabla(\mathbf{u}^h - \bar{\mathbf{u}}^h))\cdot\mathbf{n}\right)_{\Gamma_i} + \left(\bar{\mathbf{v}}_i^{\bar{h}}, \nu_T'(\nabla(\mathbf{u}^h - \bar{\mathbf{u}}^h))\cdot\mathbf{n}\right)_{\bar{\Gamma}_i} \\
&\quad = B_{\mathrm{NS}}^{\mathrm{FV}}(\mathbf{v}_i^h, q_i^h; \mathbf{u}^h, p^h) - \left(\mathbf{v}_i^h, \nu_T'((\nabla \mathbf{u}^h)\cdot\mathbf{n} - (\nabla \bar{\mathbf{u}}^h)\cdot\mathbf{n})\right)_{\Gamma_i} + \Big(\bar{\mathbf{v}}_i^{\bar{h}}, \nu_T'((\nabla \mathbf{u}^h)\cdot\mathbf{n} \\
&\qquad -(\nabla \bar{\mathbf{u}}^h)\cdot\mathbf{n})\Big)_{\bar{\Gamma}_i} \\
&\quad = (\mathbf{v}_i^h, \mathbf{f})_\Omega + (\mathbf{v}_i^h, \mathbf{h})_{\Gamma_h'}
\end{aligned} \tag{97}$$

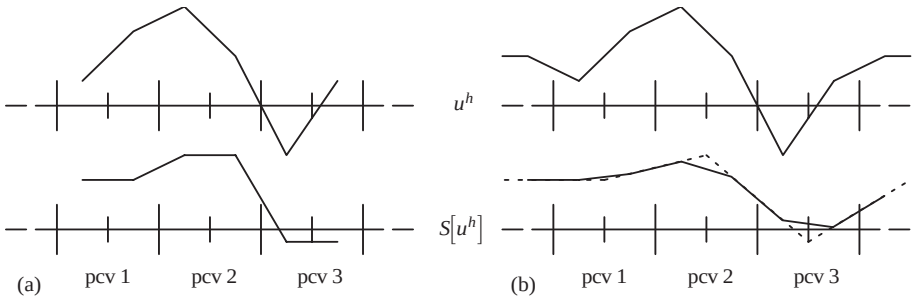

Figure 7. Applying the multigrid scale-separating operators to a 1-D graph of u^h: (a) PM; (b) SM (dashed line indicates linear interpolation of the large-scale values at the pcv centers)

where the boundary Γ_i is split up into a large-scale boundary $\bar{\Gamma}_i$ and, accordingly, a small-scale boundary subject to

$$\Gamma_i' = \Gamma_i - \bar{\Gamma}_i \tag{98}$$

and the viscous term has been written in the simpler conventional form in (97), using the continuity equation (4). A proof of the commutation between differentiation and the definition of the large scales in terms of an L_2-projection subject to (82) was provided by John and Kaya [95]. This proof was done in the context of an FE formulation for a subgrid viscosity term which was integrated by parts and then defined on the domain Ω_i rather than the boundary Γ_i. However, a similar proof may be done for the present FV case, ensuring the equality of the second and the third line in (97), analogous to the equality of (83) and (81).

A crucial difference between S^{pm} and S^{sm} was stated in Gravemeier [58]: there is no large-scale (subgrid) viscous flux for S^{pm} across the small-scale boundary subject to (98). This may already be pointed out for the 1-D case by surveying Figure 7(a) and (b), where the curve of a function and its large-scale part after applying the scale-separating operator are shown along three parent control volumes of a uniform discretization. It is obvious that S^{pm} yields the same value in both child control volumes of any parent control volume, see Figure 7(a). Thus, there is no derivative (or gradient in the two- and three-dimensional case) of the large-scale function at inner (small-scale) boundaries within each parent control volume, and the large-scale part of the subgrid viscosity term at these boundaries is ensured to be zero. As a result, (97) may be specified for S^{pm} as

$$B_{\mathrm{NS}}^{\mathrm{FV}}(\mathbf{v}_i^h, q_i^h; \mathbf{u}^h, p^h) - (\mathbf{v}_i'^h, \nu_T'(\nabla \mathbf{u}^h) \cdot \mathbf{n})_{\Gamma_i'} = (\mathbf{v}_i^h, \mathbf{f})_\Omega + (\mathbf{v}_i^h, \mathbf{h})_{\Gamma_h} \tag{99}$$

Figure 7(b) illustrates the configuration for S^{sm}. The dashed line in Figure 7(b) indicates the linear interpolation of the large-scale values at the centers of the parent control volumes, obtained as a result of the restriction (90). Here, a non-zero large-scale part of the subgrid viscosity term has to be expected, in general, even at the inner (small-scale) boundaries. Thus, equation (99) is not valid in this case.

In Figure 8, the definition of large- and small-scale boundaries in the FVM is illustrated for the two-dimensional case. The large-scale weighting function $\bar{\mathbf{v}}^{\bar{h}}$ is exclusively defined on the large-scale boundaries belonging to the parent control volume as shown in Figure 8(a). The small-scale weighting function $\bar{\mathbf{v}}^{\bar{h}}$ has non-zero values only on the inner boundaries of the child control volumes, see Figure 8(b). It was proven in Gravemeier [58] that the validity of (99) for S^{pm} in the FVM provides substantial computational savings. All calls of the scale-separating computational subroutine during the actual solution procedure, for

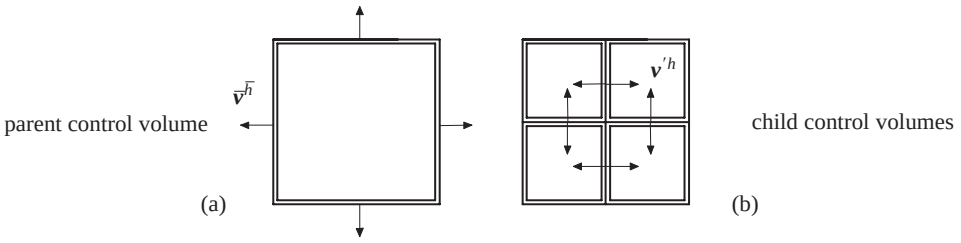

Figure 8. Geometrical locations of weighting functions in the FVM (2-D case): (a) large-scale; (b) small- scale

example, at the beginning of each solver iteration step for determining the updated large-scale velocity field for the residual calculation, are not required for S^{pm} . This is in contrast to S^{sm} and other scale-separating operators investigated in Gravemeier [58].

3.2.3 Scale separation within spectral methods and the finite difference method

The scale separation in spectral methods represents a p-type separation similar to the one in the hierarchical FEM. Fourier modes up to a certain wave number $\bar{k}$ represent the large resolved scales, and further Fourier modes up to another higher wave number k represent the complete range of resolved scales. The intermediate Fourier modes subject to (70) are associated with the small-scale space. This simple scale separation in the spectral space has already been well-known in the traditional LES as the sharp or spectral cutoff filter, which can be proven to have the property of a projector in the spectral space. Jansen and Tejada-Martinez [92] pointed out that the spectral method applications benefit from two attributes that will never be available to the hierarchical FEM:

- the ability to cut the scale spectrum at any wavenumber by choosing the wavenumber which separates large and small resolved scales, and
- a perfect separation of scales.

In fact, for the L_2-orthogonal basis functions in the spectral case, the equation system consisting of the large- and small-scale equation would amount to an *uncoupled* equation system for a *linear* problem. Merely the non-linear term within the Navier-Stokes equations "couples" the system in the spectral case, see Collis [25] for elaboration. This underlines the specific role spectral methods play in comparison to the other numerical methods.

The application of the spectral VMM to the decay of homogeneous isotropic turbulence can be found in Hughes *et al.* [84]. Turbulent channel flow was investigated in Holmen *et al.* [74], Hughes *et al.* [85], and Oberai and Hughes [123], applying modified Legendre polynomials in the inhomogeneous wall-normal direction. The separation of scales is performed by applying a sharp cutoff filter in the homogeneous flow directions and a p-type scale seperation to the Legendre polynomials. In contrast to this, Ramakrishnan and Collis [133] apply a FV method in the non-homogeneous flow direction for the same flow example and restrict the separation of scales to the remaining two homogeneous flow directions. This approach is called "planar variational multiscale" (PVMS) method by the authors. As a result, the scale separation is a pure application of the sharp cutoff filter for this specific case.

With a similar approach in the homogeneous planes and fourth-order spectral-like compact finite differences in the inhomogeneous direction, Jeanmart and Winckelmans [93] simulated the channel flow problem. In their regularized version of the variational multiscale LES, those authors used a discrete box (or top-hat) filter for the extraction of the small resolved scales which the subgrid-scale model is applied to. Discrete smooth filters,

such as the discrete box filter, do not provide a projective scale separation. Thus, this regularized version only fulfills the second of the two prerequisites for the variational multiscale LES mentioned in the introduction, the restriction of the application of the subgrid-scale model to the small resolved scales. Interestingly, however, a combination of the sharp cut-off filter in the homogeneous planes and projective sampling or "sampling + interpolation" procedures, respectively, in the inhomogeneous wall-normal direction were employed for the dynamic modeling procedure in Jeanmart and Winckelmans [93].

Adopting the notation parent grid and child grid from the previous section, the sampling procedure may be described as follows: one value every two is retained (i.e., from a sequence of field values $[f_1, f_2, f_3, \dots]$ on the child grid, the sequence $[f_1, f_3, \dots]$ is retained on the parent grid), which is a projective procedure. This first step represents a simple restriction operation. In order to obtain projected values everywhere on the child grid, Jeanmart and Winckelmans [93] linearly interpolate the sequence from the parent grid (i.e., $[f_1, (f_1 + f_3)/2, f_3, \dots]$). This second step represents a linear prolongation. Thus, the "sampling + interpolation" procedure in the finite difference method mirrors the h-type scale separation in a nodal-based FEM. It is emphasized that the just described h-type scale separation was only used for the dynamic modeling procedure in Jeanmart and Winckelmans [93], and not for the extraction of the small resolved scales to which the subgrid-scale model is ultimately applied. Another recent study merely fulfilling the second prerequisite for the variational multiscale LES was the one by Vreman [153], which also applied a discrete smooth filter for scale separation in a second-order energy-conserving finite difference method.

3.3 Summary of Approaches for Scale Separation

In Table 1, a grapical overview of the scale-separating strategies for a three-scale separation within the variational multiscale method (i.e., strategies for separating large and small resolved scales), which have been applied so far and presented in Section 3, is shown. The approaches are distinguished by the respective numerical method (including finite difference methods (FDM) and spectral methods (SM)) and the solution strategy. The inclusion of the still unresolved scales of the problem via a subgrid-scale model will be described in the subsequent section. The choice of the subgrid-scale model is, in principle, independent of the practical scale-separating procedure. Thus, the modeling approaches to be presented below are suitable for use in combination with any of the procedures in Table 1.

4 SUBGRID-SCALE MODELING WITHIN THE MULTISCALE ENVIRONMENT

The subgrid-scale modeling approaches in this section will all be based on the *subgrid (or eddy) viscosity concept* (see appendix). More precisely, they will all be based on the Smagorinsky [144] model. The Smagorinsky [144] model was the first subgrid-scale model historically and is still a commonly used one due to its attractive simplicity. A number of shortcomings of the simple Smagorinsky model based on a constant coefficient have been detected in the meantime. Germano *et al.* [53] proposed to unfix the constant and allow it to change in space and time by way of a dynamic algorithm. The procedure is basically not restricted to using the Smagorinsky model as the underlying model, although it has usually been applied with this model. The dynamic modeling procedure of Germano *et al.* [53] relies on the Germano identity in its original form. It will be presented in a consistent form here (i.e., the same multigrid scale-separating operators used in Section 3.2.2 for identifying the scales to which the subgrid-scale model is applied will be used for the necessary scale separation in the dynamic modeling procedure), as proposed in Gravemeier [57]. A modification of this identity for the underlying case of a variationally formulated problem was first proposed by Oberai and Wanderer [124]. In the final part

<table>
<tr><td></td><td>Explicit approach (sec. 3.1)</td><td colspan="2">Monolithic approach (sec. 3.2)</td></tr>
<tr><td></td><td></td><td>p-type scale separation</td><td>h-type scale separation</td></tr>
<tr><td>FEM</td><td>Two-level FEM (RFB on small-scale level)</td><td>Hierarchical FEM (continuous/disc.)
L_2-projection</td><td rowspan="2">Multigrid scale separation (project. and non-project. scale separation possible)</td></tr>
<tr><td>FVM</td><td></td><td></td></tr>
<tr><td>FDM</td><td></td><td></td><td>Discrete smooth filters (non-projective)
Sampling + interpolation (applied in dynamic model)</td></tr>
<tr><td>SM</td><td></td><td>Spectral or sharp cutoff filter
Discrete smooth filters (non-projective)</td><td></td></tr>
</table>

Table 1. Overview of approaches for separating large and small resolved scales

of this section, another dynamic modeling procedure, which aims at the extension of the two-level FEM (see Section 3.1.1) to a three-level FEM, will be addressed and compared to the previously introduced dynamic approaches.

4.1 Smagorinsky Model

Adopting the usual filter-based notation with filter width Δ to the present situation, where the resolved part of the velocity is defined by the discretization with characteristic length scale h, the subgrid viscosity can be expressed as

$$\nu_T = (C_{\mathrm{S}} h)^2 |\varepsilon(\mathbf{u}^h)| \tag{100}$$

where C_{S} denotes the Smagorinsky model constant. The actual evaluation of (100) is performed in every element or control volume Ω_i with the respective characteristic length h_i, so that a value $\nu_{T,i}$ in every element or control volume is obtained. The weak point of the Smagorinsky model is represented by the *a priori* unknown constant C_{S} in (100). As a result of investigations for homogeneous isotropic turbulence, where turbulent kinetic energy production and dissipation were balanced, a value of $C_{\mathrm{S}} = 0.18$ (see, e.g., Lilly [109]) was proposed, which has proven to be too large for most flows yet. Hence, a lower value has usually been employed. Since it does not vanish at walls, the value is often reduced artificially in the vicinity of walls by so-called "van Driest damping". Furthermore, the constant-coefficient Smagorinsky model is not a reasonable approach for the simulation of transitional flows, since it does not vanish in laminar regimes. Another problem with this model is the complete exclusion of any backscatter mechanism due to the strictly dissipative character of the model, which results in $\nu_T \geq 0$ everywhere in the flow domain at any point in time.

Despite all these well-known flaws of the constant-coefficient Smagorinsky model, the integration of this simple model into the framework of the variational multiscale method has led to good results for a number of test cases. The specific modification of the model restricting the dependence on the small scales as

$$\nu'_T = (C_S h)^2 |\varepsilon(\mathbf{u}'^h)| = (C_S h)^2 |\varepsilon(\mathbf{u}^h - \bar{\mathbf{u}}^h)| \tag{101}$$

which was named "small-small" model in Hughes *et al.* [83], seems to be the most natural version within the multiscale formalism. Other versions are a "large-small" model using only the large-scale part of the velocity for the calculation of the rate-of-deformation tensor ε, which was mainly introduced for achieving some gain in computational efficiency in Hughes *et al.* [83], and the original definition in (100) as an "all-small" model, which was applied, for instance, in a dynamic modeling procedure in Holmen *et al.* [74]. As in the case of the original model in (100), the actual evaluation of (101) is performed in every element or control volume Ω_i with the respective characteristic length h_i, so that a value $\nu'_{T,i}$ in every element or control volume is obtained.

4.2 Dynamic Modeling Procedures

4.2.1 Dynamic modeling procedure based on the classical Germano identity

All of the aformentioned negative features of the Smagorinsky model can be somehow traced back to the preliminary fixing of the constant C_S. Therefore, the idea of Germano *et al.* [53] was to unfix the constant and allow it to change in space and time (i.e., $C_S = C_S(\mathbf{x}, t)$) by way of a dynamic algorithm. Therefore, C_S will be refered to as a model *parameter* rather than a *constant* from now on. The original idea was slightly modified by Lilly [110] and generalized to inhomogeneous flows in Ghosal *et al.* [54] by the introduction of a dynamic localization model. For this dynamic localization model, a consistent version for LES based on a variational formulation has recently been proposed in Gravemeier [60]. Another interesting variant of the dynamic model is the combination of this model with the scale-similarity model of Bardina *et al.* [3] in Zang *et al.* [163], which results in a dynamic mixed model.

According to the scale-similarity hypothesis, the basic intention of the dynamic procedure in the traditional LES consists of exploiting the resolved scales, particularly the ones in the vicinity of the filter scale, in order to get information for the modeling. It is interesting to note that the dynamic modeling procedure already distinguishes large resolved scales, small resolved scales, and unresolved scales explicitly, in order to extract the small resolved scales close to the filter scale. This mirrors the type of scale separation in the variational three-scale formulation. Mathematically, the dynamic modeling procedure is based on the Germano identity (see, e.g., Germano [52]), which will be named the "classical Germano identity" (CGI) below, in order to distinguish it from the "variational Germano identity" (VGI), which will be presented in the next section. Both dynamic modeling procedures will be developed for the case of an h-type multigrid scale separation according to Section 3.2.2.

The CGI was formulated *pointwise* according to the traditional approach for LES (see appendix), not in variational form. Thus, it is started with a pointwise formulation of the Navier-Stokes equations for the discretized variables $\mathbf{u}^h$ and p^h. The momentum equation is then given as

$$\frac{\partial \mathbf{u}^h}{\partial t} + \nabla \cdot (\mathbf{u}^h \otimes \mathbf{u}^h) + \nabla p^h - 2\nu \nabla \cdot \varepsilon(\mathbf{u}^h) + \nabla \cdot \boldsymbol{\tau}^h = \mathbf{f}^h \tag{102}$$

where the subgrid-scale stress tensor is defined as

$$\boldsymbol{\tau}^h = (\mathbf{u} \otimes \mathbf{u})^h - \mathbf{u}^h \otimes \mathbf{u}^h \tag{103}$$

Note that in (102)-(103) the ususal filtered formulation (see appendix) is replaced by the actual implicit scale separation based on the chosen discretization with characteristic length scale h. A test filter with filter width $\bar{\Delta}$, which is larger than the basic LES filter (often twice as large), is introduced at this point in the traditional LES. The test filter is here replaced by the multigrid scale-separating operators of Section 3.2.2. Thus, the analog of the "sub-test-filter"-scale stress tensor can be expressed as

$$\bar{\boldsymbol{\tau}}^h = \overline{(\mathbf{u} \otimes \mathbf{u})^h} - \bar{\mathbf{u}}^h \otimes \bar{\mathbf{u}}^h = S^{\mathrm{m}}[(\mathbf{u} \otimes \mathbf{u})^h] - S^{\mathrm{m}}[\mathbf{u}^h] \otimes S^{\mathrm{m}}[\mathbf{u}^h] \tag{104}$$

The procedure based on the CGI yields a value for the constant at every degree of freedom of the child grid. Aside from this, the application of the scale-separating operators based on multigrid operators opens up the opportunity to determine the values only at the degrees of freedom of the parent grid as

$$\bar{\boldsymbol{\tau}}^{\bar{h}} = \overline{(\mathbf{u} \otimes \mathbf{u})^{\bar{h}}} - \bar{\mathbf{u}}^{\bar{h}} \otimes \bar{\mathbf{u}}^{\bar{h}} = R[(\mathbf{u} \otimes \mathbf{u})^h] - R[\mathbf{u}^h] \otimes R[\mathbf{u}^h] \tag{105}$$

by using the restriction operator exclusively.

The CGI related to the child grid discretization level states the following:

$$\mathbf{L}^h = \bar{\boldsymbol{\tau}}^h - \overline{\boldsymbol{\tau}^h} = \bar{\boldsymbol{\tau}}^h - S^{\mathrm{m}}[\boldsymbol{\tau}^h] \tag{106}$$

where $\mathbf{L}^h$ can be obtained as

$$\mathbf{L}^h = \overline{\mathbf{u}^h \otimes \mathbf{u}^h} - \bar{\mathbf{u}}^h \otimes \bar{\mathbf{u}}^h = S^{\mathrm{m}}[\mathbf{u}^h \otimes \mathbf{u}^h] - S^{\mathrm{m}}[\mathbf{u}^h] \otimes S^{\mathrm{m}}[\mathbf{u}^h] \tag{107}$$

by inserting (103) and (104) into (106). Alternatively, the CGI related to the parent grid discretization level reads

$$\mathbf{L}^{\bar{h}} = \bar{\boldsymbol{\tau}}^{\bar{h}} - \overline{\boldsymbol{\tau}^h} = \bar{\boldsymbol{\tau}}^{\bar{h}} - R[\boldsymbol{\tau}^h] \tag{108}$$

where $\mathbf{L}^{\bar{h}}$ can be obtained as

$$\mathbf{L}^{\bar{h}} = \overline{\mathbf{u}^h \otimes \mathbf{u}^h} - \bar{\mathbf{u}}^h \otimes \bar{\mathbf{u}}^h = R[\mathbf{u}^h \otimes \mathbf{u}^h] - R[\mathbf{u}^h] \otimes R[\mathbf{u}^h] \tag{109}$$

by inserting (103) and (105) into (108). The Smagorinsky model is now assumed as an appropriate modeling term at both discretization levels. Furthermore, it is accounted for the fact that the Smagorinsky model within the subgrid viscosity concept is basically a "trace-free" model in the context of incompressible flow (i.e., the rate-of-deformation tensor ε, which appears in the subgrid viscosity term, has a zero trace). Thus, only the deviatoric part dev $\mathbf{L}^h$ of the tensor $\mathbf{L}^h$ in (106) can be modeled as

$$\begin{aligned} \mathrm{dev}\mathbf{L}^h &= \mathbf{L}^h - \frac{1}{3}\mathrm{tr}\mathbf{L}^h\mathbf{I} = \\ &= -2(C_{\mathrm{S}}\bar{h})^2 |S^{\mathrm{m}}[\varepsilon(\mathbf{u}^h)]| S^{\mathrm{m}}[\varepsilon(\mathbf{u}^h)] + S^{\mathrm{m}}[2(C_{\mathrm{S}}h)^2 |\varepsilon(\mathbf{u}^h)| \varepsilon(\mathbf{u}^h)] \end{aligned} \tag{110}$$

where $\mathbf{I}$ denotes the identity tensor. It is now assumed that the model parameter C_{S} is at least constant over one control volume of the parent grid. Hence, (110) may be rewritten as

$$\mathrm{dev}\,\mathbf{L}^h = (C_{\mathrm{S}}h)^2 \left(2S^{\mathrm{m}}[|\varepsilon(\mathbf{u}^h)|\varepsilon(\mathbf{u}^h)] - 2\left(\frac{\bar{h}}{h}\right)^2 |S^{\mathrm{m}}[\varepsilon(\mathbf{u}^h)]| S^{\mathrm{m}}[\varepsilon(\mathbf{u}^h)] \right) = (C_{\mathrm{S}}h)^2 \mathbf{M}^h \tag{111}$$

The calculation of the parameter expression $(C_{\mathrm{S}}h)^2$ on the right hand side of (111) aims at minimizing the error tensor

$$\mathbf{E}^h = \operatorname{dev}\mathbf{L}^h - (C_{\mathrm{S}}h)^2\mathbf{M}^h \tag{112}$$

Using the least-squares approach proposed by Lilly [110], the formula for the parameter expression reads

$$(C_{\mathrm{S}}h)^2 = \frac{\operatorname{dev}\mathbf{L}^h\mathbf{M}^h}{\mathbf{M}^h\mathbf{M}^h} \tag{113}$$

Replacing the scale-separating operator S^{m} by the restriction operator R as well as the superscript "h" by the superscript "$\bar{h}$" in (110)-(113) yields the respective equations for the alternative case. The actual evaluation of (113) is performed in every *child* element or control volume Ω_i with the respective characteristic length h_i, so that a value $(C_{\mathrm{S},i}h_i)^2$ in every *child* element or control volume is eventually obtained. Following the alternative formulation of the CGI related to the parent grid discretization level, a value $(C_{\mathrm{S},i}h_i)^2$ in every *parent* element or control volume is eventually obtained. In both cases, the result may then be introduced in any of the three multiscale variants of the Smagorinsky model, such as the small-small model (101), as well as in the conventional formulation (100).

Potential numerical difficulties may have to be faced related to either unbounded or negative (and, thus, anti-dissipative) values of C_{S}, jeopardizing the stability of the simulation. On the one hand, appropriate measures may be taken to overcome these problems (see, e.g., Sagaut [138]). For example, an artificial condition may be introduced as

$$\nu + \nu_T^{(\prime)} \geq 0 \tag{114}$$

On the other hand, negative values of C_{S} and, consequently, of the subgrid viscosity may be physically interpreted as a modeling of the backscatter process. However, the situation becomes critical when the dynamically calculated model parameter remains too long in the negative range. This corresponds to a too high transfer of kinetic energy to the resolved scales, see Carati *et al.* [20]. In a variant of the dynamic localization model in Ghosal *et al.* [54], an energy equation is included, preventing the simulation from becoming unstable by monitoring the energy transfer.

4.2.2 Dynamic modeling procedure based on the variational Germano identity

The VGI has recently been introduced as a general methodology for evaluating unknown model parameters in a numerical method for partial differential equations as well as for the particular problem of the incompressible Navier-Stokes equations in Oberai and Wanderer [124], [125]. A variant of the VGI for the compressible Navier-Stokes equations very similar to the one in Oberai and Wanderer [124], [125], except for a slight difference, has been proposed by Farhat *et al.* [37]. Two different methods have been considered in Oberai and Wanderer [124], [125] to reduce the dimension of the equations eventually obtained: a dissipation method, such as it was originally applied in Germano *et al.* [53], and a least-squares method analogous to the one by Lilly [110]. Here, the least-squares method will be followed, which has also been used in Farhat *et al.* [37] and which enables a thorough comparison with the previously introduced dynamic modeling procedure based on the CGI. Specifying the model term in a VGI-related formulation to be a subgrid viscosity term, the general description of the VGI may be started with the respective variational equation including a variationally formulated subgrid viscosity term which is not restricted to the small resolved scales. Here, the FV equation is used, given as

$$B_{\mathrm{NS}}^{\mathrm{FV}}(\mathbf{v}_i^h, q_i^h; \mathbf{u}^h, p^h) - (\mathbf{v}_i^h, 2\nu_T\varepsilon(\mathbf{u}^h)\cdot\mathbf{n})_{\Gamma_i} = (\mathbf{v}_i^h, \mathbf{f})_\Omega + (\mathbf{v}_i^h, \mathbf{h})_{\Gamma_h} \;\forall\{\mathbf{v}_i^h, q_i^h\} \in \mathcal{V}_{up}^h \tag{115}$$

Replacing the right hand side by the exact solution in the sense of the variational formulation and rearranging yields

$$-(\mathbf{v}_i^h, 2\nu_T\varepsilon(\mathbf{u}^h)\cdot\mathbf{n})_{\Gamma_i} = B_{\mathrm{NS}}^{\mathrm{FV}}(\mathbf{v}_i^h, q_i^h; \mathbf{u}, p) - B_{\mathrm{NS}}^{\mathrm{FV}}(\mathbf{v}_i^h, q_i^h; \mathbf{u}^h, p^h)\ \forall\{\mathbf{v}_i^h, q_i^h\} \in \mathcal{V}_{up}^h \quad (116)$$

which defines a formula for the model term, in order to generate the optimal solution. Since it is, in general, impossible to get the exact solution, another numerical approximation besides the one related to the child grid with characteristic length scale h has to be relied on. In the context of the particular implementation considered here, this is the numerical approximation using the parent grid with characteristic length scale $\bar{h}$. Applying the restriction operator R, the variational equation may be formulated on the large-scale resolution level with the same model assumption analogous to (115) as

$$\begin{aligned} &B_{\mathrm{NS}}^{\mathrm{FV}}(\bar{\mathbf{v}}_i^{\bar{h}}, \bar{q}_i^{\bar{h}}; R[\mathbf{u}^h], R[p^h]) - (\bar{\mathbf{v}}_i^{\bar{h}}, 2\nu_T\varepsilon\big(R[\mathbf{u}^h]\big)\cdot\mathbf{n})_{\bar{\Gamma}_i} \\ &\quad = (\bar{\mathbf{v}}_i^{\bar{h}}, \mathbf{f})_\Omega + (\bar{\mathbf{v}}_i^{\bar{h}}, \mathbf{h})_{\Gamma_h} \qquad \forall\{\bar{\mathbf{v}}_i^{\bar{h}}, \bar{q}_i^{\bar{h}}\} \in \bar{\mathcal{V}}_{up}^{\bar{h}} \end{aligned} \quad (117)$$

where $q^{\bar{h}}$ is defined analogous to (96). Again, replacing the right hand side by the exact solution and rearranging yields

$$-(\bar{\mathbf{v}}_i^{\bar{h}}, 2\nu_T\varepsilon(\bar{\mathbf{u}}^{\bar{h}})\cdot\mathbf{n})_{\bar{\Gamma}_i} = B_{\mathrm{NS}}^{\mathrm{FV}}(\bar{\mathbf{v}}_i^{\bar{h}}, \bar{q}_i^{\bar{h}}; \mathbf{u}, p) - B_{\mathrm{NS}}^{\mathrm{FV}}(\bar{\mathbf{v}}_i^{\bar{h}}, \bar{q}_i^{\bar{h}}; \bar{\mathbf{u}}^{\bar{h}}, \bar{p}^{\bar{h}})\ \forall\{\bar{\mathbf{v}}_i^{\bar{h}}, \bar{q}_i^{\bar{h}}\} \in \bar{\mathcal{V}}_{up}^{\bar{h}} \quad (118)$$

Note that equations (117) and (118) hold only for the weighting functions contained in $\bar{\mathcal{V}}_{up}^{\bar{h}}$ and associated with the parent grid. Since it is assumed that $\bar{\mathcal{V}}_{up}^{\bar{h}} \subset \mathcal{V}_{up}^h$ with respect to the applied restriction operator R, equation (116) may also be formulated on the large-scale resolution level subject to

$$-(\bar{\mathbf{v}}_i^{\bar{h}}, 2\nu_T\varepsilon(\mathbf{u}^h)\cdot\mathbf{n})_{\bar{\Gamma}_i} = B_{\mathrm{NS}}^{\mathrm{FV}}(\bar{\mathbf{v}}_i^{\bar{h}}, \bar{q}_i^{\bar{h}}; \mathbf{u}, p) - B_{\mathrm{NS}}^{\mathrm{FV}}(\bar{\mathbf{v}}_i^{\bar{h}}, \bar{q}_i^{\bar{h}}; \mathbf{u}^h, p^h)\ \forall\{\bar{\mathbf{v}}_i^{\bar{h}}, \bar{q}_i^{\bar{h}}\} \in \bar{\mathcal{V}}_{up}^{\bar{h}} \quad (119)$$

Afterwards, (119) can be subtracted from (118) such that

$$\begin{aligned} &(\bar{\mathbf{v}}_i^{\bar{h}}, 2\nu_T\varepsilon(\mathbf{u}^h)\cdot\mathbf{n})_{\bar{\Gamma}_i} - (\bar{\mathbf{v}}_i^{\bar{h}}, 2\nu_T\varepsilon(\bar{\mathbf{u}}^{\bar{h}})\cdot\mathbf{n})_{\bar{\Gamma}_i} \\ &\quad = B_{\mathrm{NS}}^{\mathrm{FV}}(\bar{\mathbf{v}}_i^{\bar{h}}, \bar{q}_i^{\bar{h}}; \mathbf{u}, p) - B_{\mathrm{NS}}^{\mathrm{FV}}(\bar{\mathbf{v}}_i^{\bar{h}}, \bar{q}_i^{\bar{h}}; \bar{\mathbf{u}}^{\bar{h}}, \bar{p}^{\bar{h}}) \qquad \forall\{\bar{\mathbf{v}}_i^{\bar{h}}, \bar{q}_i^{\bar{h}}\} \in \bar{\mathcal{V}}_{up}^{\bar{h}} \end{aligned} \quad (120)$$

Thus, no more relations for the final calculation of the constant can be expected by this version of the VGI than there are degrees of freedom on the parent grid, which equals the dimension of $\bar{\mathcal{V}}_{up}^{\bar{h}}$. Inserting the Smagorinsky model and expanding $B_{\mathrm{NS}}^{\mathrm{FV}}$ yields

$$\begin{aligned} &(C_{\mathrm{S},i}h_i)^2 \left[\bar{\mathbf{v}}_i^{\bar{h}}, 2\left(|\varepsilon(\mathbf{u}^h)|\varepsilon(\mathbf{u}^h)\cdot\mathbf{n}) - \left(\frac{\bar{h}}{h}\right)^2 |\varepsilon(\bar{\mathbf{u}}^{\bar{h}})|\varepsilon(\bar{\mathbf{u}}^{\bar{h}})\cdot\mathbf{n}\right)\right]_{\bar{\Gamma}_i} \\ &= \left[\bar{\mathbf{v}}_i^{\bar{h}}, \frac{\partial(\mathbf{u}-\bar{\mathbf{u}}^{\bar{h}})}{\partial t}\right]_{\bar{\Omega}} + (\bar{\mathbf{v}}_i^{\bar{h}}, (\mathbf{u}^h\otimes\mathbf{u}^h - \bar{\mathbf{u}}^{\bar{h}}\otimes\bar{\mathbf{u}}^{\bar{h}})\cdot\mathbf{n})_{\bar{\Gamma}_i} + (\bar{\mathbf{v}}_i^{\bar{h}}, (p^h - \bar{p}^{\bar{h}})\mathbf{n})_{\bar{\Gamma}_i} \\ &\quad -(\bar{\mathbf{v}}_i^{\bar{h}}, 2\nu\varepsilon(\mathbf{u}^h - \bar{\mathbf{u}}^{\bar{h}})\cdot\mathbf{n})_{\bar{\Gamma}_i} - (\bar{q}_i^{\bar{h}}, (\mathbf{u}^h - \bar{\mathbf{u}}^{\bar{h}})\cdot\mathbf{n})_{\bar{\Gamma}_i} \end{aligned} \quad (121)$$

where $C_{\mathrm{S},i}$ denotes the model parameter in the control volume $\bar{\Omega}_i$ of the parent grid. It is assumed that $C_{\mathrm{S},i}$ is constant over this control volume of the parent grid, as before in the

context of the CGI. An error vector is formulated in the respective parent control volume such that

$$\mathbf{e}_i^{\bar{h}} = \mathbf{r}_{\mathrm{NS,i}}^{\bar{h}} - (C_{\mathrm{S},i} h_i)^2 \mathbf{m}_i^{\bar{h}} \tag{122}$$

where $\mathbf{r}_{\mathrm{NS,i}}^{\bar{h}}$ denotes the residual vector related to the Navier-Stokes equations on the right hand side of (121) and $\mathbf{m}_i^{\bar{h}}$ the model vector on the left hand side of (121). The least-squares method of Lilly [110] may be transfered to the VGI yielding

$$(C_{\mathrm{S}_i} h_i)^2 = \frac{\mathbf{r}_{\mathrm{NS,i}}^{\bar{h}} \mathbf{m}_i^{\bar{h}}}{\mathbf{m}_i^{\bar{h}} \mathbf{m}_i^{\bar{h}}} \tag{123}$$

A value for the parameter expression $(C_{\mathrm{S},i} h_i)^2$ may eventually be calculated in every control volume of the *parent* grid. As before in the context of the CGI, an alternative formulation may be pursued, yielding a value for the parameter expression $(C_{\mathrm{S},i} h_i)^2$ in every control volume of the *child* grid. This alternative formulation has been used in Farhat *et al.* [37]. For this purpose, equation (117) is rather formulated on the level of complete resolution, using the complete multigrid scale-separating operator S^{m} instead of the restriction operator R. Thus,

$$\begin{aligned} &B_{\mathrm{NS}}^{\mathrm{FV}}(\mathbf{v}_i^h, q_i^h; S^{\mathrm{m}}[\mathbf{u}^h], S^{\mathrm{m}}[p^h]) - (\mathbf{v}_i^h, 2\nu_T \varepsilon(S^{\mathrm{m}}[\mathbf{u}^h]) \cdot \mathbf{n})_{\Gamma_i} \\ &\quad = (\mathbf{v}_i^h, \mathbf{f})_\Omega + (\mathbf{v}_i^h, \mathbf{h})_{\Gamma_h} \qquad \forall \{\mathbf{v}_i^h, q_i^h\} \in \bar{\mathcal{V}}_{up}^h \end{aligned} \tag{124}$$

is obtained, which may also be rearranged analogous to (118). Subtracting (115) or (116) from (124) or its rearranged version, respectively, yields

$$\begin{aligned} &(\mathbf{v}_i^h, 2\nu_T \varepsilon(\mathbf{u}^h) \cdot \mathbf{n})_{\Gamma_i} - (\mathbf{v}_i^h, 2\nu_T \varepsilon(\bar{\mathbf{u}}^{\bar{h}}) \cdot \mathbf{n})_{\Gamma_i} \\ &\quad = B_{\mathrm{NS}}^{\mathrm{FV}}(\mathbf{v}_i^h, q_i^h; \mathbf{u}^h, p^h) - B_{\mathrm{NS}}^{\mathrm{FV}}(\mathbf{v}_i^h, q_i^h; \bar{\mathbf{u}}^{\bar{h}}, \bar{p}^{\bar{h}}) \qquad \forall \{\mathbf{v}_i^h, q_i^h\} \in \mathcal{V}_{up}^h \end{aligned} \tag{125}$$

which represents the analog to equation (120) on the level of complete resolution. Finally, it is remarked that the potential numerical problemes mentioned in the context of the CGI-related dynamic modeling procedure may also appear for the present procedure, and appropriate measures would have to be taken to prevent the simulation from becoming unstable, see Farhat *et al.* [37].

The three basic differences between the dynamic modeling procedures based on the CGI and the VGI are summarized in the following, see also Oberai and Wanderer [125].

- The CGI aims at satisfying the identity pointwise, whereas the VGI aims at satisfying the identity weakly.
- As a result of using the CGI, a tensor-based formula for the calculation of the model parameter is obtained, whereas the calculation originating from the VGI is vector-based.
- The CGI only takes into account the non-linear convective term of the Navier-Stokes equations, whereas the VGI takes into account all terms of the Navier-Stokes equations.

4.2.3 Dynamic modeling procedure based on elementwise sub-submeshes

This dynamic modeling procedure is a particular approach for improving the two-level FEM presented in Section 3.1.1. In the end, it amounts to a three-level FEM. The presentation of the two-level FEM closed with the variational problem (68), which is formulated on each element of the basic discretization. If one were able to solve this variational problem, at least up to the necessary resolution limit for a complete incorporation of all existing scales in the sense of a DNS, a fully satisfying local solution for the small scales within every individual element domain Ω_i would be achieved. Of course, this solution is limited from a global perspective by the aforementioned assumptions, in particular the crucial residual-free bubble assumption that the scales crossing the element boundaries are not taken into account. As attractive this thought may still be, as unlikely is it, in general, due to limited computer power. However, obtaining at least a good approximation of $\mathcal{B}_1$ would be the second best choice and, more importantly, the one which can be afforded in general.

The idea for this is basically the same as the idea underlying the subgrid viscosity concept in a global context. Here, the elementwise equations are likewise enhanced by the addition of a subgrid viscosity term. Thus, the quality of the approximation as a whole depends on the quality of the approximation of the elementwise subgrid viscosity $\nu'_{T,i}$. The enhanced variational problem is given as

$$\left(w^{h'}, \frac{1}{\delta t}\mathcal{B}_1^{h'} + \mathbf{u}\nabla\mathcal{B}_1^{h'} \right)_{\Omega_i} + (\nabla w^{h'}, (\nu + \nu'_{T,i})\nabla\mathcal{B}_1^{h'})_{\Omega_i} = (w^{h'}, 1)_{\Omega_i} \tag{126}$$

For the determination of the subgrid viscosity, a dynamic modeling procedure is chosen here as well, which is, however, quite different from the previously introduced procedures based on the CGI and the VGI, respectively.

In Brezzi *et al.* [14], a dynamic tune-up for $\nu'_{T,i}$ was proposed, from which a reasonably good value should arise. Brezzi *et al.* [14] assumed the model formulation previously suggested by Guermond [64] to be the basis of their dynamic algorithm. The model formulation in Guermond [64] exhibits an obvious similarity with (100). It was shown in Gravemeier *et al.* [61] that there was actually no need for any model assumption, since a direct calculation of the subgrid viscosity is possible. Thus, the subgrid viscosity directly represents the "unknown parameter". An elementwise sub-submesh with characteristic element length $\hat{h}$ is chosen, slightly finer than the original submesh (i.e., $\hat{h} < h'$). On these elementwise sub-submeshes, the variational equation (126) has to be solved as well. Comparing these two solutions (i.e., the one on the submesh and the one on the sub-submesh), the desired value for $\nu'_{T,i}$ may be achieved.

However, for this dynamic tune-up to be workable in that an explicit value for $\nu'_{T,i}$ can actually be obtained in the end, a criterion must be established. Motivated by insights from the theory of stabilized methods, the average integral of $\mathcal{B}_1$ on the large-scale element domain Ω_i is required to be equal to the corresponding value of the adequately resolved bubble for $\nu'_{T,i} = 0$ in (126), such that

$$\frac{1}{|\Omega_i|}\int_{\Omega_i} \mathcal{B}_1(\nu'_{T,i} = 0)\,\mathrm{d}\Omega_i \approx \frac{1}{|\Omega_i|}\int_{\Omega_i} \mathcal{B}_1^{h'}(\nu'_{T,i})\,\mathrm{d}\Omega_i \approx \frac{1}{|\Omega_i|}\int_{\Omega_i} \mathcal{B}_1^{\hat{h}}(\nu'_{T,i})\,\mathrm{d}\Omega_i \tag{127}$$

where the solution on the sub-submesh is indicated by its characteristic element length $\hat{h}$. Criterion (127) governs an iterative algorithm, which amounts to an extrapolation, with the target of this extrapolation being the goal: a "good" approximation of the analytical residual-free bubble $\mathcal{B}_1$ (i.e., the one with $\nu'_{T,i} = 0$). Further details of the dynamic modeling procedure can be found in Gravemeier [56] or Gravemeier *et al.* [61], respectively. The three-

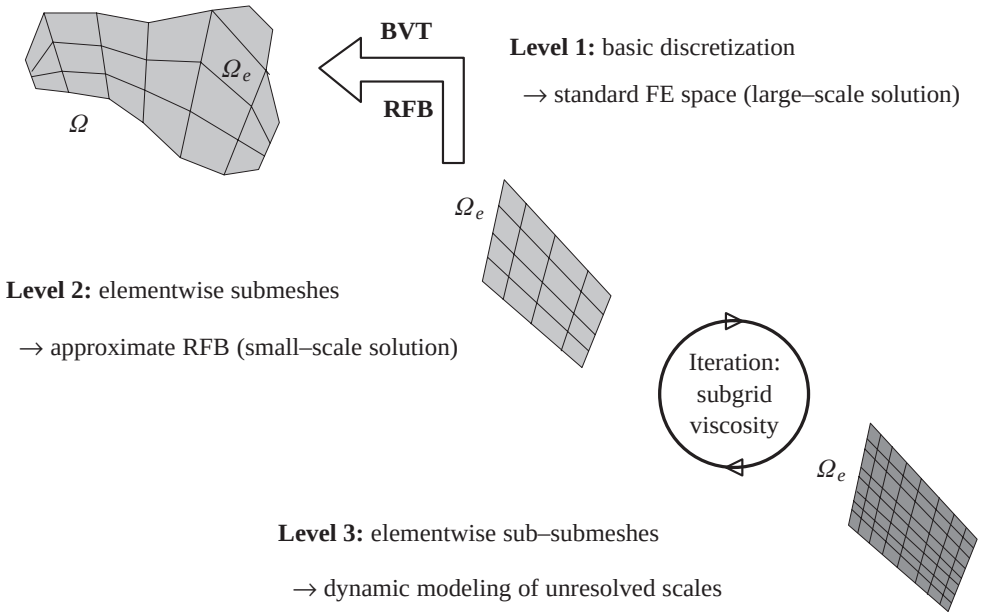

Figure 9. Three-level FEM: discretizations and strategy

level FEM is graphically summarized in Figure 9. Figure 9 extends Figure 4, which has already depicted the two-level FEM, by including the third level.

Comparing the dynamic modeling procedures based on the CGI and the VGI to the three-level FEM with the dynamic modeling procedure just outlined, it is stated that the crucial difference refers to the range of scales exploited to fix the undetermined "parameter" in the respective model, see Figure 10. In the dynamic modeling procedures based on the CGI and the VGI, the small resolved scales are exploited, and the model parameter is calculated based on the CGI or its variational counterpart, respectively. In the three-level FEM, the unresolved scales are, in a crude manner so far (see Gravemeier [56] for discussion), exploited, and the subgrid viscosity is directly determined. The approximation of the small resolved scales via the localized residual-free bubble strategy is reemphasized in Figure 10(b). The underlying idea and the reason for the success of the dynamic modeling procedures based on the CGI and the VGI has to be attributed to the hypothesis of the similarity between the unresolved scales and the small resolved scales. It is, however, certainly unquestionable that no scales are more similar to the unresolved scales than the unresolved scales themselves. Thus, a dynamic modeling procedure exploiting the unresolved scales appears to be promising from the authors' point of view, although the actual estimation in the presented approach is still crude.

5 NUMERICAL EXAMPLES

In this section, the results from the numerical simulations of three flow examples, a laminar and two turbulent flow situations, which were all conducted by the author, will be summarized. Additionally, the reader is provided with an overview of those turbulent flow examples which have been simulated with the variational multiscale LES and published to date.

5.1 Laminar Flow Example: Beltrami Flow

The results from numerical simulations of a laminar flow example, the so-called Beltrami flow, using the two- and three-level FEM as described in Sections 3.1.1 and 4.2.3, re-

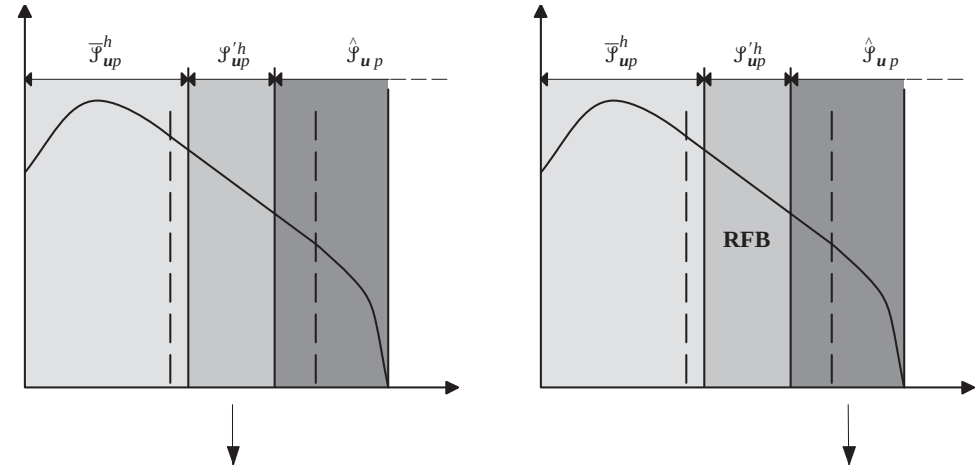

Figure 10. Exploited scale groups for dynamic modeling: (a) CGI/VGI; (b) elementwise submeshes

spectively, will be presented in the following. This laminar flow example combines three attractive features which cannnot be met elsewhere in this unification according to Ethier and Steinman [33]: it describes a fully three-dimensional instationary flow situation, all terms in the Navier-Stokes equations play a crucial role (i.e., there is no degeneration in the sense that one or more terms are identically zero), and a closed-form analytical solution exists. This flow example was developed by Ethier and Steinman [33] for three-dimensional benchmarking purposes, although it is unlikely to be physically realized eventually. Possibly more familiar to the reader is the two-dimensional counterpart of this flow, the Taylor [146] problem, which was used by Kim and Moin [102] for benchmarking purposes in two dimensions. Further laminar flow examples simulated with the two- and the three-level FEM may be found in Gravemeier [56] and Gravemeier *et al.* [61].

The problem is solved on the flow domain $\Omega = [-1,1] \times [-1,1] \times [-1,1]$. The analytical solutions for the velocity and the pressure are given as

$$u_1 = -a[e^{ax_1} \sin(ax_2 \pm dx_3) + e^{ax_3} \cos(ax_1 \pm dx_2)]e^{-\nu d^2 t} \tag{128}$$

$$u_2 = -a[e^{ax_2} \sin(ax_3 \pm dx_1) + e^{ax_1} \cos(ax_2 \pm dx_3)]e^{-\nu d^2 t} \tag{129}$$

$$u_3 = -a[e^{ax_3} \sin(ax_1 \pm dx_2) + e^{ax_2} \cos(ax_3 \pm dx_1)]e^{-\nu d^2 t} \tag{130}$$

$$\begin{aligned} p = -\frac{a^2}{2}\lceil & e^{2ax_1} + e^{2ax_2} + e^{2ax_3} + 2\sin(ax_1 \pm dx_2)\cos(ax_3 \pm dx_1)e^{a(x_2+x_3)} \\ & + 2\sin(ax_2 \pm dx_3)\cos(ax_1 \pm dx_2)e^{a(x_3+x_1)} \\ & + 2\sin(ax_3 \pm dx_1)\cos(ax_2 \pm dx_3)e^{a(x_1+x_2)}\rceil e^{-2\nu d^2 t} \end{aligned} \tag{131}$$

where a and d are open parameters, defining a family of solutions. These parameters will be fixed according to Ethier and Steinman (1994) with the values $a = \pi/4$ and $d = \pi/2$. The characteristic feature of this flow is a series of counter-rotating vortices intersecting one

another at oblique angles. The time-dependent terms in (128)-(131) indicate the exponential decay in time of the initial flow configuration.

Two different flow regimes, a diffusion-dominated flow with $\nu = 1.0$ and a convection-dominated flow with $\nu = 0.001$, are investigated. The Reynolds number based on the respective viscosity, the length of the domain, and the maximum velocity is $\mathrm{Re} = 6.62$ and $\mathrm{Re} = 6620$. The initial flow state is the same for both the diffusion- and the convection-dominated flow regime, since the viscosity has no effect at $t = 0$. Depictions of the initial velocity and pressure fields can be found in Gravemeier [56] or Gravemeier *et al.* [61], respectively. A simple backward Euler time integration scheme is applied. The simulation is started with the initial field given by (128)-(131) for $t = 0$. Thereafter, Dirichlet boundary conditions based on (128)-(131) are applied on all boundaries of the flow domain. The calculation is run 16 time steps with $\delta t = 0.00625$ and then stopped at $t = 0.1$, in order to quantify the current errors for the velocity and the pressure in the L_2-norm and in the H_1-norm. The error measure for the velocity in the L_2-norm is defined as

$$e_0^{\mathbf{u}} = \frac{\|\mathbf{u} - \mathbf{u}^h\|_0}{\|\mathbf{u}\|_0} = \left[\frac{\int_\Omega (\mathbf{u} - \mathbf{u}^h)^2 \, \mathrm{d}\Omega}{\int_\Omega \mathbf{u}^2 \, \mathrm{d}\Omega} \right]^{\frac{1}{2}} \tag{132}$$

and in the H^1-norm as

$$e_1^{\mathbf{u}} = \frac{\|\mathbf{u} - \mathbf{u}^h\|_1}{\|\mathbf{u}\|_1} = \left[\frac{\int_\Omega (\mathbf{u} - \mathbf{u}^h)^2 + (\nabla \mathbf{u} - \nabla \mathbf{u}^h)^2 \, \mathrm{d}\Omega}{\int_\Omega \mathbf{u}^2 + (\nabla \mathbf{u})^2 \, \mathrm{d}\Omega} \right]^{\frac{1}{2}} \tag{133}$$

The same error measure in the L_2-norm in (132) is also used for the evaluation of the error in the pressure field. The results obtained with the two- and three-level FEM are compared to the ones obtained with a stabilized method of USFEM-type according to Franca and Valentin [49]. Stabilized FEMs of this and other type have been established as adequate methods for the numerical simulation of laminar flows in the meantime. For the two- and three-level method, the bubble functions are assumed to be quasi-static, see Gravemeier [56]. In the USFEM, there is no explicit small-scale part of the velocity. However, for the two- and three-level methods, the small-scale part of the velocity is explicitly incorporated in the error calculations for the velocity by setting $\mathbf{u}^h = \bar{\mathbf{u}}^{\bar{h}} + \mathbf{u}'^{h'}$, where the small-scale part of the velocity depends on the characteristic element length h' of the submesh. Uniform discretizations with $4 \times 4 \times 4$, $8 \times 8 \times 8$, and $16 \times 16 \times 16$ trilinear hexahedral elements are used as the basic discretization. Furthermore, uniform $4 \times 4 \times 4$-element discretizations for the submeshes of the two-level FEM and the sub-submeshes of the three-level FEM, respectively, are chosen. Uniform $3 \times 3 \times 3$-element discretizations represent the submeshes of the three-level FEM.

Figures 11 and 12 depict the velocity error in the L_2-norm and in the H^1-norm for the diffusion- and convection-dominated flow, respectively. For the diffusion-dominated flow, the convergence rates which have to be expected from a theoretical error analysis are accurately matched by all methods. Moreover, they cannot be distinguished from one another in terms of the absolute error. The situation is quite different for the convection-dominated flow. The stabilized method of USFEM-type and the three-level FEM still work fine, although the absolute velocity error in the H^1-norm for the three-level FEM is not as good as the one for the stabilized method. This tendency could also be observed for bilinear elements in the two-dimensional example of an impinging fluid flow, see Gravemeier

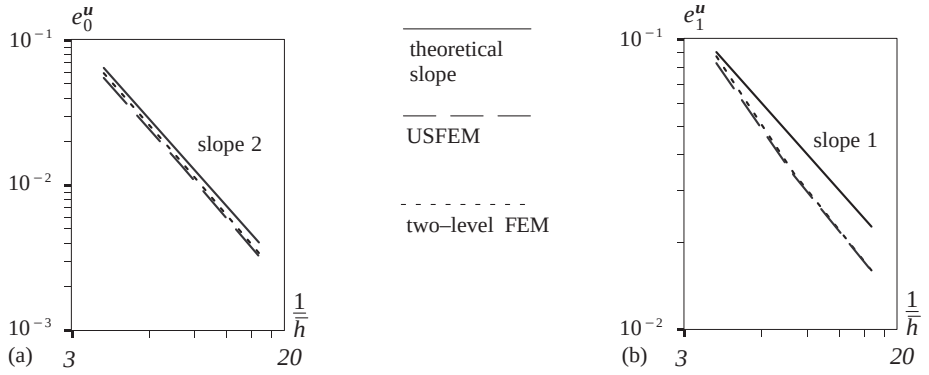

Figure 11. Velocity error for diffusion-dominated flow: (a) L_2-norm; (b) H_1-norm

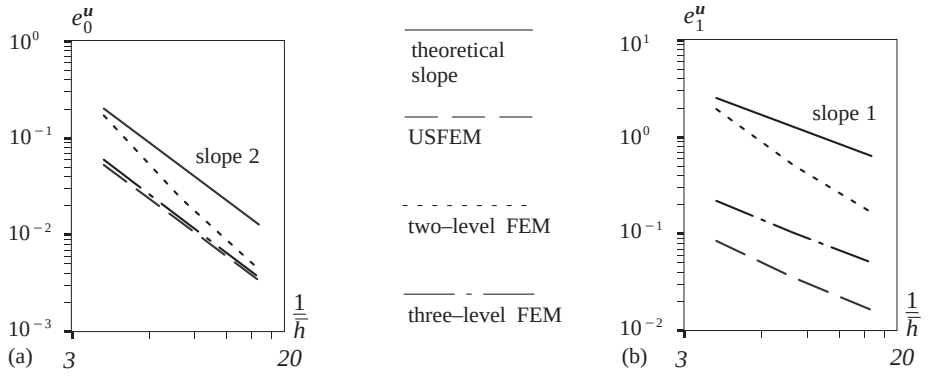

Figure 12. Velocity error for convection-dominated flow: (a) L_2-norm; (b) H_1-norm

et al. [61]. It may supposably be blamed on the negative effect of the stringent zero Dirichlet boundary conditions in the context of the residual-free bubble method. In the two-dimensional applications, this performance is, however, then reversed for higher-order elements in favor of the three-level FEM. Similar behaviour might be expected in the three-dimensional case. The crucial surveillance is that the two-level FEM is no longer able to guarantee an acceptable absolute error in both the L_2-norm and the H^1-norm for a relatively coarse basic discretization. In Figure 13, the pressure error is reported. In both diagrams, lines are included displaying the slopes of suboptimal (slope 1) and optimal (slope 2) rate. It is observed that all three methods match the optimal rate in both the diffusion- and the convection-dominated case. The stabilized method shows but a slightly negative deviation from this behaviour in the diffusion-dominated flow regime, and the two- and three-level FEM exhibit a slightly positive deviation.

Concluding this laminar flow example, it is stated that a two-level FEM with the present discretizations on the two levels is not able to resolve enough scales to guarantee an acceptable velocity error. To remedy this deficiency, it is necessary to take into account the effect of the unresolved scales of the problem, which is here done by a dynamic modeling procedure in the context of the three-level FEM. It is important to note that the three-level FEM employs a coarser submesh ($3 \times 3 \times 3$ elements) than the two-level FEM ($4 \times 4 \times 4$ elements) in the present implementation, which emphasizes the beneficial effect of the third level.

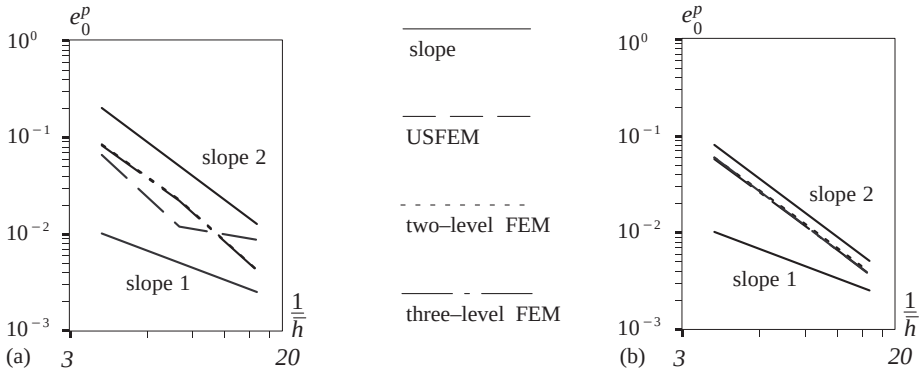

Figure 13. Pressure error in L_2-norm: (a) diffusion-dominated flow; (b) convection-dominated flow

5.2 Overview of Turbulent Flow Applications

A couple of test cases have been studied by several researchers so far, in order to investigate the performance of the variational multiscale method in turbulent flow situations. However, most of these studies have been on relatively simple geometrical flow domains. In the following, a brief overview of the flow problems addressed and published so far will be given along with the respectively applied numerical method and the respective approach for separating the large and small resolved scales. Most of these studies have already been examined from the methodical point of view in Section 3.

The simplest turbulent flow problem and, thus, a well-suited initial test case is homogeneous isotropic turbulence. Hughes *et al.* [84] presented simulations of this flow using a spectral method with the sharp cutoff filter for separating the scale groups. For the same flow example, Jansen and Tejada-Martinez [92] applied a continuous Galerkin FEM with hierarchical shape function bases. In two recent studies, the influence of the resolution level (Hughes *et al.* [88]) as well as the applied numerical method (Oberai *et al.* [122]) on the energy transfer in the context of homogeneous isotropic turbulence were investigated.

Turbulent channel flow is the most famous representative of the test cases exhibiting one inhomogeneous direction. This flow example was studied in Hughes *et al.* [85] and Oberai and Hughes [123], applying a spectral method in the homogeneous planes of the channel and modified Legendre polynomials in the inhomogeneous wall-normal direction. The sharp cutoff filter in Fourier space, as in their work on homogeneous isotropic turbulence, and a p-type separation for the Legendre polynomials enabled the separation of the problem scales. A spectral method in the homogeneous planes and a FVM in the inhomogeneous direction, with scale separation only in the homogeneous planes, was the approach for simulating channel flow in Ramakrishnan and Collis [133]. With a similar approach in the homogeneous planes and fourth-order spectral-like compact finite differences in the inhomogeneous direction, Jeanmart and Winckelmans [93] simulated the channel flow problem. In their regularized version of the variational multiscale LES, those authors used the discrete box (or top-hat) filter for the extraction of the small resolved scales which the subgrid-scale model is applied to. Another recent study applying a discrete smooth filter for the turbulent flow in a channel was the one by Vreman [153], using a second-order energy-conserving finite difference method. Gravemeier [58] applied a FVM with an h-type multigrid scale separation for the numerical simulation of this particular flow situation. A summary of the results from this application will be given in Section 5.3.

Further test cases beside these two flow examples have been studied. The turbulent flow

in a lid-driven cavity was investigated in Gravemeier *et al.* [62], using the three-level FEM. The flow problem of a plane mixing layer was also simulated with the three-level FEM in Gravemeier *et al.* [62]. A three-dimensional mixing layer and turbulent flow past a square cylinder were simulated in John and Kaya [95], using a p-type scale separation within a FEM. Koobus and Farhat [103] applied a combined FEM/FVM with an h-type multigrid scale separation for the numerical simulation of turbulent flow past a square cylinder. The same method was used in Farhat *et al.* [37] for the simulation of turbulent flow past a prolate spheroid and a forward swept scaled wing. In Gravemeier [59], turbulent flow in a planar asymmetric diffuser was simulated, using a FVM with an h-type scale separation. A summary of the results from this application will also be given in Section 5.3.

5.3 Turbulent Flow Examples: Channel and Diffuser

In this section, the results from numerical simulations of two turbulent flow examples, turbulent flow in a channel and turbulent flow in a planar asymmetric diffuser, will be presented. The detailed description of the numerical setup and further results can be found in Gravemeier [58] and Gravemeier [59], respectively. All numerical simulations described in this section have been conducted using the CDP-α code. CDP-α is an unstructured FV-based CFD code of the Center for Turbulence Research, which has been designed for LES of variable density low Mach-number flows on very large grids using massively parallel computers (see, e.g., Ham *et al.* [66] and references therein). The main features of the code are the use of a fractional-step procedure with a four-step scheme and a momentum interpolation method for unstructured grids, see Kim and Choi [101]. The Crank-Nicolson scheme, a fully implicit time-stepping scheme of second-order accuracy, is applied to the convective and viscous terms, and the non-linear convective term is linearized about the result from the previous time step. All spatial and temporal approximations are of second-order accuracy. Furthermore, discrete conservation of energy is enforced. See Ham and Iaccarino [67] and Mahesh *et al.* [112] for this important aspect of the code. The momentum equation in the first step of the fractional-step procedure is solved using a simple iterative SOR procedure. For the solution of the pressure Poisson equation in the third step of the fractional-step procedure, an algebraic multigrid solver is used. See Ham *et al.* [66] for the details as well as results from investigations concerning the performance of this multigrid solver. Three different ways of subgrid-scale modeling are compared:

- dynamic Smagorinsky (DS) (i.e., the dynamic modeling procedure based on the CGI according to Section 4.2.1 in a non-multiscale application with the subgrid viscosity subject to (100)),
- constant multiscale Smagorinsky (CMS) (i.e., the constant-coefficient Smagorinsky model within the multiscale environment subject to (97) or (99), respectively, with the subgrid viscosity according to (101)), and
- dynamic multiscale Smagorinsky (DMS) (i.e., the dynamic modeling procedure based on the CGI according to Section 4.2.1 within the multiscale environment subject to (97) or (99), respectively, with the subgrid viscosity according to (101)).

All of these methods are investigated for the scale-separating operators S^{pm} and S^{sm}, which have been presented in Section 3.2.2. The results are compared to results from simulations with discrete smooth filters based on the trapezoidal rule and Simpson's rule (see appendix), which are denoted S^{tf} and S^{sf}, respectively. In the following diagrams, the abbreviation DMS-PM, for instance, indicates the variational multiscale LES incorporating a dynamic Smagorinsky model with the scale-separating operator S^{pm} applied. Results are

also reported for simulations using the constant-coefficient Smagorinsky model in a non-multiscale environment (CS) (only for the channel flow) as well as applying no subgrid-scale model at all (NM), which represents a coarse (i.e., not sufficiently resolved) DNS. It is reemphasized that CMS is merely the combination of these last two approaches by applying no model to the large resolved scales and the constant-coefficient Smagorinsky model to the small resolved scales. Based on the evaluation of results in Gravemeier [58], the characteristic length scale ratio $\bar{h}/h$ is set to 2.5 for S^{pm} and 2.0 for S^{sm} for all DS and DMS simulations. For S^{tf} and S^{sf}, ratios of 2.0 and 1.5, respectively, are applied. The computational effort required for the various methodical combinations is also evaluated.

Test simulations by the author have shown at most comparable results for the large-small and all-small model with respect to the small-small model, but no superior results. Thus, the small-small model (101) is exclusively used for the variational multiscale LES. The constant C_{S} is chosen to be 0.1 for the channel flow simulations according to the original choice in Deardorff [28], although this choice was by no means designed for a multiscale LES in the present sense. The choice of a constant C_{S} for the non-dynamic variational multiscale LES in the case of turbulent flow in a diffuser is not an easy one, since there is an entire lack of available data for this case. The choice of 0.1 is maintained for the inflow channel simulations in the diffuser applications. For the actual diffuser, a value of $C_{\mathrm{S}} = 0.18$ is applied. It represents the value obtained in Lilly's [109] analysis for homogeneous isotropic turbulence. However, this choice is supported by a simple comparison of values observed during the dynamic calculations in the inflow channel and in the diffuser. Considering a volume-averaged value of C_{S} over the entire domain, values of approximately 0.15 and 0.25 are obtained in the inflow channel and in the diffuser, respectively (i.e., a ratio of about 0.6). Setting 0.1 in this ratio, a constant $C_{\mathrm{S}} \approx 0.17$ can be calculated for the diffuser using this rough approximation, which is close to the chosen value of 0.18.

5.3.1 Turbulent channel flow

Flows at two different Reynolds numbers, $\mathrm{Re}_\tau = u_\tau \delta_{\mathrm{c}}/\nu = 180$ and $\mathrm{Re}_\tau = 590$, were simulated in Gravemeier [58], marking the lower and upper end of the DNS study in Moser *et al.* [118]. The turbulent wall-shear velocity $u_\tau = \sqrt{\tau_w}$, where τ_w denotes the wall shear stress, and the channel half-width δ_{c} define the Reynolds number Re_τ, besides the kinematic visosity ν. The channel dimensions are chosen according to Moser *et al.* [118] for the two cases. Here, only the results for the flow at the higher Reynolds number $\mathrm{Re}_\tau = 590$ are shown. A parabolic velocity profile perturbed by a random velocity fluctuation of 10%-amplitude of the bulk mean streamwise velocity represents the initial condition $\mathbf{u}_0$ for the velocity field, see Gravemeier [58] for details. No-slip boundary conditions are applied at the upper and lower wall perpendicular to the x_2-direction. In the homogeneous x_1- and x_3-direction, periodic boundary conditions for the velocity are applied. As the driving mechanism for the flow, a body force is imposed in form of a driving pressure gradient in the streamwise x_1-direction. The respective time step value for the temporal discretization is evaluated based on a fixed choice of the CFL number as 0.65. 5,000 time steps are performed to allow the flow to develop, and the statistics are collected during another 5,000 time steps.

A relatively coarse spatial discretization with 64 control volumes in all coordinate directions is employed. The distribution of control volumes in the wall-normal x_2-direction obeys a cosine function, refining towards the walls for the parent grid. The isotropic subdivision procedure, which has been briefly addressed in Section 3.2.2, is applied subsequently. The characteristic length scales are, as usual, expressed in non-dimensional length units $h^+ = h/\delta_\nu = h u_\tau/\nu$, scaling the actual characteristic control volume length by the viscous length scale δ_ν. The child grid control volume lengths in the respective coordinate directions eventually are $h_1^+ = 57.92$, $h_{2,\mathrm{min}}^+ = 1.42$, $h_{2,\mathrm{max}}^+ = 28.92$, and $h_3^+ = 28.96$. Results for

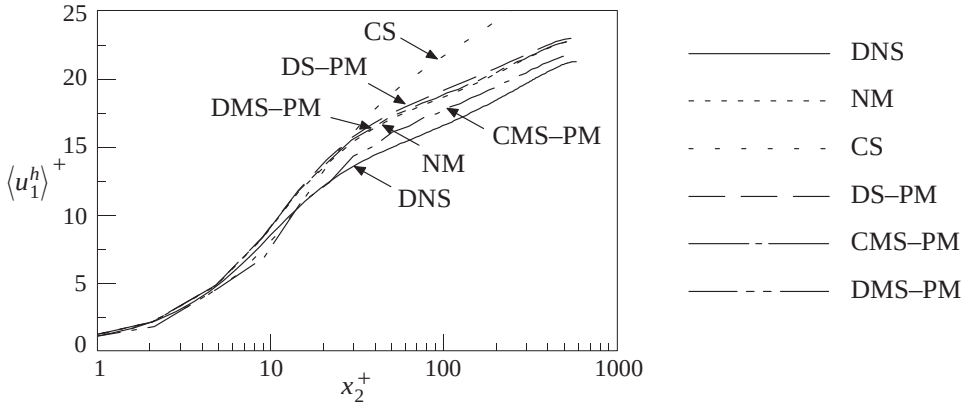

Figure 14. Comparing methods (PM-separation): mean streamwise velocity

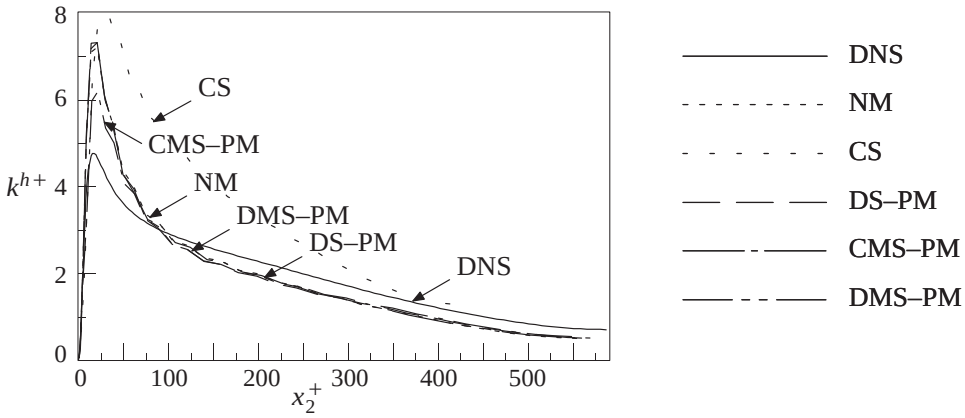

Figure 15. Comparing methods (PM-separation): turbulent kinetic energy

a finer discretization may be found in Gravemeier [58].

In order to compare the various methods, the scale-separating operator S^{pm} is used for DS, CMS, and DMS, since it is the most important operator due to its projective property. Figures 14 and 15 depict the mean streamwise velocity profile $\langle u_1^h \rangle$, scaled by the wall-shear velocity u_τ, and the turbulent kinetic energy k^h, scaled by u_τ^2, respectively. The larger numerical error introduced by a second-order accurate method in combination with a relatively coarse discretization comes into play for all methods applied (see, e.g., Gravemeier [58], Terracol *et al.* [150], and references therein). Surprisingly, however, the lower accuracy of the basic method affects CMS-PM to a far lesser extent than the other methods towards the channel center. It is considerably closer to the DNS profile in this part of the channel than NM, DS-PM, and DMS-PM. DMS-PM shows no improvement in comparison to NM, and DS-PM performs even slightly worse. Despite the higher accuracy in the inertial layer (usually expected to start at $x_2^+ = 30$), CMS-PM slightly underpredicts the velocity profile in the buffer layer (usually expected to range from $x_2^+ = 5$ to $x_2^+ = 30$). The profile for the turbulent kinetic energy shows a much better agreement for the height of the peak in comparison to the DNS profile than the other methods. Of course, CS is far worse than all other methods with respect to both the mean streamwise velocity and the turbulent kinetic energy profile.

An objective comparison of the computational effort for the simulations using the afore-

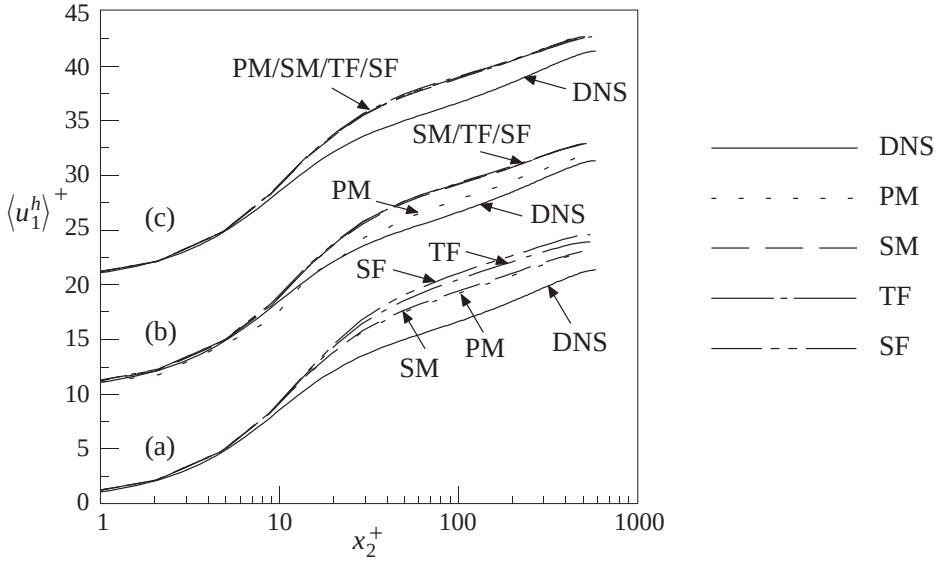

Figure 16. Comparing scale-separating operators: mean streamwise velocity: (a) DS; (b) CMS (+10); (c) DMS (+20)

mentioned methods is difficult, since it strongly depends on the amount of computational time spent within the actual solvers in CDP-α. These time measures can vary considerably from one calculation to another. Thus, only approximate measures for the necessary computational effort are reported as a mean value of the actual simulation times covering all calculations in Gravemeier [58]. Setting the computational effort for NM to 1.0, the relative measures for CS, DS-PM, CMS-PM, and DMS-PM are circa 1.10, 1.15, 1.10, and 1.15, respectively. Thus, CMS in combination with PM is a very efficient method computationally, even more efficient than the non-multiscale method DS. Taking into account other scale-separating operators, the numbers increase drastically for CMS and DMS, as will be seen below.

A second important issue concerns the differences between the various scale-separating operators. In Figures 16 and 17, the mean streamwise velocity and the turbulent kinetic energy, respectively, for four different scale-separating operators, which are applied with DS, CMS, or DMS, respectively, are pictured. There are hardly any differences visible for DMS in Figure 16(c), but the scale-separating operators PM and SM perform better than TF and SF in the context of DS, see Figure 16(a). This presumption is, at least to a certain degree, reinforced for the turbulent kinetic energy profiles in Figures 17(a) and (c). A remarkable difference between the projective scale-separating operator PM and the other operators shows up in the context of CMS for the mean streamwise velocity, in particular, as well as for the turbulent kinetic energy profile, although to a lesser degree, see Figures 16(b) and 17(b). Thus, the favourable behaviour of CMS-PM in the inertial layer as well as the slightly underpredictive performance in the buffer layer and parts of the viscous sublayer seems to be attributed to CMS only depending on this specific scale-separating operator.

Specifying the necessary computational effort for the various scale-separating operators results in the following approximate numbers. Setting the relative computational simulation time for the operator PM to 1.0, the measures for SM, TF, and SF are approximately 1.25, 1.40, and 2.50, respectively. In particular, SF in this implementation is an extremely time-consuming operator and is therefore not recommended for further use as a scale-separating

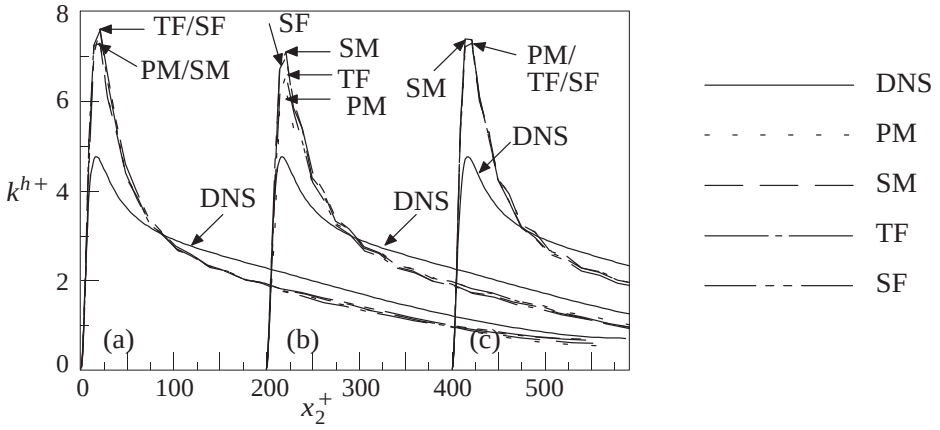

Figure 17. Comparing scale-separating operators: turbulent kinetic energy: (a) DS; (b) CMS (+200); (c) DMS (+400)

operator. The reason for the additional effort linked with such non-projective operators can be traced back to a necessary call of the scale-separating routine at the beginning of each iteration step in the solution procedure for the momentum equation. This call is required to determine the updated large-scale velocity field for the residual calculation. Such a call is not necessary for PM.

In order to analyze the specific behaviour of CMS-PM in comparison to all other scale-separating operator in the context of CMS, the small scales haven been extracted and investigated explicitly. Figures 18 and 19 depict the mean streamwise small-scale velocity and the small-scale turbulent kinetic energy, respectively. The small-scale velocity of CMS-PM shows an oscillating behaviour with large amplitudes particularly in the buffer layer. For CMS-SM, the frequency of the oscillation is about the same, but the amplitudes are considerably smaller. In case of CMS-TF and CMS-SF, one oscillation period can be seen throughout one half-width of the channel with the amplitude being larger for CMS-TF than for CMS-SF. The largest small-scale turbulent kinetic energy is obtained for CMS-PM by evidence of the x_2-*integral* of the profile (although the peak close to the wall is also matched by CMS-SM) and the smallest one for CMS-SF, see Figure 19. This indicates a measure for the amount of small scales extracted by the respective scale- separating operator and was quantified in Gravemeier [58].

5.3.2 Turbulent flow in a planar asymmetric diffuser

The diffuser geometry, which basically matches the experimental configuration of Obi *et al.* [126] and Buice and Eaton [18] as well as the numerical setup in Kaltenbach *et al.* [98] and Wu *et al.* [162], is shown in Figure 20. The inlet plane is located at $x_1 = -5$, followed by an inlet channel of length $5\delta_c$. The inlet channel half-width δ_c, which matches the half-width of the preceding inflow channel, is fixed to be of unit length. The asymmetric diffuser of length $42\delta_c$ opens with an angle of 10°. This corresponds to an expansion ratio of $h_{in}/h_{out} = 4.7$. It is followed by an outlet channel of height $9.4\delta_c$ and length of approximately $58\delta_c$, which locates the outlet plane at about $x_1 = 100$. The outlet channel length matches the one in Wu *et al.* [162] and is considerably longer than the one in Kaltenbach *et al.* [98]. Due to the relatively long distance between the last point of measurement and the outlet plane, any significant upstream influence of the outlet plane is minimized to the greatest extent. Nevertheless, the recovery into a canonical channel flow will not be reached even within this longer outlet channel, see Buice and Eaton [18] and Kaltenbach *et al.* [98]. Both the

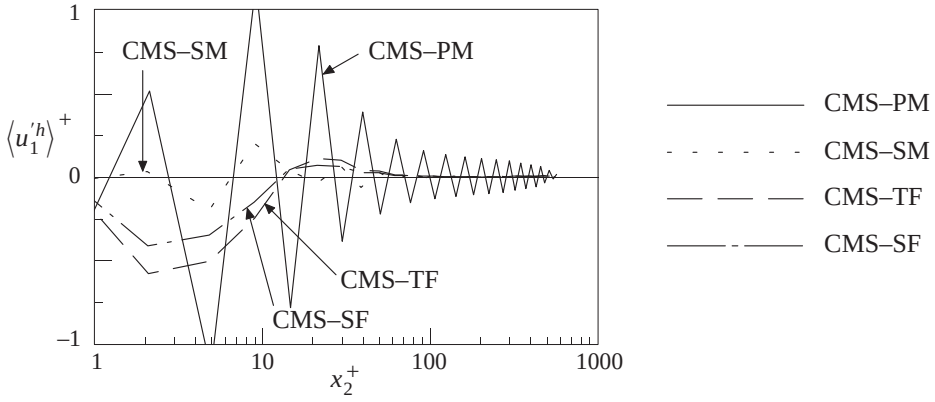

Figure 18. Comparing scale-separating operators for CMS: mean streamwise small-scale velocity

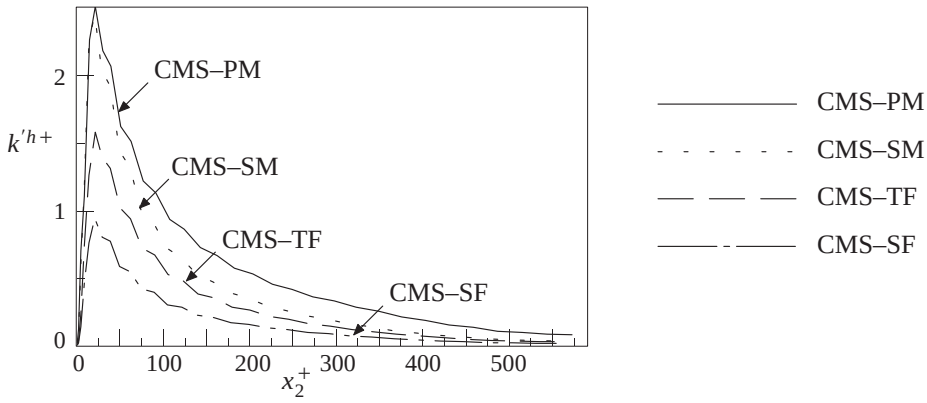

Figure 19. Comparing scale-separating operators for CMS: small-scale turbulent kinetic energy

upstream corner at $x_1 = 0$ and the downstream corner at $x_1 = 42$ are rounded with a radius of $r = 19.4$, where the curvature centers are located as shown in Figure 20. The length of the domain in x_3-direction (i.e., orthogonal to the depiction in Figure 20), is chosen to be $8\delta_c$, matching the spanwise length in Wu *et al.* [162] and representing the largest value for the spanwise length investigated in Kaltenbach *et al.* [98]. The inflow channel matches the inlet channel in its dimensions in x_2- and x_3-direction. According to Wu *et al.* [162], an inflow channel length of $12\delta_c$ is chosen.

A zero velocity field is assumed to be the initial condition for the velocity. At the walls Γ_w, no-slip boundary conditions (i.e., $\mathbf{g} = \mathbf{0}$ in (7)) are assumed throughout the simulation time T. At the inflow boundary Γ_{in}, a time-dependent inflow velocity vector $\mathbf{g} = \mathbf{u}^{\text{in}}(t)$ is prescribed. The inflow velocity $\mathbf{u}^{\text{in}}(t)$ is generated in the inflow channel as a result of a fully developed turbulent flow. At the outflow boundary Γ_{out}, a convective boundary condition is prescribed subject to

$$\frac{\partial \mathbf{u}}{\partial t} + u^{\text{out}} \frac{\partial \mathbf{u}}{\partial x_1} = \mathbf{0} \qquad \text{on} \quad \Gamma_{\text{out}} \times (0, T) \tag{134}$$

where u^{out} is calculated such that overall conservation is maintained (i.e., the mass flux through the outflow boundary equals the mass flux through the inflow boundary). Fi-

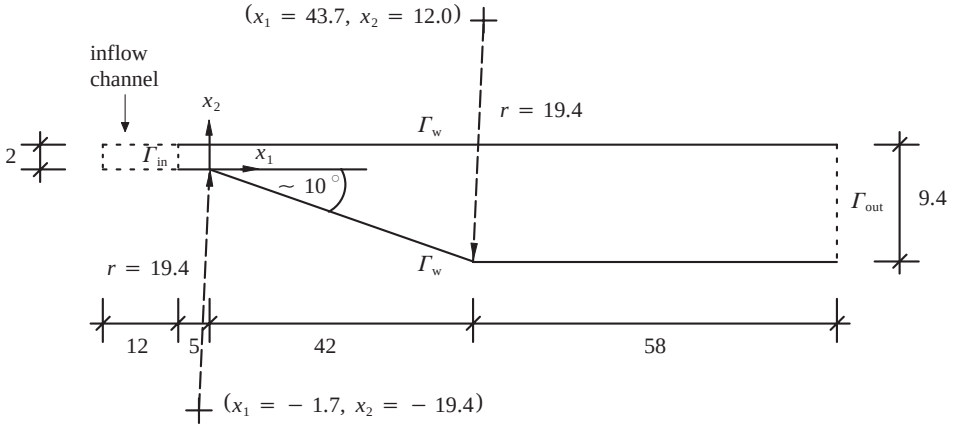

Figure 20. Diffuser geometry in $x_1 - x_2$-plane

nally, periodic boundary conditions are assumed on the boundaries in x_3-direction (i.e., this periodicity is assumed orthogonal to the depiction in Figure 20).

Flow at Reynolds number $\mathrm{Re}_\tau = u_\tau \delta_\mathrm{c}/\nu = 500$ is simulated in the inflow channel. The velocity at the outlet plane of the inflow channel represents the inflow velocity $\mathbf{u}^\mathrm{in}$ for the diffuser. The Reynolds number for the flow in the diffuser is determined based on the streamwise bulk mean velocity u_b (i.e., $\mathrm{Re}_\mathrm{b} = u_\mathrm{b}\delta_\mathrm{c}/\nu$). The corresponding Reynolds numbers Re_b range from about 10,800 to 11,200 and are, thus, slightly higher than 9,000, which is the approximate Reynolds number in the aforementioned experimental and numerical studies. However, the flow appears to be insensitive to the Reynolds number in this higher Reynolds number range according to Kaltenbach *et al.* [98].

The inflow channel is spatially discretized using 80, 64, and 80 control volumes in x_1-, x_2-, and x_3- direction, respectively. The distribution of control volumes in the wall-normal direction obeys a cosine function refining towards the walls for the parent grid, with the isotropic subdivison procedure subsequently applied. Compared to the discretization of the inflow channel in Wu *et al.* [162], which employed 128 control volumes in each coordinate direction, less than 20% the number of control volumes are used in the present case. The actual diffuser including inlet and outlet channel is discretized using 290, 64, and 80 control volumes in x_1-, x_2-, and x_3-direction, respectively. The control volumes are uniformly distributed in the spanwise direction as in the inflow channel. In the wall-normal direction, the same cosine function for refinement towards the walls is used as in the inflow channel. This leads to an equivalent distribution in the inlet channel, which is then spreaded in the asymmetric part of the diffuser. In the streamwise direction, the following control volume distribution is employed: in the inlet channel, h_1 decreases linearly from 0.15 to 0.05, in the asymmetric diffuser part, h_1 increases linearly from 0.05 to 0.475, in the first part of the outlet channel (ranging from $x_1 = 42$ to $x_1 = 74.5$), h_1 increases linearly from 0.475 to 0.825, and in the remaining part of the outlet channel, the control volumes are uniformly distributed with $h_1 = 0.825$. Comparing the discretization of the diffuser to the finer discretization in Wu et al. [162], which employed 590, 100, and 110 control volumes in x_1-, x_2-, and x_3-direction, respectively, it is stated that less than 23% the number of control volumes are used in the present case.

Both for the inflow channel and the diffuser simulation, the time step δt is fixed to be 0.002. 5,000 time steps are performed to allow the flow to develop, and the statistics as well as the inflow velocity data are collected during another 10,000 time steps. As a consequence, inflow data for 20 time units are available, which represents a sufficient period

for a fluid particle to be convected over a distance roughly equal to the streamwise diffuser dimension, including inlet and outlet channel. In the actual diffuser simulation, 40,000 time steps, corresponding to 80 time units, are performed to allow the flow to develop, and the statistics are collected during another 40,000 time steps. Thus, the inflow data are recycled 8 times during the diffuser simulation. The characteristic length scale ratios $\bar{h}/h$ for the various scale-separating operators are chosen as in the previous example.

In the diffuser, the mean streamwise velocity $\langle u_1^h \rangle$ is evaluated as profiles in the wall-normal direction at four different locations in streamwise direction. These locations are distributed along the diffuser as follows: one behind the entry to the asymmetric diffuser section ($x_1 = 6.4$), one in the middle ($x_1 = 22.4$), one close to the end ($x_1 = 38.4$), and one in the outlet channel ($x_1 = 58.4$). These locations correspond to locations where experimental as well as numerical results are available from the studies in Obi *et al.* [126] and Wu *et al.* [162]. The mean values in the diffuser are obtained by averaging over all time steps of the statistical period as well as over the homogeneous x_3-direction. In the diagrams, they are scaled by the streamwise bulk mean velocity u_b. The velocity results are compared to the numerical data from Wu *et al.* [162], hereafter refered to as "Wu-LES", and to the experimental data from Obi *et al.* [126], hereafter refered to as "Obi-experiment".

Both along the upper and lower wall of the diffuser, the wall static pressure coefficient defined as

$$C_{p_\mathrm{w}}(x_1) = \frac{\langle p_\mathrm{w}^h \rangle(x_1) - \langle p_\mathrm{w}^h \rangle(x_1 = -5)}{\frac{1}{2}\rho u_\mathrm{b}^2} \tag{135}$$

where p_w^h denotes the discrete pressure value at the wall, and the skin friction coefficient subject to

$$C_\mathrm{f}(x_1) = \frac{\langle \tau_\mathrm{w}^h \rangle(x_1)}{\frac{1}{2}\rho u_\mathrm{b}^2} \tag{136}$$

where τ_w^h denotes the discrete value of the wall shear stress, are evaluated as functions of the streamwise direction x_1, respectively. In both (135) and (136), the fluid density ρ is assumed to be of unit value. The results for the two coefficients in (135) and (136) are compared to the numerical data from the Wu-LES. Furthermore, the results for the skin friction coefficient are compared to the experimental data from Buice and Eaton [18], hereafter refered to as "Buice-experiment". Due to the fact that the reference pressure value was chosen at a different location in the Buice-experiment, namely $x_1 = -3.4$ for the present configuration, it is not possible to accurately compare the results for the wall static pressure coefficient as well.

The results for the wall static pressure coefficient along the upper and lower wall of the diffuser are displayed in Figures 21 and 22, respectively. Overall, it is stated that all methods tend to overpredict $C_{p\mathrm{w}}$ compared to the results from the Wu-LES, and that the results are qualitatively the same for both the upper and the lower wall. The most remarkable observation is that the best and worst approximations are both produced by the same method. CMS-PM yields results which are very close to the results from the Wu-LES. On the contrary, CMS-SM yields by far the worst results. The second best results are obtained with DS-PM, which slightly outperforms DMS-PM. NM produces the worst results in terms of the pressure gradient component in streamwise direction. It predicts the highest value of all methods for the adverse pressure *gradient* at the diffuser throat and further downstream, and then changes relatively rapidly again, almost predicting a slightly favorable pressure gradient in the rear part of the diffuser, where a slightly adverse pressure gradient is expected.

Figures 23 and 24 depict the results for the skin friction coefficient along the upper and lower wall of the diffuser, respectively. Results from the Wu-LES are not available for the

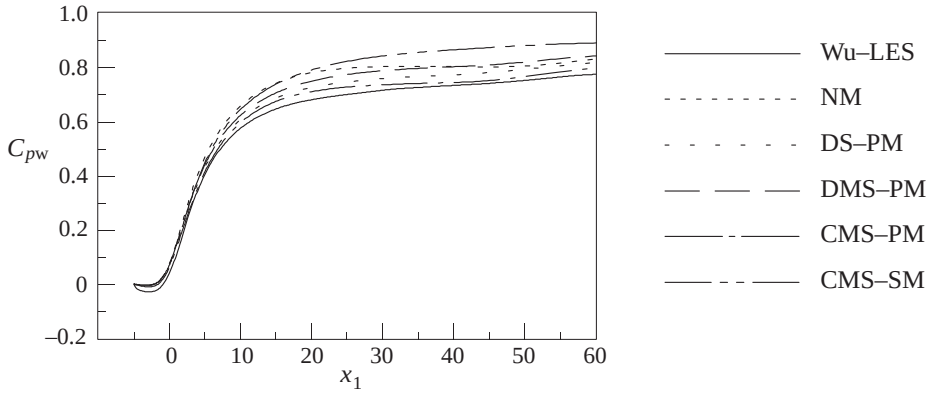

Figure 21. Wall static pressure coefficient along the upper wall of the diffuser

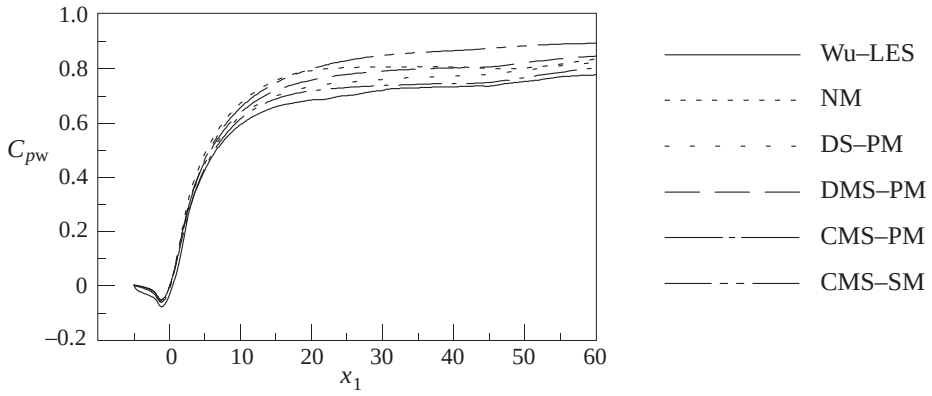

Figure 22. Wall static pressure coefficient along the lower wall of the diffuser

inlet channel at both walls. At the lower wall, the first value was measured at $x_1 \approx 10$ in the Buice-experiment. Nevertheless, the values for the inlet channel are also included for the present methods in both diagrams. Qualitative comparison with the respective results in Kaltenbach *et al.* [98] confirm the reasonability of the results in the inlet channel, in particular the abrupt drop of C_f to approximately zero close to the diffuser throat at the lower deflected wall. For the upper wall, it may be stated that all methods tend to underpredict C_f compared to the results from the Wu-LES and the Buice-experiment, with one exception. The worst results are again produced by CMS-SM. The profile for NM is closest to the ones from the Wu-LES and the Buice-experiment immediately behind the diffuser throat, but gets worse in its prediction further downstream. DS-PM yields a fairly good prediction throughout the diffuser, and DMS-PM again produces worse results than DS-PM. Although the results for CMS-PM are worse than the one for NM immediately behind the diffuser throat, the predicition is again the best overall. It is the only method yielding results which almost match the experimental results in the section of the diffuser between $x_1 \approx 18$ and $x_1 \approx 46$ at the upper wall. In this part of the diffuser, which is approximately the region where the flow is separated, as will be seen below, CMS-PM appears to produce even better results than the substantially finer Wu-LES. Furthermore, it seems to be the only one of the present methods which would have been able to predict the first point from the Buice-experiment at $x_1 \approx -10$, if the inlet channel had been elongated. A complete comparison at the lower wall may only be done from $x_1 \approx 10$, where the experimental data is available. After producing results close to the one from the

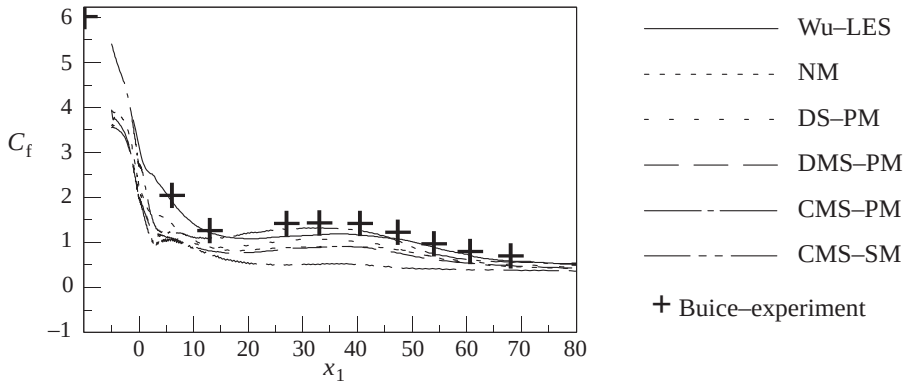

Figure 23. Skin friction coefficient (factor 1000) along the upper wall of the diffuser

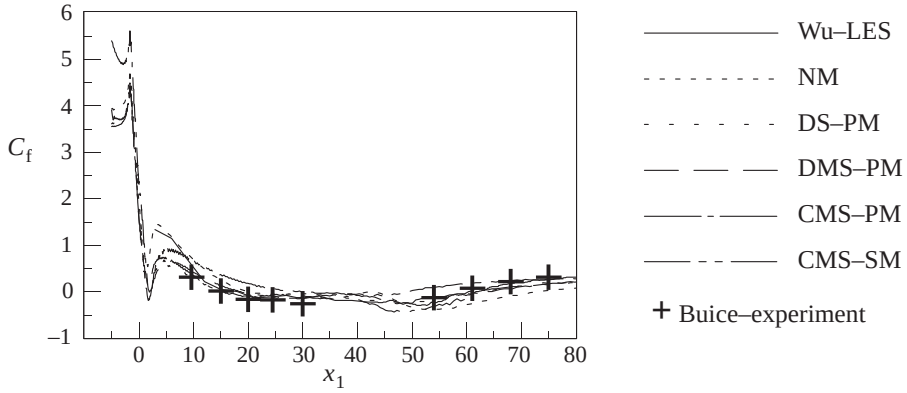

Figure 24. Skin friction coefficient (factor 1000) along the lower wall of the diffuser

Wu-LES immediately behind the diffuser throat, NM gets worse in its prediction further downstream. CMS-SM overpredicts the profile from $x_1 \approx 10$ throughout the diffuser. DS-PM, DMS-PM, and CMS-PM yield very similar results at the lower wall, representing a very good prediction from $x_1 \approx 15$ throughout the diffuser, compared to both the data from the Wu-LES and the Buice-experiment.

In Figures 25–28, the profiles for the mean streamwise velocity at the four locations along the diffuser specified above are displayed. Behind the entry to the asymmetric diffuser section, all methods predict a velocity profile which is in qualitative agreement with the ones from the Wu-LES and the Obi-experiment, although all of them underpredict the maximum velocity, see Figure 25. The best prediction is produced by CMS-PM followed by DS-PM, DMS-PM, CMS-SM, and NM in descending order of their quality of approximation. CMS-PM even appears to underpredict the experimental data by approximately the same amount as the Wu-LES overpredicts. The second location depicted in Figure 26 is slightly more than halfway down the diffuser, and the flow separation, which should be expected at $x_1 \approx 16$ according to the Buice-experiment, has already taken place. By observing Figure 26 as well as Figures 27 and 28, it is apparent that CMS-SM is inadequate, since it is the only method failing to predict the flow separation. The best approximation of the results from the Obi-experiment in Figure 26 is provided by CMS-PM and the second best by DS-PM, both being even closer to the experimental data than the Wu-LES towards the lower wall. Compared to the experimental data, the Wu-LES does not predict the separation point as accurately as CMS-PM and DS-PM. At the next location further downstream

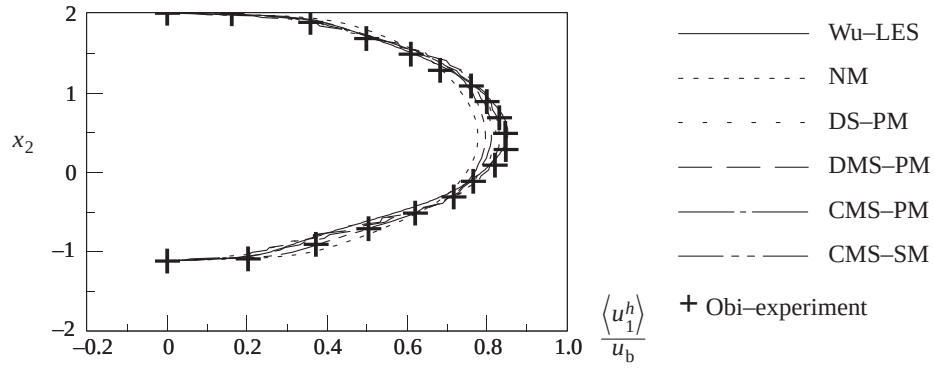

Figure 25. Mean streamwise velocity at $x_1 = 6.4$

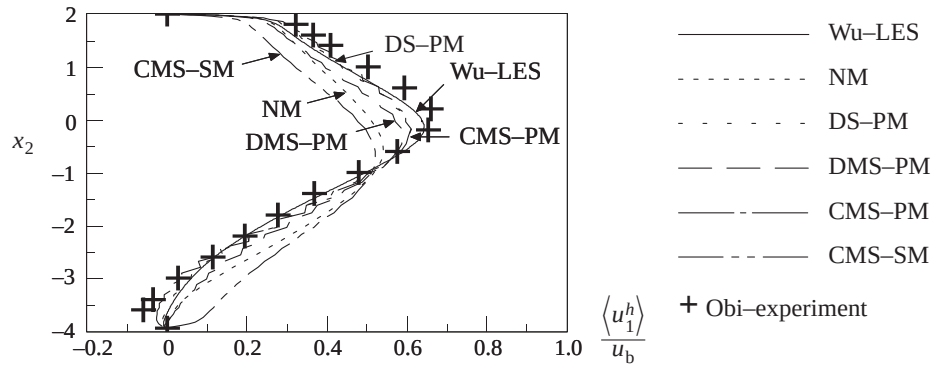

Figure 26. Mean streamwise velocity at $x_1 = 22.4$

depicted in Figure 27, CMS-PM almost matches the experimental data in the lower part of the diffuser, predicting the reversed flow very accurately. In the outlet channel, this very good approximation cannot be completely maintained, see Figure 28. DMS-PM is less accurate at all three locations shown in Figures 26-28. Aside from CMS-SM, NM produces the worst prediction, with the exception of Figure 27 (i.e., close to the end of the asymmetric diffuser section), where it is, at least, slightly better than DMS-PM. However, the most obvious failure of NM is its clear overestimation of the recirculating velocity in the outlet channel. Thus, it does not provide a reasonable approximation of the flow separation as well as the reattachment point, which should be expected at $x_1 \approx 52$ according to the Buice-experiment.

For profiles showing the root-mean-square velocity in streamwise and wall-normal direction, it is refered to Gravemeier [59]. Results from explicit investigations of the small scales, the dynamically determined parameter of the subgrid-scale model, and the subgrid viscosity introduced by the model may also be found in Gravemeier [59]. Evaluating the necessary computational effort provides the following numbers. Setting the computational effort for NM to 1.0, the relative measures for CMS-PM, CMS-SM, DS-PM, and DMS- PM are approximately 1.08, 1.34, 1.27, and 1.32, respectively. These numbers are even more impressively in favor of CMS-PM than the ones for the channel. Thus, it is confirmed that CMS in combination with PM is a very efficient method computationally, in the present case substantially more efficient than, for instance, DS. As in the previous flow example, the numbers increase drastically for CMS in combination with the scale-separating operator SM.

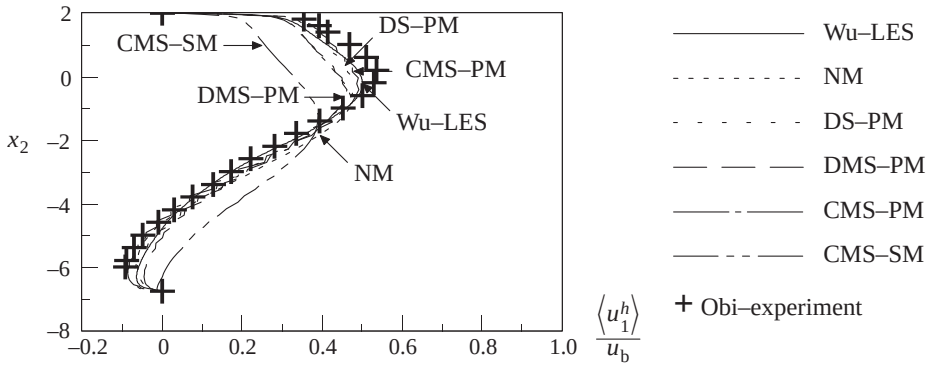

Figure 27. Mean streamwise velocity at $x_1 = 38.4$

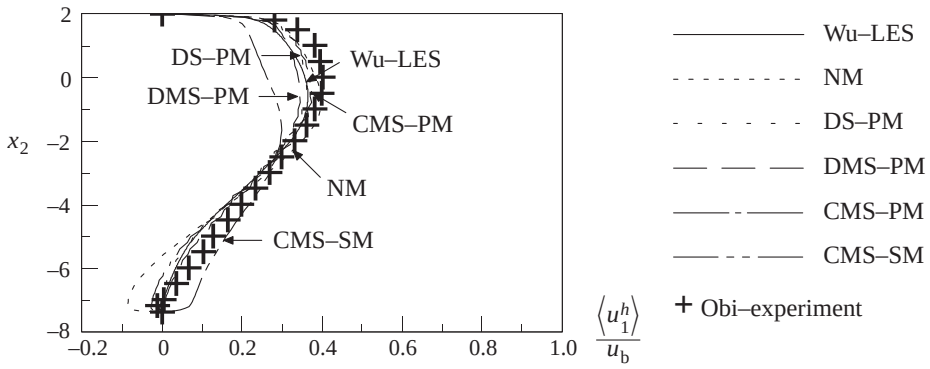

Figure 28. Mean streamwise velocity at $x_1 = 58.4$

5.3.3 Summary of observations

Taking into account all results for both test cases provided in Gravemeier [58] and Gravemeier [59], the most important observations are summarized as follows.

- Taking into account all flow aspects investigated in the context of the channel and the diffuser, CMS-PM has provided the most accurate predictions overall. Only one shortcoming is noted: a slight underprediction of the mean streamwise velocity profile in the buffer layer of the channel.

- Aside from the observation that it has produced the best results overall, CMS-PM has also represented the most computationally efficient approach. This advantage of CMS-PM appears to increase with increasing problem size, as the comparison of the numbers for the diffuser problem to the smaller channel problem indicate.

- Both positive features linked with CMS-PM have to be attributed to the use of the projective scale-separating operator PM in this context. Already for the channel flow application, PM has outperformed traditional discrete smooth filters, both in terms of quality of results and required computational effort. In the diffuser flow application, the alternative multigrid scale-separating operator SM has failed to predict one of the most important aspects of the diffuser flow. Furthermore, a comparison of the computational effort has emphasized the superiority of PM over SM. Thus, the theoretical especialness of a projective operator has been confirmed in the practical applications.

- A surprising result is that DMS-PM has not been proven to be a superior alternative to CMS-PM, despite its more sophisticated (and, simultaneously, more expensive) subgrid- scale modeling approach. Throughout all investigations, it has produced less accurate predictions. In contrast to the channel flow application, it has also yielded worse results than DS-PM in the diffuser application. The latter observation appears to be related to the relatively coarser discretization level applied to the diffuser, and is thus consistent with similar observations by Hughes *et al.* [88] in the context of homogeneous isotropic turbulence.

- A potential explanation for the success of CMS-PM in the channel flow application was given in Gravemeier [58] by analyzing the crucial benefit of adding a substantial amount of subgrid viscosity to the small resolved scales, particularly in the buffer layer of the channel. Similar mechanisms might also guarantee its success in the present diffuser application. A still existing potential deficiency due to the inability to account for backscatter with the present subgrid-scale models was also addressed in Gravemeier [58].

Finally, it is emphasized that these perceptions have been gained in the context of the particular implementation in a second-order accurate FVM. The results from the turbulent channel flow example, which have been briefly shown here and can be found in more detail in Gravemeier [58], may be compared to the results from the same flow example for applications of the variational multiscale LES within a spectral method in Holmen *et al.* [74], Hughes *et al.* [85], and Oberai and Hughes [123], in the first reference with dynamic subgrid-scale modeling. A direct comparison of the results achieved with the constant-coefficient and the dynamic Smagorinsky model in those references is not available. However, a cross-comparison appears to indicate that the influence of a dynamic modeling procedure within the multiscale environment is less favorable for a FVM than for a spectral method.

6 CONCLUSIONS AND FUTURE RESEARCH DIRECTIONS

The variational multiscale method has been presented as a new approach for the numerical simulation of laminar and turbulent flows. In particular, for the simulation of turbulent flows, this new approach has been refered to as a variational multiscale large eddy simulation. The main focus of this article has been on reviewing the practical realization of the theoretically prescribed variational projection for separating the spectrum of resolved scales into larger and smaller resolved scales. For this purpose, several solution strategies have been addressed and classified, where the emphasis has been on viable approaches within the finite element and finite volume method. The unresolved scales of the problem have been taken into account by constant-coefficient and dynamic subgrid-scale modeling based on the Smagorinsky model, which has been the usual procedure in the applications to date. Potential stabilizing features, which are inherent in some of the solution strategies, have been addressed. At the end of this article, results from the numerical simulation of a laminar as well as two turbulent flow examples have been presented and analyzed.

Two main features of the variational multiscale method make it a well-suited framework for the numerical simulation of laminar and, in particular, turbulent flows. On the one hand, replacing the traditional filtering approach by a variational projection obviates filtering problems particularly encountered in bounded flow domains as soon as the boundary is approached. On the other hand, the restriction of the direct influence of the subgrid-scale model to the smaller resolved scales corresponds better to the quantification of Richardson's energy cascade than the traditional approach, which directly influences all resolved scales by the model. However, there are still aspects demanding for further investigation. In the author's opinion, some of them are:

- the "surrounding" numerical method,
- a more flexible treatment of the scale groups in terms of the influence of the subgrid-scale model, and
- a more sophisticated inclusion of the unresolved scales of the problem (i.e., improved subgrid-scale modeling).

The numerical method within which the variational multiscale approach is applied has a huge influence on the actual performance. Already in the traditional large eddy simulation, it has often been learned that the application of the same subgrid-scale model within two different numerical methods might lead to larger discrepancies than the application of two different subgrid-scale models within the same numerical method. Due to the restriction of the model's influence to only part of the resolved scale range, this dependence appears to be reduced to a certain degree. Nevertheless, it is still existent. As mentioned in the context of the turbulent channel flow example, a realization within a second-order accurate finite volume method appears to lead to different results compared to the application within a spectral method. Oberai et al. [122] were able to show a strong dependence on the numerical method for the relatively simple flow problem of homogeneous isotropic turbulence by comparing a finite element and a spectral method (The specific role of spectral methods in comparison to the other numerical methods has already been mentioned in Section 3.2.3). In view of future applications in more complex geometries, a good performance of the variational multiscale method in the computational environments emphasized in this article (i.e., the finite element and finite volume method, which are basically suited for unstructured grid applications) appears to be of particular relevance.

So far, two scale groups within the range of resolved scales have been distinguished (i.e., large and small resolved scales). The large scales are then resolved without any direct model influence, and the small scales receive the direct model influence completely. Although this "model distribution" appears to be closer to the perceptions of turbulence theory than the traditional way of applying the model to all resolved scales, an even more flexible distribution of the model influence might be instrumental in achieving improved results. In order to give an example for the sake of imagination, one may think of a distribution of about 25% of the model influence to the large resolved scales and the remaining 75% to the small resolved scales. Combined with a variation of the model distribution, the relative sizes of the large- and small-scale space may also be varied, which leaves a multitude of "set screws" to be turned, as already discussed at the end of Section 2.5.

Of course, thinking about altering the distribution of the model influence within the resolved scale groups and the relative sizes of these groups does not improve the subgrid-scale model itself. The subgrid-scale model in the form applied so far (i.e., as a constant-coefficient or dynamic Smagorinsky model based on the subgrid viscosity concept) is still a weak point, from the author's point of view. The limitations and, consequently, potential deficiencies not only of the simple Smagorinsky model realization (see Section 4.1), but also of the underlying subgrid viscosity concept, in general, have been addressed in the respective literature (see, e.g., Sagaut [138] and Wilcox [161]). As only one aspect in this context, the inability of this concept to adequately take into account the (relatively weak but existing) backscatter process has to be mentioned. A residual-based variant of the variational multiscale method for LES of turbulent flows, which has recently been developed by Calo [19], should be mentioned as a new approach beyond the subgrid viscosity concept. This new variant may be regarded as a sophisticated stabilized method, which takes into account the non-linear nature of the underlying Navier-Stokes problem. It obviates the use of a subgrid-scale model based on the subgrid viscosity concept. This method has been applied to the problem of bypass transition of a boundary layer, and it is refered to Calo

[19] for further elaboration. Several other approaches going beyond modeling based on the subgrid viscosity concept have been developed for the traditional way of performing large eddy simulation (see, e.g., the survey in Sagaut [138]), and might also be favorably integrated in the framework of the variational multiscale large eddy simulation in the future.

ACKNOWLEDGEMENTS

The author would like to express his sincere appreciation to Ekkehard Ramm and Wolfgang Wall for their support during his PhD studies at the University of Stuttgart in 2000-2003. In those years, the basis for this article was established. The author's postdoctoral research stay at the Center for Turbulence Research at Stanford University in 2004, during which another considerable part of the author's work involved in this article originated, was supported by a Feodor Lynen Research Fellowship of the Alexander von Humboldt-Foundation. The support through this Fellowship, which was jointly funded by the Center for Turbulence Research and the Alexander von Humboldt-Foundation, is gratefully acknowledged. The author is also grateful to Greg Burton, Frank Ham, Parviz Moin, and Xiaohua Wu for helpful discussions during that time.

REFERENCES

1 Baiocchi, C., Brezzi, F. and Franca, L.P. (1993). Virtual bubbles and Galerkin-least-squares type methods. *Comput. Methods Appl. Mech. Engrg.*, **105**, 125–141.

2 Barbone, P. and Harari, I. (2001). Nearly H1-optimal finite element methods. *Comput. Methods Appl. Mech. Engrg.*, **190**, 5679–5690.

3 Bardina, J., Ferziger, J.H. and Reynolds, W.C. (1983). Improved turbulence models based on large eddy simulation of homogeneous, incompressible, turbulent flows. Report TF-19, Thermosciences Division, Department of Mechanical Engineering, Stanford University.

4 Baumann, C.E. and Oden, J.T. (1999). A discontinuous hp finite element method for the Euler and Navier-Stokes equations. *Int. J. Numer. Meth. Fluids*, **31**, 79–95.

5 Boussinesq, J. (1877). Thorie de l'Écoulement Tourbillant. *Mem. Présentés par Divers Savants Acad. Sci. Inst. Fr.*, **23**, 46–50.

6 Bradshaw, P. (1994). Turbulence: the chief outstanding difficulty of our subject. *Exp. Fluids*, **16**, 203–216.

7 Brezzi, F. (2000). Interacting with the subgrid world. In Griffiths, D.F. and Watson, G.A. (Eds.): Numerical Analysis 1999, Chapman & Hall/CRC, Boca Raton, FL, 69–82.

8 Brezzi, F. (2002). Recent results in the treatment of subgrid scales. In Blouza, A., Danaila, I., Joly, P., Kaber, S.M., Lucquin, B., Murat, F. and Postel, M. (Eds.): *Editeurs ESAIM: Proceedings Volume 11*, 61–84.

9 Brezzi, F., Bristeau, M.-O., Franca, L.P., Mallet, M. and Roge, G. (1992). A relationship between stabilized finite element methods and the Galerkin method with bubble functions. *Comput. Methods Appl. Mech. Engrg.*, **96**, 117–129.

10 Brezzi, F. and Fortin, M. (1991), *Mixed and hybrid finite element methods*, Springer, New York.

11 Brezzi, F., Franca, L.P., Hughes, T.J.R. and Russo, A. (1996). Stabilization techniques and subgrid scale capturing. Pubb. 1011, Istituto di Analisi Numerica, Pavia.

12 Brezzi, F., Franca, L.P., Hughes, T.J.R. and Russo, A. (1997). "$b = \int g$". *Comput. Methods Appl. Mech. Engrg.*, **145**, 329–339.

13 Brezzi, F., Franca, L.P. and Russo, A. (1998). Further considerations on residual-free bubbles for advective-diffusive equations. *Comput. Methods Appl. Mech. Engrg.*, **166**, 25–33.

14 Brezzi, F., Houston, P., Marini, D. and Süli, E. (2000). Modeling subgrid viscosity for advection-diffusion problems. *Comput. Methods Appl. Mech. Engrg.*, **190**, 1601–1610.

15 Brezzi, F. and Marini, L.D. (2002). Augmented spaces, two-level methods and stabilizing subgrids. *Int. J. Numer. Meth. Fluids*, **40**, 31–46.

16 Brezzi, F. and Russo, A. (1994). Choosing bubbles for advection-diffusion problems. *Math. Models Methods Appl. Sci.*, **4**, 571–587.

17 Brooks, A.N. and Hughes, T.J.R. (1982). Streamline upwind/Petrov-Galerkin formulations for convection dominated flows with particular emphasis on the incompressible Navier-Stokes equations. *Comput. Methods Appl. Mech. Engrg.*, **32**, 199–259.

18 Buice, C.U. and Eaton, J.K. (1997). Experimental investigation of flow through an asymmetric plane diffuser. Report TSD-107, Thermosciences Group, Department of Mechanical Engineering, Stanford University.

19 Calo, V.M. (2004). Residual-based multiscale turbulence modeling: finite volume simulations of bypass transition. PhD Thesis, Department of Civil and Environmental Engineering, Stanford University (http://www.ices.utexas.edu/victor/vmc-thesis.pdf).

20 Carati, D., Ghosal, S. and Moin, P. (1995). On the representation of backscatter in dynamic localization models. *Phys. Fluids*, **7**, 606–616.

21 Cockburn, B., Karniadakis, G.E. and Shu, C.-W. (Eds.) (2000). Discontinuous Galerkin methods - theory, computation and applications, *Lecture Notes in Computational Science and Engineering*, **11**, Springer, Berlin.

22 Codina, R. (1998). Comparison of some finite element methods for solving the diffusion-convection-reaction equation. *Comput. Methods Appl. Mech. Engrg.*, **156**, 185–210.

23 Codina, R. (2001). A stabilized finite element method for generalized stationary incompressible flows. *Comput. Methods Appl. Mech. Engrg.*, **190**, 2681–2706.

24 Codina, R. (2002). Stabilized finite element approximation of transient incompressible flows using orthogonal subscales. *Comput. Methods Appl. Mech. Engrg.*, **191**, 4295–4321.

25 Collis, S.S. (2001). Monitoring unresolved scales in multiscale turbulence modeling. *Phys. Fluids*, **13**, 1800–1806.

26 Collis, S.S. (2002). Discontinuous Galerkin methods for turbulence simulation. In: Proceedings of the Summer Program 2002, Center for Turbulence Research, Stanford University and NASA Ames Research Center, 155–167.

27 Collis, S.S. (2002). The DG/VMS method for unified turbulence simulation. AIAA Paper 2002-3124, St. Louis, Missouri, June 24–27.

28 Deardorff, J.W. (1970). A numerical study of three-dimensional turbulent channel flow at large Reynolds numbers. *J. Fluid Mech.*, **41**, 453–465.

29 Domaradzki, J.A., Loh, K.C. and Yee, P.P. (2002). Large eddy simulations using the subgrid-scale estimation model and truncated Navier-Stokes dynamics. *Theoret. Comput. Fluid Dyn.*, **15**, 421–450.

30 Donea, J. and Huerta, A. (2003). *Finite element methods for flow problems*, John Wiley & Sons, Chichester.

31 Dubois, T., Jauberteau, F. and Temam, R. (1999). *Dynamic multilevel methods and the numerical simulation of turbulence*, Cambridge University Press, Cambridge.

32 Engel, G., Garikipati, K., Hughes, T.J.R., Larson, M.G., Mazzei, L. and Taylor, R.L. (2002). Continuous/discontinuous finite element approximations of fourth-order elliptic problems in structural and continuum mechanics with applications to thin beams and plates, and strain gradient elasticity. *Comput. Methods Appl. Mech. Engrg.*, **191**, 3669–3750.

33 Ethier, C.R. and Steinman, D.A. (1994). Exact fully 3D Navier-Stokes solution for benchmarking. *Int. J. Numer. Meth. Fluids*, **19**, 369–375.

34 Ferziger, J.H. and Peric, M. (1999). *Computational methods for fluid dynamics*, 2nd edition, Springer, Berlin.

35 Farhat, C., Harari, I. and Franca, L.P. (2001). The discontinuous enrichment method. *Comput. Methods Appl. Mech. Engrg.*, **190**, 6455–6479.

36 Farhat, C., Harari, I. and Hetmaniuk, U. (2003). The discontinuous enrichment method for multiscale analysis. *Comput. Methods Appl. Mech. Engrg.*, **192**, 3195–3209.

37 Farhat, C., Rajasekharan, A. and Koobus, B. (2006). A dynamic variational multiscale method for large eddy simulations on unstructured meshes. *Comput. Methods Appl. Mech. Engrg.*, **195**, 1667–1691.

38 Franca, L.P. and Farhat, C. (1995). Bubble functions prompt unusual stabilized finite element methods. *Comput. Methods Appl. Mech. Engrg.*, **123**, 299–308.

39 Franca, L.P., Farhat, C., Lesoinne, M. and Russo, A. (1998). Unusual stabilized finite element methods and residual free bubbles. *Int. J. Numer. Meth. Fluids*, **27**, 159–168.

40 Franca, L.P. and Frey, S. (1992). Stabilized finite element methods: II. The incompressible Navier- Stokes equations. *Comput. Methods Appl. Mech. Engrg.*, **99**, 209–233.

41 Franca, L.P., Frey, S. and Hughes, T.J.R. (1992). Stabilized finite element methods: I. Application to the advective-diffusive model. *Comput. Methods Appl. Mech. Engrg.*, **95**, 253–276.

42 Franca, L.P. and Macedo, A.P. (1998). A two-level finite element method and its application to the Helmholtz equation. *Int. J. Numer. Meth. Engrg.*, **43**, 23–32.

43 Franca, L.P., Madueira, A.L. and Valentin, F. (2005). Towards multiscale functions: enriching finite element spaces with local but not bubble-like functions. *Comput. Methods Appl. Mech. Engrg.*, **194**, 3006–3021.

44 Franca, L.P. and Nesliturk, A. (2001). On a two-level finite element method for the incompressible Navier-Stokes equations. *Int. J. Numer. Meth. Engrg.*, **52**, 433–453.

45 Franca, L.P., Nesliturk, A. and Stynes, M. (1998). On the stability of residual-free bubbles for convection-diffusion problems and their approximation by a two-level finite element method. *Comput. Methods Appl. Mech. Engrg.*, **166**, 35–49.

46 Franca, L.P. and Oliveira, S.P. (2003). Pressure bubbles stabilization features in the Stokes problem. *Comput. Methods Appl. Mech. Engrg.*, **192**, 1929–1937.

47 Franca, L.P., Ramalho, J.V.A. and Valentin, F. (2005). Multiscale and residual-free bubble functions for reaction-advection-diffusion problems. *Int. J. Multiscale Comput. Engrg.*, **3**, 297–312.

48 Franca, L.P. and Russo, A. (1996). Approximation of the Stokes problem by residual-free macro bubbles. *East-West J. Numer. Math.*, **4**, 265–278.

49 Franca, L.P. and Valentin, F. (2000). On an improved unusual stabilized finite element method for the advective-reactive-diffusive equation. *Comput. Methods Appl. Mech. Engrg.*, **190**, 1785–1800.

50 Fröhlich, J. and Rodi, W. (2002). Introduction to large eddy simulation of turbulent flows. In Launder, B.E. and Sandham, N.D. (Eds.): *Closure Strategies for Turbulent and Transitional Flows, Cambridge University Press*, Cambridge, 267–298.

51 Gelhard, T., Lube, G., Olshanskii, M.A. and Starcke, J.H. (2005). Stabilized finite element schemes with LBB-stable elements for incompressible flows. *J. Comp. Appl. Math.*, **177**, 243–267.

52 Germano, M. (1992). Turbulence: the filtering approach. *J. Fluid Mech.*, **238**, 325-336.

53 Germano, M., Piomelli, U., Moin, P. and Cabot, W.H. (1991). A dynamic subgrid-scale eddy viscosity model. *Phys. Fluids A*, **3**, 1760–1765.

54 Ghosal, S., Lund, T.S., Moin, P. and Akselvoll, K. (1995). A dynamic localization model for large-eddy simulation of turbulent flows. *J. Fluid Mech.*, **286**, 229–255.

55 Ghosal, S. and Moin, P. (1995). The basic equations for the large-eddy simulation of turbulent flows in complex geometry. *J. Comput. Phys.*, **118**, 24–37.

56 Gravemeier, V. (2003). The variational multiscale method for laminar and turbulent incompressible flow. PhD Thesis, Report No. 40, Institute of Structural Mechanics, University of Stuttgart (http://www.uni-stuttgart.de/ibs/publications/phd/2000/fulltext/phdgravem.pdf).

57 Gravemeier, V. (2004). Variational multiscale large eddy simulation of turbulent flows using a finite volume method. In: *Annual Research Briefs - 2004*, Center for Turbulence Research, Stanford University and NASA Ames Research Center, 131–144.

58 Gravemeier, V. (2006). Scale-separating operators for variational multiscale large eddy simulation of turbulent flows. *J. Comput. Phys.*, **212**, 400–435.

59 Gravemeier, V. (2006). Variational multiscale large eddy simulation of turbulent flow in a diffuser. *Comput. Mech.*, in press, available online.

60 Gravemeier, V. (2006). A consistent dynamic localization model for large eddy simulation of turbulent flows based on a variational formulation. *J. Comput. Phys.*, in press, available online.

61 Gravemeier, V., Wall, W.A. and Ramm, E. (2004). A three-level finite element method for the instationary incompressible Navier-Stokes equations. *Comput. Methods Appl. Mech. Engrg.*, **193**, 1323–1366.

62 Gravemeier, V., Wall, W.A. and Ramm, E. (2004). Large eddy simulation of turbulent incompressible flows by a three-level finite element method. *Int. J. Numer. Meth. Fluids.*, **48**, 1067–1099.

63 Gresho, P.M. and Sani, R.L. (1998). *Incompressible flow and the finite element method: advection-diffusion and isothermal laminar flow*, John Wiley & Sons, Chichester.

64 Guermond, J.-L. (1999). Stabilization of Galerkin approximations of transport equations by subgrid modeling. *Math. Mod. Num. Anal.*, **33**, 1293–1316.

65 Guermond J.-L., Oden, J.T. and Prudhomme, S. (2004). Mathematical perspectives on large eddy simulation models for turbulent flows. *J. Math. Fluid Mech.*, **6**, 194–248.

66 Ham, F., Apte, S., Iaccarino, G., Wu, X., Herrmann, M., Constantinescu, G., Mahesh, K. and Moin, P. (2003). Unstructured LES of reacting multiphase flows in realistic gas turbine combustors. In: *Annual Research Briefs - 2003*, Center for Turbulence Research, Stanford University and NASA Ames Research Center, 139–160.

67 Ham, F. and Iaccarino, G. (2004). Energy conservation in collocated discretization schemes on unstructured meshes. In: *Annual Research Briefs - 2004*, Center for Turbulence Research, Stanford University and NASA Ames Research Center, 3–14.

68 Hansbo, P. and Szepessy, A. (1990). A velocity-pressure streamline diffusion finite element method for the incompressible Navier-Stokes equations. *Comput. Methods Appl. Mech. Engrg.*, **84**, 175–192.

69 Harari, I., Franca, L.P. and Oliveira, S.P. (2001). Streamline design of stability parameters for advection-diffusion problems. *J. Comput. Phys.*, **171**, 115–131.

70 Haselbacher, A. and Vasilyev, O. (2003). Commutative discrete filtering on unstructured grids based on least-squares techniques. *J. Comput. Phys.*, **187**, 197–211.

71 Haworth, D.C. and Jansen, K. (2000). Large-eddy simulation on unstructured deforming meshes: towards reciprocating IC engines. *Comput. Fluids*, **29**, 493–524.

72 Hirsch, C. (1988), *Numerical computation of internal and external flows, Vol. I: Fundamentals of numerical discretization*, John Wiley & Sons, New York.

73 Hirsch, C. (1990), *Numerical computation of internal and external flows, Vol. II: Computational methods for inviscid and viscous flows*, John Wiley & Sons, New York.

74 Holmen, J., Hughes, T.J.R., Oberai, A.A. and Wells, G.N. (2004). Sensitivity of the scale partition for variational multiscale large-eddy simulation of channel flow. *Phys. Fluids*, **1**6, 824–827.

75 Hou, T.Y. and Wu, X.-H. (1997). A multiscale finite element method for elliptic problems in composite materials and porous media. *J. Comput. Phys.*, **134**, 169–189.

76 Hughes, T.J.R. (1995). Multiscale phenomena: Green's functions, the Dirichlet-to-Neumann formulation, subgrid scale models, bubbles and the origins of stabilized methods. *Comput. Methods Appl. Mech. Engrg.*, **127**, 387–401.

77 Hughes, T.J.R. (2000). *The finite element method: linear static and dynamic finite element analysis*, Dover, Mineola, NY.

78 Hughes, T.J.R., Engel, G., Mazzei, L. and Larson, M.G. (2000). The continuous Galerkin method is locally conservative. *J. Comput. Phys.*, **163**, 467–488.

79 Hughes, T.J.R., Feijoo, G.R., Mazzei, L. and Quincy, J.-B. (1998). The variational multiscale method-a paradigm for computational mechanics. *Comput. Methods Appl. Mech. Engrg.*, **166**, 3–24.

80 Hughes, T.J.R., Franca, L.P. and Balestra, M. (1986). A new finite element formulation for computational fluid dynamics:V. Circumventing the Babuška-Brezzi condition: A stable Petrov-Galerkin formulation of the Stokes problem accomodating equal-order interpolation. *Comput. Methods Appl. Mech. Engrg.*, **59**, 85–99.

81 Hughes, T.J.R., Franca, L.P. and Hulbert, G.M. (1989). A new finite element formulation for computational fluid dynamics: VIII. The Galerkin/least-squares method for advective-diffusive equations. *Comput. Methods Appl. Mech. Engrg.*, **73**, 173–189.

82 Hughes, T.J.R., Hauke, G., Jansen, K. and Johan, Z. (1994). Stabilized finite element methods in fluids: inspirations, origins, status and recent developments. In Hughes, T.J.R., Oñate, E. and Zienkiewicz, O.C. (Eds.): *Recent Developments in Finite Element Analysis*, CIMNE, Barcelona, 272–292.

83 Hughes, T.J.R., Mazzei, L. and Jansen, K.E. (2000). Large eddy simulation and the variational multiscale method. *Comput. Visual. Sci.*, **3**, 47–59.

84 Hughes, T.J.R., Mazzei, L., Oberai, A.A. and Wray, A.A. (2001). The multiscale formulation of large eddy simulation: decay of homogeneous isotropic turbulence. *Phys. Fluids*, **13**, 505–512.

85 Hughes, T.J.R., Oberai, A.A. and Mazzei, L. (2001). Large eddy simulation of turbulent channel flows by the variational multiscale method. *Phys. Fluids*, **13**, 1784–1799.

86 Hughes, T.J.R., Scovazzi, G. and Franca, L.P. (2004). Multiscale and stabilized methods. In Stein, E., de Borst, R. and Hughes, T.J.R. (Eds.): *Encyclopedia of Computational Mechanics*, John Wiley & Sons, Chichester.

87 Hughes, T.J.R. and Wells, G.N. (2005). Conservation properties for the Galerkin and stabilised forms of the advection-diffusion and incompressible Navier-Stokes equations. *Comput. Methods Appl. Mech. Engrg.*, **194**, 1141–1159.

88 Hughes, T.J.R., Wells, G.N. and Wray, A.A. (2004). Energy transfers and spectral eddy viscosity in large eddy simulations of homogeneous isotropic turbulence: comparison of dynamic Smagorinsky and multiscale models over a range of discretizations. *Phys. Fluids*, **16**, 4044–4052.

89 Idelsohn, S.R. and Oñate, E. (1994). Finite volumes and finite elements: two 'good friends'. Int. J. *Numer. Meth. Engrg.*, **37**, 3323–3341.

90 Jansen, K.E. (1999). A stabilized finite element method for computing turbulence. *Comput. Methods Appl. Mech. Engrg.*, **174**, 299–317.

91 Jansen, K.E., Collis, S.S., Whiting, C. and Shakib, F. (1999). A better consistency for low-order stabilized finite element methods. *Comput. Methods Appl. Mech. Engrg.*, **174**, 153–170.

92 Jansen, K.E. and Tejada-Martinez, A.E. (2002). An evaluation of the variational multiscale model for large-eddy simulation while using a hierarchical basis. *AIAA Paper 2002-0283*, Reno, NV, January 14–17.

93 Jeanmart, H. and Winckelmans, G.S. (2002). Comparison of recent dynamic subgrid-scale models in turbulent channel flow. In: *Proceedings of the Summer Program 2002, Center for Turbulence Research*, Stanford University and NASA Ames Research Center, 105–116.

94 John, V. (2004). *Large eddy simulation of turbulent incompressible flows: analytical and numerical results for a class of LES models*, Lecture Notes in Computational Science and Engineering, **34**, Springer, Berlin.

95 John, V. and Kaya, S. (2005). A finite element variational multiscale method for the Navier-Stokes equations. *SIAM J. Sci. Comp.*, **26**, 1485–1503.

96 John, V., Kaya, S. and Layton, W.J. (2005). A two-level variational multiscale method for convection-diffusion equations. *Technical Report TR-MATH 05-02, Department of Mathematics*, University of Pittsburgh.

97 Johnson, C. and Saranen, J. (1986). Streamline diffusion methods for the incompressible Euler and Navier-Stokes equations. *Math. of Comp.*, **47**, 1–18.

98 Kaltenbach, H.-J., Fatica, M., Mittal, R., Lund, T.S. and Moin, P. (1999). Study of flow in a planar asymmetric diffuser using large-eddy simulation. *J. Fluid Mech.*, **390**, 151–185.

99 Karamanos, G.S. and Karniadakis, G.E. (2000). A spectral vanishing viscosity method for large-eddy simulations. *J. Comput. Phys.*, **163**, 22–50.

100 Kaya, S. and Layton, W.J. (2003). Subgrid-scale eddy viscosity methods are variational multiscale methods. *Technical Report TR-MATH 03-05*, Department of Mathematics, University of Pittsburgh.

101 Kim, D. and Choi, H. (2000). A second-order time-accurate finite volume method for unsteady incompressible flow on hybrid unstructured grids. *J. Comput. Phys.*, **162**, 411–428.

102 Kim, J. and Moin, P. (1985). Application of a fractional-step method to incompressible Navier-Stokes equations. *J. Comp. Phys.*, **21**, 308–323.

103 Koobus, B. and Farhat, C. (2004). A variational multiscale method for the large eddy simulation of compressible turbulent flows on unstructured meshes - application to vortex shedding. *Comput. Methods Appl. Mech. Engrg.*, **193**, 1367–1383.

104 Kolmogorov, A.N. (1941). The local structure of turbulence in incompressible viscous fluid for very large Reynolds numbers. (in Russian), Dokl. Akad. Nauk SSSR, **30**, 299–303.

105 Lallemand, M.H., Steve, H., and Dervieux, A. (1992). Unstructured multigridding by volume agglomeration: current status. *Comput. Fluids*, **21**, 397–433.

106 Layton, W.J. (2003). A mathematical introduction to large eddy simulation. *Technical Report TR-MATH 03-03*, Department of Mathematics, University of Pittsburgh.

107 Leonard, A. (1974). Energy cascade in large eddy simulation of turbulent fluid flow. *Adv. Geophys.*, **18A**, 237–248.

108 Lesieur, M. and Metais, O. (1996). New trends in large-eddy simulations of turbulence. *Ann. Rev. Fluid Mech.*, **28**, 45–82.

109 Lilly, D.K. (1967). The representation of small-scale turbulence in numerical simulation experiments. In: *Proceedings of the IBM Scientific Computing Symposium on Environmental Sciences*, Yorktown Heights, NY.

110 Lilly, D.K. (1992). A proposed modification of the Germano subgrid-scale closure method. *Phys. Fluids A*, **4**, 633–635.

111 Lund, T.S. (1997). On the use of discrete filters for large eddy simulation. In: *Annual Research Briefs - 1997*, Center for Turbulence Research, Stanford University and NASA Ames Research Center, 83–95.

112 Mahesh, K., Constantinescu, G. and Moin, P. (2004). A numerical method for large-eddy simulation in complex geometries. *J. Comput. Phys.*, **197**, 215–240.

113 Marsden, A.L., Vasilyev, O. and Moin, P. (2002). Construction of commutative filters for LES on unstructured meshes. *J. Comput. Phys.*, **175**, 584–603.

114 Mavriplis, D.J. (1997). Adaptive meshing techniques for viscous flow calculations on mixed element unstructured meshes. *ICASE-Report 97-20*, NASA Langley Research Center, Hampton, VA.

115 Meneveau, C. and Katz, J. (2000). Scale-invariance and turbulence models for large-eddy simulation. *Ann. Rev. Fluid Mech.*, **32**, 1–32.

116 Moin, P. (2002). Advances in large eddy simulation methodology for complex flows. *Int. J. of Heat Fluid Flow*, **23**, 710–720.

117 Moin, P. and Mahesh, K. (1998). Direct numerical simulation: a tool in turbulence research. *Ann. Rev. Fluid Mech.*, **30**, 539–578.

118 Moser, R.D., Kim, J. and Mansour, N.N. (1999). Direct numerical simulation of turbulent channel flow up to $Re_\tau = 590$. *Phys. Fluids*, **11**, 943–945.

119 Mullen, J.S. and Fischer, P.F. (1999). Filtering techniques for complex geometry fluid flows. *Comm. Numer. Meth. Engrg.*, **15**, 9–18.

120 Nesliturk, A.I. (1999). Approximating the incompressible Navier Stokes equations using a two level finite element method. PhD Thesis, University of Colorado, Denver.

121 Nesliturk, A.I. and Harari, I. (2003). The nearly-optimal Petrov-Galerkin method for convection-diffusion problems. *Comput. Methods Appl. Mech. Engrg.*, **192**, 2501–2519.

122 Oberai, A.A., Gravemeier, V. and Burton, G.C. (2004). Transfer of energy in the variational multiscale formulation of LES. In: *Proceedings of the Summer Program 2004, Center for Turbulence Research*, Stanford University and NASA Ames Research Center, 123–132.

123 Oberai, A.A. and Hughes, T.J.R. (2002). The variational multiscale formulation of LES: channel flow at $Re_\tau = 590$. *AIAA Paper 2002-1056*, Reno, NV, January 14–17.

124 Oberai, A.A. and Wanderer, J. (2005). A dynamic approach for evaluating parameters in a numerical method. *Int. J. Numer. Meth. Engrg.*, **62**, 50–71.

125 Oberai, A.A. and Wanderer, J. (2005). Variational fomulation of the Germano identity for the Navier-Stokes equations. *Journal of Turbulence*, **6**, 1–17.

126 Obi, S., Aoki, K. and Masuda, S. (1993). Experimental and computational study of turbulent separating flow in an asymmetric plane diffuser. *Ninth Symp. on Turbulent Shear Flows*, Kyoto, Japan, August 16–19.

127 Oñate, E., Garcia, J. and Idelsohn, S. (1997). Computation of the stabilization parameter for the finite element solution of advective-diffusive problems. *Int. J. Numer. Meth. Fluids*, **25**, 1385–1407.

128 Oñate, E. (1998). Derivation of stabilized equations for numerical solution of advective-diffusive transport and fluid flow problems. *Comput. Methods Appl. Mech. Engrg.*, **151**, 233–265.

129 Oñate, E. (2000). A stabilized finite element method for incompressible viscous flows using a finite increment calculus formulation. *Comput. Methods Appl. Mech. Engrg.*, **182**, 355–370.

130 Piomelli, U. (1999). Large-eddy simulation: achievements and challenges. *Progress in Aerospace Science*, **35**, 335–362.

131 Pope, S.B. (2000). *Turbulent flows*, Cambridge University Press, Cambridge.

132 Ramakrishnan, S. (2004). Towards multi-scale modeling for turbulence simulation in complex geometries. PhD Thesis, Rice University, Houston, Texas.

133 Ramakrishnan, S. and Collis, S.S. (2002). Variational multiscale modeling for turbulence control. *AIAA Paper 2002-3280*, Houston, Texas, June 24–27.

134 Ramakrishnan, S. and Collis, S.S. (2004). Multiscale modeling for turbulence simulation in complex geometries. *AIAA Paper 2004-241*, Reno, Nevada, January 5–8.

135 Richardson, L.F. (1922). Weather prediction by numerical process, Cambridge University Press, Cambridge.

136 Rogallo, R.S. and Moin, P. (1984). Numerical simulation of turbulent flows. *Ann. Rev. Fluid Mech.*, **16**, 99–137.

137 Russo, A. (1996). Bubble stabilization of finite element methods for the linearized incompressible Navier-Stokes equations. *Comput. Methods Appl. Mech. Engrg.*, **132**, 335–343.

138 Sagaut, P. (2002). *Large eddy simulation for incompressible flows*, 2nd edition, Springer, Berlin.

139 Sagaut, P. and Grohens, R. (1999). Discrete filters for large eddy simulation. *Int. J. Numer. Meth. Fluids*, **31**, 1195–1220.

140 Sangalli, G. (2003). Capturing small scales in elliptic problems using a residual-free bubbles finite element method. *Multiscale Modeling and Simulation*, **1**, 485–503.

141 Sarghini, F., Piomelli, U. and Balaras, E. (1999). Scale-similar models for large-eddy simulation. *Phys. Fluids*, **11**, 1596–1607.

142 Schumann, U. (1975). Subgrid scale model for finite difference simulations of turbulent flows in plane channels and annuli. *J. Comput. Phys.*, **18**, 376–404.

143 Shephard, M., Dey, S. and Flaherty, J.E. (1997). A straightforward structure to construct shape functions for variable p-order meshes. *Comput. Methods Appl. Mech. Engrg.*, **147**, 209–233.

144 Smagorinsky, J. (1963). General circulation experiments with the primitive equations. I. The basic experiment. *Mon. Weather Rev.*, **91**, 99–164.

145 Szabo, B. and Babuška, I. (1991) *Finite element analysis*. John Wiley & Sons, New York.

146 Taylor, G.I. (1923). On the decay of vortices in a viscous fluid. *Philos. Mag.*, **46**, 671–674.

147 Tejada-Martinez, A.E. and Jansen, K.E. (2003). Spatial test filters for dynamic model large eddy simulation with finite elements. *Comm. Numer. Meth. Engrg.*, **19**, 205–213.

148 Tejada-Martinez, A.E. and Jansen, K.E. (2004). A dynamic Smagorinsky model with dynamic determination of the filter width ratio. *Phys. Fluids*, **16**, 2514–2528.

149 Tennekes, H. and Lumley, J.L. (1972). *A first course in turbulence*. MIT Press, Cambridge, MA.

150 Terracol, M., Sagaut, P. and Basdevant, C. (2001). A multilevel algorithm for large-eddy simulation of turbulent compressible flows. *J. Comput. Phys.*, **167**, 439–474.

151 Tezduyar, T.E. and Osawa, Y. (2000). Finite element stabilization parameters computed from element matrices and vectors. *Comput. Methods Appl. Mech. Engrg.*, **190**, 411–430.

152 Vasilyev, O., Lund, T.S. and Moin, P. (1998). A general class of commutative filters for LES in complex geometries. *J. Comput. Phys.*, **146**, 82–104.

153 Vreman, A.W. (2003). The filtering analog of the variational multiscale method in large-eddy simulation. *Phys. Fluids*, **15**, L61–L64.

154 Vreman, A.W. (2004). The adjoint filter operator in large-eddy simulation of turbulent flow. *Phys. Fluids*, **16**, 2012–2022.

155 Wagner, G.J. and Liu, W.K. (2000). Turbulence simulation and multiple scale subgrid models. *Comput. Mech.*, **25**, 117–136.

156 Wall, W.A. (1999). Fluid-Struktur-Interaktion mit stabilisierten Finiten Elementen. (in German), PhD Thesis, Report No. 31, Institute of Structural Mechanics, University of Stuttgart.

157 Wesseling, P. (1992). *An introduction to multigrid methods*. John Wiley & Sons, Chichester.

158 Whiting, C.H. (1999). Stabilized finite element methods for fluid dynamics using a hierarchical basis. PhD Thesis, Rensselaer Polytechnic Institute.

159 Whiting, C.H. and Jansen, K.E. (2001). A stabilized finite element method for the incompressible Navier-Stokes equations using a hierarchical basis. *Int. J. Numer. Meth. Fluids*, **35**, 93–116.

160 Whiting, C.H., Jansen, K.E. and Dey, S. (2003). Hierarchical basis for stabilized finite element methods for compressible flows. *Comput. Methods Appl. Mech. Engrg.*, **192**, 5167–5185.

161 Wilcox, D.C. (1998). *Turbulence Modeling for CFD*. 2nd edition, DCW Industries Inc., La Canada, CA.

162 Wu, X., Schlüter, J., Moin, P., Pitsch, H., Iaccarino, G. and Ham, F. (2006). Computational study on the internal layer in a diffuser. *J. Fluid Mech.*, **550**, 391–412.

163 Zang, Y., Street, R.L. and Koseff, J.R. (1993). A dynamic mixed subgrid-scale model and its application to turbulent recirculating flows. *Phys. Fluids A*, **5**, 3186–3196.

164 Zienkiewicz, O.C., de S.R. Gago, J.P. and Kelly, D.W. (1983). The hierarchical concept in finite element analysis. *Comput. Struct.*, **16**, 53–65.

165 Zienkiewicz, O.C. and Taylor, R.L. (2000). *The finite element method, Vol. 1: The basis*. 5th edition, Butterworth-Heinemann, Oxford.

Please address your comments or questions on this paper to:
International Center for Numerical Methods in Engineering
Edificio C-1, Campus Norte UPC
Grand Capitán s/n
08034 Barcelona, Spain
Phone: 34-93-4016035; Fax: 34-93-4016517
E-mail: onate@cimne.upc.edu

A TRADITIONAL FILTER-BASED LARGE EDDY SIMULATION

A.1 Explicit Spatial Filtering of the Navier-Stokes Equations

The first step in a traditional LES is the application of a spatial filter G with characteristic filter width Δ to the unknown velocity field $\mathbf{u}$ resulting in the filtered velocity field

$$\mathbf{u}^{\Delta}(\mathbf{x},t) = \int_{\Omega} G(\mathbf{x}-\xi)\mathbf{u}(\xi,t)\,d\xi \tag{A.1}$$

This filtering procedure was first proposed by Leonard [107]. The three most commonly used filters for LES are the box or top-hat filter, the Gaussian filter, and the sharp or spectral cutoff filter. These filters are displayed in physical space along with their associated version in the spectral space, for instance, in Sagaut [138], and it is refered to this textbook for an extensive discussion of these classical filters as well as some other ways of filtering. It should be remarked that only the sharp cutoff filter has the property of a projector in the spectral space for the multiple application of the operator, which may be expressed as

$$\hat{G}^n = \hat{G} \circ \hat{G} \circ \cdots \circ \hat{G} = \hat{G}, \qquad n > 1 \tag{A.2}$$

In practical applications in the physical space, the situation is usually much more complicated with regard to the filtering issue than in the spectral space. Discrete filters with compact support are widely used in practical applications in the physical space. They may be identified as discrete approximations of the filter G in (A.1) (i.e., usually as discrete approximations of the box filter or the Gaussian filter in physical space), see Sagaut and Grohens [139]. Such discrete smooth filters will be particularly adressed in Section A.3. All those filters commute with differentiation, a prerequisite for the formulation of the filtered Navier-Stokes equations, in the *homogeneous* case, see Sagaut [138]. However, problems occur both for the continuous filter itself and the discrete approximation when using homogeneous filters for *inhomogenous* cases, for instance, as soon as a domain boundary is approached. The need for the filtering to be commutative with differentiation also in inhomogeneous cases was emphasized in Ghosal and Moin [55], and moreover, second-order commuting continuous filters were developed to address this problem. In Vasilyev *et al.* [152], this strategy was extended to higher-order commuting filters as well as discrete approximations of the continuous filters.

After applying the spatial filter G to (3)-(4), the Navier-Stokes equations for the filtered velocity $\mathbf{u}^{\Delta}$ and the filtered pressure p^{Δ} are given as

$$\frac{\partial \mathbf{u}^{\Delta}}{\partial t} + \nabla\cdot(\mathbf{u}^{\Delta}\otimes\mathbf{u}^{\Delta}) + \nabla p^{\Delta} - 2\nu\nabla\cdot\varepsilon(\mathbf{u}^{\Delta}) + \nabla\cdot\boldsymbol{\tau}^{\Delta} = \mathbf{f}^{\Delta} \qquad \text{in} \quad \Omega\times(0,T) \tag{A.3}$$

$$\nabla\cdot\mathbf{u}^{\Delta} = 0 \qquad \text{in} \quad \Omega\times(0,T) \tag{A.4}$$

where

$$\boldsymbol{\tau}^{\Delta} = (\mathbf{u}\otimes\mathbf{u})^{\Delta} - \mathbf{u}^{\Delta}\otimes\mathbf{u}^{\Delta} \tag{A.5}$$

The tensor $\boldsymbol{\tau}^{\Delta}$ is refered to as a "subfilter"-scale stress tensor here, in order to emphasize its origin due to a filtering process. The non-linear convective term incorporates the effect of the subfilter scales on the filtered (i.e., resolved) scales. Since one is only able to compute $\mathbf{u}^{\Delta}\otimes\mathbf{u}^{\Delta}$, the difference between the filtered non-linear term $(\mathbf{u}\otimes\mathbf{u})^{\Delta}$ and $\mathbf{u}^{\Delta}\otimes\mathbf{u}^{\Delta}$ has to be modeled. This describes the *closure problem* of the traditional LES.

A.2 Implicit and Effective Filtering

According to Sagaut [138], four different types of filters in a LES may be identified:

- an explicit analytical filter G represented by a convolution product as in (A.1),
- an implicit filter induced by the numerical scheme applied to the underlying problem, which may be, for instance, ascribed to the approximation of continuous differential operators by discrete operators (The introduction of an implicit filter due to the use of artificial dissipation (e.g., in the context of an upwinding scheme) should also been mentioned here, although this filtering is very similar to the filtering introduced by a subgrid viscosity model, which is stated below.),
- an implicit filter linked to the chosen discretization (It is obvious that no frequency higher than the Nyquist frequency associated with the respective computational grid can be resolved.), and
- an implicit filter associated with a potentially applied subgrid-scale model, due to the inherent length scale of the model (In the context of a subgrid viscosity model, this may, for instance, be interpreted as the mixing length.).

It is a difficult but crucial question how the effective filter assembled by all or some of the filters just mentioned looks like. It is refered to the exhaustive discussion of this important question in Sagaut [138]. One way of clearly identifying the effective filter is by letting one of the filters become predominant over the other filters. This may be done by the so-called "pre-filtering technique" (i.e., actually applying an explicit filter). The pre-filtering technique allows strict control of the form of the filter and the cutoff length by applying a filter with a filter width Δ which is larger than the characteristic length h of the computational grid. The drawback of this procedure lies in the fact that subfilter scales appear, which are resolved by the computational grid, but are not resolved scales in the sense of a traditional LES and therefore useless. Thus, computational demands are substantially increased without increasing the amount of resolved scales. As a result, an explicit filter does not appear in virtually all LES codes, unless it is necessary, for example, to carry out a dynamic modeling procedure for the unresolved scales, as shown in Section 4.2. Two explicit discrete filters for this purpose will be addressed, and references for further discrete filters will be given in the subsequent section.

As a result, the usual way of filtering is an implicit one, which is mainly based on the chosen discretization, with the other aforementioned implicit filters potentially having an impact. This may be viewed, in principle, as a variant of the "volume-balance" approach of Schumann [142], where the respective control volume of a FVM was utilized as a "filter", which was identified to be very similar to a box filter. Thus, problems associated with necessary modifications of explicit filters in wall-bounded flows become obsolete for such a purely implicit filtering technique. In the main part of this article, variational projection has been identified as another implicit "filter" for the Navier-Stokes equations. There is also a close relationship of the variational projection with Schumann's volume-balance approach, at least in the context of the FVM.

A.3 Discrete Smooth Filters

The use of discrete filters for LES is addressed, for instance, in Lund [111] and Sagaut and Grohens [139]. The two most prominent representatives of discrete smooth filters are obtained by applying either the trapezoidal rule or Simpson's rule. In Sagaut and Grohens [139], it is shown that discrete filters may be constructed in two steps. Firstly,

the continuous convolution filter in (A.1) is approximated by a truncated Taylor series expansion in the sense of a continuous differential operator. Secondly, this continuous differential operator is discretized to obtain a discrete form of the operator.

In the following, it is assumed that the usual implicit filtering approach based on the chosen discretization has been applied to identify the resolved scales of the problem, as mentioned above. The discrete smooth filter may then be required for the identification of the large resolved scales, for example, for a dynamic modeling procedure as described in Section 4.2. For instance, the large-scale part $\bar{u}_i^h$ of the discrete scalar unknown u_i^h in the control volume Ω_i of a uniform 1-D FV discretization, is computed as

$$\bar{u}_i^h = \frac{1}{4}(u_{i-1}^h + 2u_i^h + u_{i+1}^h) \tag{A.6}$$

for the trapezoidal rule and

$$\bar{u}_i^h = \frac{1}{6}(u_{i-1}^h + 4u_i^h + u_{i+1}^h) \tag{A.7}$$

for Simpson's rule, including the neighbour control volumes Ω_{i-1} and Ω_{i+1}. In the three-dimensional case, a discrete filter for a structured grid of hexahedra may be constructed in two ways: either by linear combination or by product. Following the strategy of construction by linear combination, a face-based filter as described in Jansen [90] may be achieved. However, it is well known that filters constructed by linear combination are less sensitive to the cross modes than the ones constructed by product, see Sagaut [138]. Following the rules for construction by product in Sagaut and Grohens [139], the large-scale velocity vector in the center of the control volume Ω_i of a three-dimensional FV discretization is obtained as

$$\bar{\mathbf{u}}_i^h = \frac{1}{8}\mathbf{u}_i^h + \frac{1}{16}\sum_{f=1}^{n_{\mathrm{fpcv}}} \mathbf{u}_f^h + \frac{1}{32}\sum_{e=1}^{n_{\mathrm{epcv}}} \mathbf{u}_e^h + \frac{1}{64}\sum_{n=1}^{n_{\mathrm{npcv}}} \mathbf{u}_n^h \tag{A.8}$$

for the trapezoidal filter and

$$\bar{\mathbf{u}}_i^h = \frac{8}{27}\mathbf{u}_i^h + \frac{2}{27}\sum_{f=1}^{n_{\mathrm{fpcv}}} \mathbf{u}_f^h + \frac{1}{54}\sum_{e=1}^{n_{\mathrm{epcv}}} \mathbf{u}_e^h + \frac{1}{216}\sum_{n=1}^{n_{\mathrm{npcv}}} \mathbf{u}_n^h \tag{A.9}$$

for Simpson's filter with the number of faces n_{fpcv}, edges n_{epcv}, and nodes n_{npcv} per control volume being 6, 12, and 8, respectively. $\mathbf{u}_f^h$, $\mathbf{u}_e^h$, and $\mathbf{u}_n^h$ denote the velocity vectors at the center of control volumes sharing at most one face, one edge, and one node with Ω_i, respectively.

On unstructured grids, the discrete filters have to be altered in general. Commutative discrete filters for unstructured grids were developed in Marsden *et al.* [113], using the work of Vasilyev *et al.* [152] as a starting point. Subsequently, a new construction procedure based on least-squares techniques was presented in Haselbacher and Vasilyev [70]. Filters for unstructured cases based on the numerical solution of high-order elliptic problems were proposed in Mullen and Fischer [119]. For the FEM, in particular, a number of discrete filters suited for the application on unstructured grids were described in Jansen [90]. One of them, a node-oriented discrete version of a box filter, was then further investigated in Tejada-Martinez and Jansen [147], [148] on structured FE grids.

For the two filters mentioned above (i.e., the filters according to the trapezoidal and Simpson's rule), a two-step procedure for constructing the filters in the unstructured case may be performed, with the goal of reproducing formulas (A.8) and (A.9) in the structured

case, as shown in Gravemeier [58]. For the trapezoidal filter, a volume-weighted averaging procedure at every node including all control volumes Ω_k attached to this node is performed subject to

$$\bar{\mathbf{u}}_n^h = \frac{\sum\limits_{k=1}^{n_{\text{cvpn}}} |\Omega_k| \mathbf{u}_k^h}{\sum\limits_{k=1}^{n_{\text{cvpn}}} |\Omega_k|} \tag{A.10}$$

with n_{cvpn} denoting the number of control volumes attached to node n. As a result, a large-scale velocity $\bar{\mathbf{u}}_n^h$ at node n is obtained. It should be noted that for unstructured grids with abrupt variations of the volume measures within small distances, it may be advisable to use a simple non-volume-weighted average instead of (A.10). In any case, the large-scale velocity at the center of the control volume is afterwards collected as the averaged value calculated by including all nodes of this control volume according to

$$\bar{\mathbf{u}}_i^h = \frac{1}{n_{\text{npcv}}} \sum_{n=1}^{n_{\text{npcv}}} \bar{\mathbf{u}}_n^h \tag{A.11}$$

A filter created by this two-step procedure was used in Haworth and Jansen [71]. It may be verified by the reader that the formula in (A.8) can be recovered for the structured case by removing the volume weighting in (A.10).

An unstructured analog of Simpson's filter is more involved in that it uses an edge- as well as a face-based data transfer in addition to the node-based transfer for the trapezoidal filter, see Gravemeier [58]. The volume-weighted averaging at edges and faces reads

$$\bar{\mathbf{u}}_e^h = \frac{\sum\limits_{l=1}^{n_{\text{cvpe}}} |\Omega_l| \mathbf{u}_l^h}{\sum\limits_{l=1}^{n_{\text{cvpe}}} |\Omega_l|}, \qquad \bar{\mathbf{u}}_f^h = \frac{\sum\limits_{m=1}^{n_{\text{cvpf}}} |\Omega_m| \mathbf{u}_m^h}{\sum\limits_{m=1}^{n_{\text{cvpf}}} |\Omega_m|} \tag{A.12}$$

with n_{cvpe} and n_{cvpf} indicating the number of control volumes attached to the interiors of edge e and face f, respectively. The node-, edge-, and face-based values in (A.10) and (A.12) are now collected in an averaged sense, including the actual value in the control volume, in order to obtain the large-scale velocity at the center of the control volume as

$$\bar{\mathbf{u}}_i^h = \frac{1}{n_{\text{npcv}} + n_{\text{epcv}} + n_{\text{fpcv}} + 1} \left[\sum_{n=1}^{n_{\text{npcv}}} \bar{\mathbf{u}}_n^h + \sum_{e=1}^{n_{\text{epcv}}} \bar{\mathbf{u}}_e^h + \sum_{f=1}^{n_{\text{fpcv}}} \bar{\mathbf{u}}_f^h + \mathbf{u}_i^h \right] \tag{A.13}$$

Again, it may be verified by the reader that the formula in (A.9) can be recovered for the structured case by removing the volume weighting in (A.10) and (A.12). The two-step procedures for the trapezoidal filter as well as for Simpson's filter may also be used for other types of control volumes, such as tetrahedra, prisms, and pyramids, which may appear in hybrid unstructured grids, although it is not possible to follow the same line of argument with respect to the structured case as for hexahedra.

A.4 Functional vs. Structural Modeling and the Subgrid Viscosity Concept

The closure problem, which has been introduced at the end of Section A.1, will now be addressed by appropriate modeling approaches. Two different modeling strategies may be

distinguished according to Sagaut [138]. On the one hand, it may be intended to approximate the subfilter-scale stress tensor $\boldsymbol{\tau}^{\Delta}$ itself. Thus, a functional relation as

$$\boldsymbol{\tau}^{\Delta} = \mathcal{F}(\mathbf{u}^{\Delta}) \tag{A.14}$$

is assumed. This first strategy is called *structural modeling*. Perhaps the most famous structural modeling approach is the Bardina model (see, e.g., Bardina *et al.* [3]). The basic idea behind this model is the hypothesis of a similarity between the subfilter (or subgrid) scales, which have to be modeled, and the smallest resolved scales, which are available for modeling purposes. This basic idea is also instrumental in the dynamic modeling procedure (see Section 4.2). The drawback of the Bardina models lies in its merely slightly dissipative character and its underestimation of the energy cascade, as a result of this. In order to remedy this problem, the Bardina model is often used in a mixed form along with a functional (and usually more dissipative) model, such as the Smagorinsky model (see, e.g., Sarghini *et al.* [141] and Zang *et al.* [163]). For an exhaustive list of structural models, it is refered to Sagaut [138], Chapter 6.

The second strategy aims at modeling the (energetic) action of the subfilter (or subgrid) scales on the resolved scales, and not the tensor $\boldsymbol{\tau}^{\Delta}$ itself. This functional relation is given as

$$\nabla \cdot \boldsymbol{\tau}^{\Delta} = \mathcal{F}(\mathbf{u}^{\Delta}) \tag{A.15}$$

This second strategy is called *functional modeling*. Perhaps the most popular and widespread way of functional modeling relies on the *subgrid (or eddy) viscosity concept*, which is based on Boussinesq's [5] turbulent (or eddy) viscosity assumption (see, e.g., Wilcox [161]). It is assumed that the energy transfer mechanism from the resolved to the unresolved scales is similar to the molecular mechanism based on the physical viscosity of the respective fluid. Thus, the tensor $\boldsymbol{\tau}^{\Delta}$ or, more precisely, the deviatoric part of it is calculated as a product of a subgrid viscosity ν_T and the rate-of-velocity tensor of the resolved scales $\boldsymbol{\varepsilon}(\mathbf{u}^{\Delta})$ such that

$$-\operatorname{dev} \boldsymbol{\tau}^{\Delta} = 2\nu_T \boldsymbol{\varepsilon}(\mathbf{u}^{\Delta}) \tag{A.16}$$

The reason for restricting the modeling efforts to the deviatoric part of the subfilter-scale tensor is justified by the fact that, for incompressible flows, $\boldsymbol{\varepsilon}(\mathbf{u})$ has a zero trace, which results in an identity between the tensor and its deviatoric part. Depending on such a deviatoric tensor, one is only able to model a deviatoric tensor as well. The complementary spherical tensor is usually added to the pressure term, which then reads in modified form as

$$\tilde{p}_{\mathrm{mod}} = \tilde{p} + \frac{1}{3}\mathrm{tr}\boldsymbol{\tau}^{\Delta} \tag{A.17}$$

and, hence, requires no modeling. However, the picture would not be complete without describing what should be modelled by ν_T. There are two main phenomena in the interaction between the resolved scales, particularly the small resolved scales, and the unresolved scales. The main process is generated by a drainage of energy from the resolved scales to the unresolved scales. Aside from this, a weak backscatter occurs in the opposite direction. All functional modeling efforts are based on the hypothesis that the action of the unresolved scales on the resolved scales can be viewed as an energetic action whose respective energy transfer balance should be sufficient for its description. Another interesting functional modeling approach, called *implicit diffusion*, is based on the applied numerical scheme as well as the hypothesis that the subfilter-(or subgrid-)scale action is strictly dissipative. Here, the associated truncation error is expected to create the desired effects. The most popular examples for this strategy are constituted by a variety of upwind schemes. Stabilized FEMs may also be arranged in this class, although they have not been designed for this purpose

initially. In Donea and Huerta [30], for instance, it is outlined that all three approaches (i.e., the direct introduction of numerical diffusion (or viscosity), the use of an upwinding scheme, and a stabilized method) may basically be viewed as equivalent methodologies in that all of them eventually introduce some kind of numerical diffusion (or viscosity). However, the distinction between stabilized methods and the other two techniques is slight but crucial.

The reader may consult Sagaut [138], Chapters 4 and 5, for a comprehensive description of functional models, which are basically developed for the isotropic case, and their adjustment to the anisotropic case. An analysis of the subfilter-(or subgrid-)scale models emphasized in Section 4 (i.e., the Smagorinsky model and the dynamic modeling procedure based on the Smagorinsky model) as well as further models based on the scale-similarity hypothesis may be found in Meneveau and Katz [115].